5-2009

A Geologic and Hydrochemical Investigation of the Suitability of Central Utah's Navajo Sandstone for the Disposal of Saline Process Water and CO2

Kevin L. Randall
Utah State University

A GEOLOGIC AND HYDROCHEMCIAL INVESTIGATION OF THE SUITABILITY OF CENTRAL UTAH'S NAVAJO SANDSTONE FOR THE DISPOSAL OF SALINE PROCESS WATER AND CO_2

by

Kevin Lewis Randall

A thesis submitted in partial fulfillment
of the requirements for the degree

of

MASTER OF SCIENCE

in

Geology

Approved:

Thomas E. Lachmar Major Professor	James P. Evans Committee Member
William Doucette Committee Member	Byron R. Burnham Dean of Graduate Studies

UTAH STATE UNIVERSITY
Logan, Utah

2009

ABSTRACT

A Geologic and Hydrochemical Investigation of the Suitability of Central Utah's Navajo Sandstone for the Disposal of Saline Process Water and CO_2

by

Kevin Lewis Randall, Master of Science

Utah State University, 2009

Major Professor: Dr. Thomas E. Lachmar
Department: Geology

Salt water is produced from the Ferron Sandstone Member of the Mancos Shale in central Utah as part of the production of coalbed methane (CBM) and is disposed of by injection predominantly into the Navajo Sandstone between 4,500 feet to 7,300 feet and is considered to be a hazardous waste. Local government agencies are concerned about the potential impacts on shallow groundwater because of this disposal method.

Water samples were gathered from four shallow water-supply wells, and nine salt water disposal (SWD) wells to compare hydrochemistries as an indicator of potential mixing. Shallow water-supply wells are likely recharged by local precipitation while the source of CO_2 is from atmospheric and/or soil CO_2 gas and comparatively, are low in total dissolved solids. Carbonate mineral dissolution is the source of CO_2 in the SWD wells and is exceptionally high in TDS. The SWD water appears to be old water and displays an evaporative signature.

A geologic analysis was conducted for the Drunkards Wash gas field using 479 digital gas well logs. Three subsurface faults were identified with one fault in the north and the other two in the central part of the gas field near the eastern and western flanks. These faults were further confirmed by comparing average monthly gas and water production from the first 24 months in these faulted areas to adjacent control areas. Areas near faults reveal two to six times greater gas production than that of the associated control areas, and water production is greater by nearly an order of magnitude. This difference is likely due to the fracturing associated with the damage zone near the faults allowing for increased flow of gas and water.

Due to the high injection pressures the vertical hydraulic gradient has been reversed from downward to upward. However, due to the thick sequences of shale separating the disposal aquifers and the shallow aquifers the estimated time required for the disposal waters to migrate to the surface would be at least 2,000 years. I conclude that the saline waters produced from the Ferron Sandstone are being safely sequestered in deeply buried, extensive and geologically-sealed aquifers.

(153 pages)

ACKNOWLEDGMENTS

I wish to extend my gratitude for the research grants received from the Community/University Research Initiative. I also greatly appreciate the teaching assistant position granted from the Department of Geology at Utah State University. In addition, I am grateful to ConocoPhillips, Anadarko and XTO Energy for their assistance in gathering water samples as well providing valuable data for this project.

I would like my committee to know how much I appreciate their time and patience. I was well taken care of by my committee members: Tom Lachmar, Jim Evans and Bill Doucette. Bill has been a great asset as he has been very willing to meet with me and listen to ideas about the chemical aspect of this project and provide useful insight. Jim was easy to work with and always willing to take time from his busy schedule to help guide me in the right direction and listen to interpretations. I especially want to thank my major professor, Tom Lachmar, who helped make this project enjoyable in many different ways. I appreciate Tom's honesty and constant encouragement. I also appreciate how thorough and constructive Tom has been with the writing and revision part of this process. Over the course of this project and several others Tom has become a good friend whom I admire and respect. Thanks for the laughs Tom.

In addition to my committee I would like to recognize and thank Dave Liddell and Pete Kolesar. Dave was very patient with me over the course of several visits as he guided me through the statistical analysis, which I could not have done without his help. Pete was very willing to help with ideas and interpretations regarding the geochemical aspect of this project and I am very grateful for his time and abilities in helping me think about ideas in a different way.

I would also like to thank my mother and father who taught me the value of education and to set high goals and then to work hard to achieve those goals, my brothers and grandparents for their love and support and my mother- and father-in-law who are very encouraging and helpful in so many ways. Most of all I would like to thank my sweetheart Camille for so many things: for always providing me with the time I needed to complete graduate school, for always listening to me, for kind and encouraging words when I needed them most and for being a wonderful mother to our two handsome boys. And special thanks to those two handsome boys, Samuel and Jonah, for being much of my motivation.

Kevin Lewis Randall

CONTENTS

Page

ABSTRACT……ii

ACKNOWLEDGMENTS……iv

LIST OF TABLES……viii

LIST OF FIGURES……ix

CHAPTER

I. INTRODUCTION…… 1

Problem Statement and Location…… 1
Purpose and Objectives…… 2

II. BACKGROUND…… 4

Geologic Setting…… 4
Structure…… 4
Stratigraphy…… 7
Ferron Sandstone CBM Play…… 15
Hydrogeology…… 19
CO_2 Sequestration…… 28

III. METHODS…… 31

Well Selection and Sampling…… 31
Hydrochemistry…… 39
Structural Analysis …… 43

IV. RESULTS…… 55

Hydrochemistry…… 55
Structural Analysis…… 60

V. SUMMARY AND DISCUSSION…… 81

Hydrochemistry…… 81
Structural Analysis…… 85
Conceptual Model…… 88

VI. CONCLUSIONS, IMPLICATIONS AND RECOMMENDATIONS……. 96

Conclusions…….. 96
Implications……. 98
Recommendations for Further Work……... 99

REFERENCES…….. 103

APPENDICES……... 107

Appendix A: Interpreted well logs…… 108
Appendix B: Uninterpreted well logs……..... 120
Appendix C: Contour maps……..... 137

LIST OF TABLES

Table		Page
1	Select data from Waddell et al. (1978)	23
2	Select data from Sumsion (1979)	24
3	Data from the disposal reservoirs	27
4	Sampling status for all shallow water-supply wells	32
5	Relevent information for SWD wells	38
6	Chemical data from shallow water-supply wells	56
7	Chemical data from SWD wells	56
8	Fault throws from areas A, B, and C	62
9	Summary of gas and water production for faulted and control areas	67
10	Statistical analysis using Mann-Whitney test	75
11	Shale smear factor calculations	80
12	Changes in water levels for SWD wells due to injection	91
13	Freshwater well elevations and depths to water	92
14	Hydraulic conductivity and stratigraphic thickness approximations	93

LIST OF FIGURES

Figure		Page
1	Location map of study area	2
2	Cross section extending from the Wasatch Plateau to the San Rafael Swell	6
3	General stratigraphic column of rocks	8
4	Interpreted regional extent of the two major delta systems	16
5	Drunkards Wash, central Utah	18
6	Potentiometric contour map within the vicinity of the Ferron CBM fairway	20
7	Locations of the four shallow water-supply wells and nine SWD wells	33
8	Variation in δD and $\delta^{18}O$	42
9	Map showing locations of the 479 wells in the Drunkards Wash gas field	45
10	East-west cross sections created using digital well logs and PETRA	50
11	North-south cross sections created using digital well logs and PETRA	51
12	Trilinear (Piper, 1944) diagram of well samples	57
13	Delta D and $\delta^{18}O$ from shallow, water-supply wells and SWD wells plotted with the GMWL	58
14	North-south trending faults and anticline identified in the Drunkards Wash CBM gas field	61
15	Faulted areas (A, B, C, and D) and associated control areas for gas and water production	65
16	Gas production for areas A (upper) and A-control (lower)	69
17	Gas production for areas B (upper) and B-control (lower)	70
18	Gas production for areas C (upper) and C-control (lower)	72
19	Gas production for areas D (upper) and D-control (lower)	73

20 Interpreted log for well 43-007-30428 from area A 77

21 Interpreted log for well 43-007-30224 from area B.....78

22 Interpreted log for well 43-007-30731 from area C.....79

23 Conceptual model 89

24 Effects of salt water injection on water level elevations.....92

25 Cross section B-B’ with interpreted fault 109

26 Cross section C-C’ with interpreted fault 109

27 Cross section D-D’ with interpreted fault.....110

28 Cross section E-E’ with interpreted faults 110

29 Cross section I-I’ with interpreted fault.....111

30 Cross section J-J’ with interpreted fault.....111

31 Cross section K-K’ with interpreted fault.....112

32 Cross section K-K’ close up of interpreted fault showing 10 feet of offset 112

33 Cross section L-L’ with interpreted fault.....113

34 Cross section M-M’ with interpreted fault.....113

35 Cross section N-N’ with interpreted fault.....114

36 Cross section O-O’ with interpreted faults 114

37 Cross section P-P’ with interpreted fault 115

38 Cross section Q-Q’ with interpreted fault.....115

39 Cross section R-R’ with interpreted fault 116

40 Cross section S-S’ with interpreted fault 116

41 Cross section T-T’ with interpreted fault.....117

42 Cross section B1-B2’ showing northern part of Huntington anticline 117

43 Cross section C1-C2’ showing Huntington anticline.....118

44 Cross section D1-D2’ showing Huntington anticline 118

45 Cross section of E1-E2’ showing southern part of Huntington anticline 119

46 Cross section A-A’ (not interpreted).....121

47 Cross section B-B’ (not interpreted) 121

48 Cross section C-C’ (not interpreted) 122

49 Cross section D-D’ (not interpreted).....122

50 Cross section E-E’ (not interpreted) 123

51 Cross section F-F’ (not interpreted) 123

52 Cross section G-G’ (not interpreted).....124

53 Cross section H-H’ (not interpreted).....124

54 Cross section I-I’ (not interpreted).....125

55 Cross section J-J’ (not interpreted) 125

56 Cross section K-K’ (not interpreted).....126

57 Cross section L-L’ (not interpreted) 126

58 Cross section M-M’ (not interpreted) 127

59 Cross section N-N’ (not interpreted).....127

60 Cross section O-O’ (not interpreted).....128

61 Cross section P-P’ (not interpreted).....128

62 Cross section Q-Q’ (not interpreted).....129

63 Cross section R-R’ (not interpreted) 129

64 Cross section S-S’ (not interpreted).....130

65 Cross section T-T’ (not interpreted) 130

66 Cross section U-U’ (not interpreted).....131

67 Cross section V-V’ (not interpreted).....131

68 Cross section W-W’ (not interpreted).....132

69 Cross section X-X’ (not interpreted).....132

70 Cross section Y-Y’ (not interpreted).....133

71 Cross section Z-Z’ (not interpreted) 133

72 Cross section A1-A2’ (not interpreted).....134

73 Cross section B1-B2’ (not interpreted).....134

74 Cross section C1-C2’ (not interpreted).....135

75 Cross section D1-D2’ (not interpreted).....135

76 Cross section E1-E2’ (not interpreted) 136

77 Elevation of top of Ferron Sandstone (ft above mean sea level) 138

78 Elevation of top of coal (ft above mean sea level).....139

79 Elevation of base of coal (ft above mean sea level).....140

80 Elevation of top of Blue Gate Shale (ft above mean sea level) 141

CHAPTER I

INTRODUCTION

Problem Statement and Location

Coalbed methane (CBM) is produced from the Ferron Sandstone member of the Mancos Shale (Cretaceous) in the Drunkards Wash, Helper, and the Buzzard Bench gas fields, located in the northwestern portion of the Colorado Plateau physiographic province in central Utah (Figure 1). The Ferron play is unique in terms of high gas content and production, and may well represent one of the most productive CBM areas in North America (Montgomery et al., 2001). Typically, CBM is produced by pumping water from the coalbed, lowering the hydrostatic pressure of the reservoir causing the methane to desorb from the fracture surfaces, which then flows as a free gas to the wellbore. Water pumped from the Drunkards Wash, Helper, and Buzzard Bench fields is very high in total dissolved solids, particularly sodium and chloride, and is considered by the U.S. EPA to be a hazardous material (Class II UIC [Underground Injection Control] water). It is disposed of by injecting it primarily into the Navajo Sandstone and to a lesser extent the Kayenta, Wingate and Shinarump Formations at depths ranging from 4,558 to 7,296 ft (1,389 to 2,221 m) below the surface as a means of permanent storage. Concern has been expressed by several local government entities in the area regarding the disposal method of this hazardous material and the possibility of contaminating overlying fresh-water aquifers.

This research has been conducted to determine if the disposal method currently being utilized to sequester the saline class II UIC waters by Anadarko Corporation,

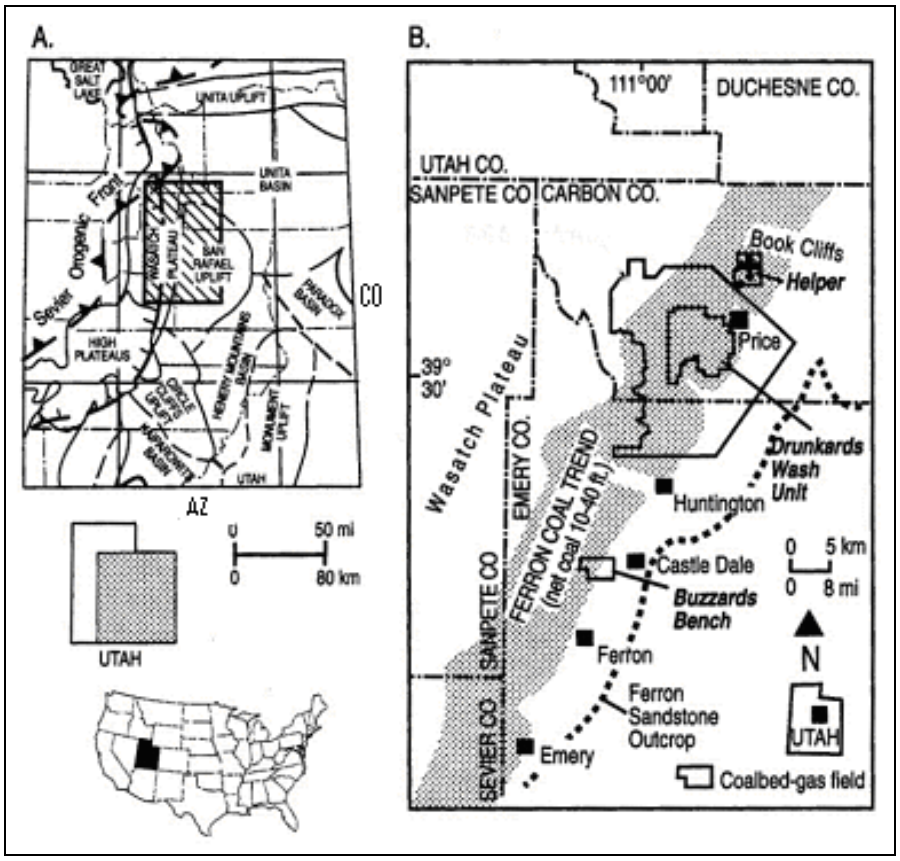

Figure 1: Location map of study area (A). Location map of the Drunkard's Wash, Helper and Buzzard Bench CBM gas fields (B). (adapted from Montgomery et al., 2001).

ConocoPhillips and XTO Energy is safe and has no negative impacts on shallow groundwater. Based on the findings of this study, further research may be warranted to determine the suitability of the Navajo Sandstone for permanently sequestering carbon dioxide (CO_2), a major greenhouse gas and contributor to global warming, in addition to the disposal of salt water.

Purpose and Objectives

The purpose of this research is to determine if salt-water injected into deep aquifers, primarily the Navajo Sandstone, in the Drunkards Wash, Helper, and Buzzard Bench gas fields in central Utah has the potential to, or currently is migrating to shallow

water-supply aquifers. The objectives of the study are to: 1) acquire geologic information from published and unpublished sources; 2) collect and analyze water samples from a representative number of salt-water disposal wells and shallow water-supply wells for major and minor ions, trace metals, and stable isotopes of hydrogen, oxygen and carbon; 3) perform a geologic survey consisting of a structural and stratigraphic analysis of the Drunkards Wash CBM gas field by creating cross sections and subsurface contour maps constructed from digital gas well logs; and 4) recommend one or more location(s) for an exploratory borehole for testing and evaluation of the Navajo Sandstone as a potential reservoir for the sequestration of CO_2.

Insight will be gained from the analysis of the geochemical and the structural and stratigraphic data into the suitability of the Navajo Sandstone for the sequestration of CO_2 within the study area. By analyzing water samples for major and minor ions, trace metals and the heavy to light ratios of hydrogen, oxygen and carbon from shallow water-supply wells and salt-water disposal wells it should be possible to determine if mixing between the disposal aquifers and shallow aquifers is occurring. Structural analysis will help identify any subsurface faults, as these faults are the most likely conduits for the migration of disposal waters.

CHAPTER II

BACKGROUND

Geologic Setting

The study area lies within the Colorado Plateau physiographic province and contains the Drunkards Wash, Helper, and Buzzard Bench CBM gas fields, which are located in central Utah (see Figure 1). The Colorado Plateau is a high-standing crustal block of relatively undeformed rocks surrounded by the highly deformed Rocky Mountains and Basin and Range Provinces. The Laramide Orogeny occurred from the end of the Cretaceous to early Tertiary periods and was responsible for the formation of the Rocky Mountains. Deformation was more gentle on the Colorado Plateau, resulting in the formation of monoclines and normal faults. During the Eocene the Colorado Plateau was at a low elevation surrounded by mountains. These mountains were eroded and sediments were deposited in intervening basins, resulting in burial of Laramide structures. As stated by Hunt (1956), approximately 5 million years ago the entire Rocky Mountains and Colorado Plateau were uplifted 4,000 feet to 6,000 feet (1,300 to 2,000 m) from the migration of magmas during the Oligocene resulting in volcanic activity and intrusion of laccoliths. On the Colorado Plateau, uplift was facilitated by reactivation of preexisting faults and accompanied by tilting of the plateau toward the north (Hunt, 1956).

Structure

Late Cretaceous sedimentation in east-central Utah was greatly influenced by two orogenic events. The Sevier orogeny (Armstrong, 1968) was characterized by east-

directed imbricate thrusting and folding within Proterozoic to Mesozoic miogeosynclinal sediments in Nevada and Utah, whereas the Laramide orogeny was characterized by basement uplifting in eastern Utah, Colorado and Wyoming. Sevier deformation is mostly Cretaceous in age, while Laramide deformation is latest Cretaceous through Eocene. A significant portion of the Cretaceous continental and shallow marine sediments were derived from the rising Sevier Mountains and deposited near the western edge of the Cretaceous Interior Seaway (Newman and Chan, 1991).

The Wasatch Plateau covers an area 50 mi (80 km) long and 16 mi (25 km) wide. It trends approximately north 20° east, and separates Sanpete Valley on the west from Castle Valley on the east (Tripp, 1991). Tripp (1991) utilizes a series of compressional and extensional events to explain the complex structural evolution of central Utah, including the Wasatch Plateau.

The San Rafael Swell (Laramide) is a broad, asymmetric northeast-trending upwarp about 70 mi (115 km) long, and some 30 mi (50 km) across (Figure 2). The northern half of the Swell, a salient physiographic feature in east-central Utah, appears as a broad wedge with a northeast-pointing apex. The wedge is flanked on the west by northeast-trending Castle Valley, and on the east by an unnamed northwest-trending valley traversed by U.S. Highway 6. Strata on the western flank of the Swell commonly dip 2° to 6° westward; by contrast those on the eastern flank of the Swell commonly dip steeply 45° to 85° eastward to form an imposing monocline. Locally, the strata along the east flank are vertical or overturned (Hawley et al., 1968). The Swell is mainly an area of barren rock that has been deeply

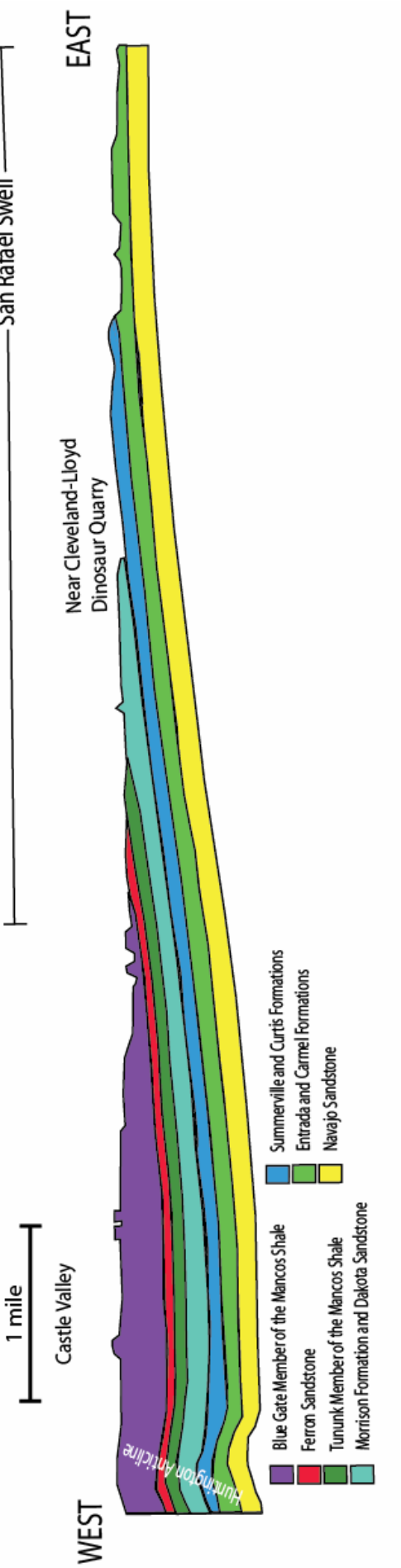

Figure 2: Cross section extending from near the base of the Wasatch Plateau (Huntington Anticline[West]) to the central portion of the San Rafael Swell (East) (modified from the Huntington 30x60 geologic map [Witkind, 1988]).

dissected by streams that cross and are incised transversely into the folded rocks. Erosion has removed the upper rocks in the center of the Swell; an inward-facing cliff delineates the Jurassic sandstone aquifers in the north and south ends of the Swell (Hood and Patterson, 1984).

Stratigraphy

Coalbed methane is produced from the Cretaceous Ferron Sandstone Member of the Mancos Shale. Salt water, from the production of CBM, is injected at depth into the Jurassic Navajo Sandstone, the Kayenta Formation and the Wingate Sandstone. The fresh-water wells in the area are completed in either Tertiary or Quaternary geologic deposits, thus this study is focused primarily on rocks from the Mesozoic and younger. A stratigraphic column containing these rocks is presented in Figure 3 and they are described in detail in this section.

Triassic Stratigraphy

The two Triassic formations are the early Triassic Moenkopi Formation and the late Triassic Chinle Formation. The Moenkopi Formation consists of four different members, from oldest to youngest: 1) the Black Dragon Member, with a thickness of 300 ft (92 m); 2) the Sinbad Limestone Member, at 60 ft (18 m) thick; 3) the Torrey Member, at 220 ft (67 m) thick; and 4) the Moody Canyon Member, at 200 ft (60 m) thick. The Moenkopi Formation is predominantly a mudstone that was deposited on a broad, flat coastal plain that sloped gently westward towards the miogeocline in southern Nevada. Thin tongues of marine limestone indicate times when the seas spread out of Nevada

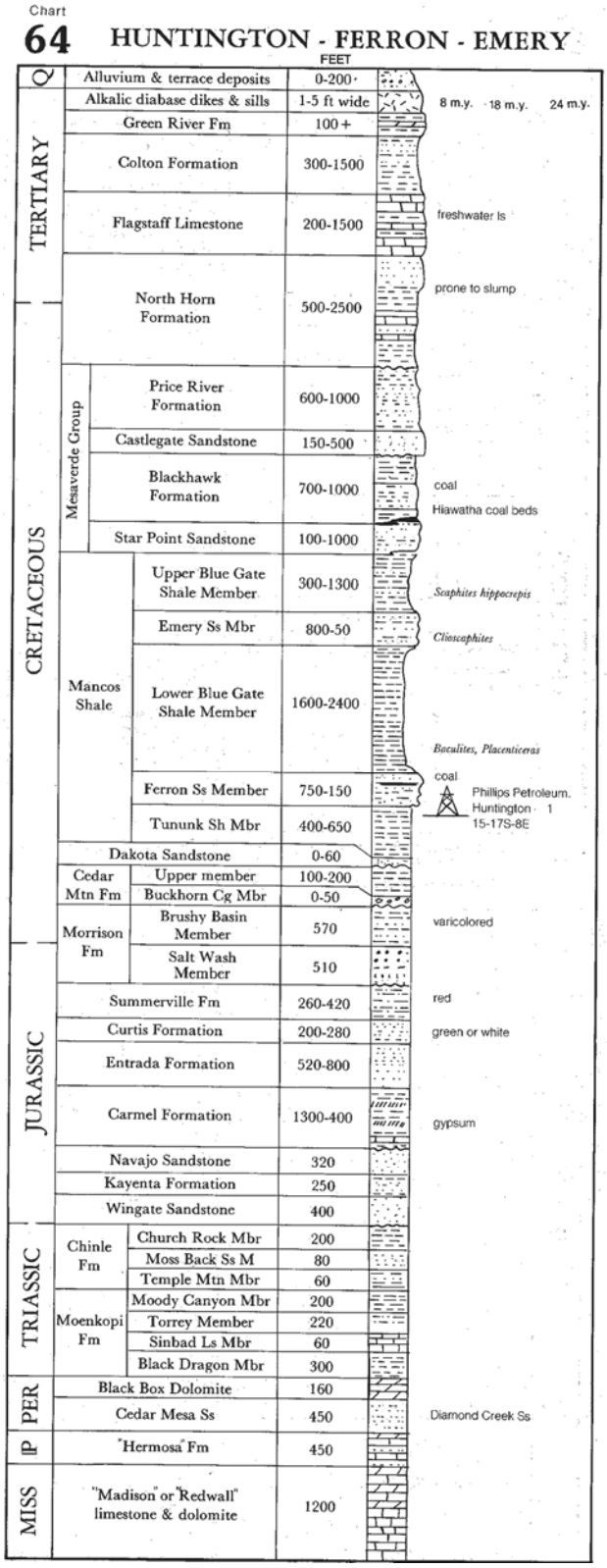

Figure 3: General stratigraphic column of rocks in Huntington, Ferron, and Emery (adapted from Hintze, 1988).

across the Moenkopi flats. Moenkopi environments, as interpreted from preserved sedimentary features, include stream channels, flood plains, fresh or brackish ponds, playas, and shallow seas. Beds of gypsum and casts of salt cubes preserved in red beds indicate evaporation (Hintze, 1988). It is typically a permeable unit.

The Chinle Formation consists of three different members, from oldest to youngest: 1) the Temple Mountain Member, with a thickness of 60 ft (18 m); 2) the Moss Back Sandstone Member, at 80 ft (24 m) thick; and 3) the Church Rock Member, at 200 ft (60 m) thick (Hintze, 1988). Deposition of the Chinle Formation occurred in an enclosed continental basin and represents a complex of alternating fluvial and lacustrine depositional systems (Hintze, 1988). Typical rocks of the Chinle are red to dark-brown, thin- to medium-bedded sandstone, conglomeratic sandstone, shaly siltstone, and minor interbedded mudstone (Witkind, 1988). It is typically a permeable unit.

Jurassic Stratigraphy

Within the Jurassic there are eight formations: 1) the early Jurassic Wingate Sandstone, which ranges in thickness from 350 to 450 ft (105 to 135 m); 2) the Kayenta Formation, from 100 to 250 ft (30 to 75 m) thick; 3) the Navajo Sandstone, from 400 to 1,000 ft (120 to 305 m) thick; 4) the Carmel Formation, from 280 to 350 ft (85 to 105 m) thick; 5) the Entrada Sandstone, from 200 to 300 ft (60 to 95 m) thick; 6) the Curtis Formation, from 75 to 250 ft (20 to 75 m) thick; 7) the Summerville Formation, from 120 to 250 ft (35 to 75 m) thick; and 8) the late Jurassic Salt Wash Member of the Morrison Formation, at about 180 ft (55 m) thick (Hintze, 1988).

The Wingate Sandstone is an eolian deposit and its rocks are typically reddish-brown to brown, thick-bedded to massive, crossbedded, fine-grained quartz sandstone that is well cemented by calcium carbonate and is strongly stained by manganese oxide (desert varnish) (Witkind, 1988). The Wingate Sandstone is a permeable aquifer. Salt-water disposal wells inject into this aquifer.

The Kayenta Formation is a fluvial deposit, and its rocks are typically lavender, reddish-brown, and pale-red, thin- to medium-bedded, irregularly bedded and crossbedded, fine- to coarse-grained sandstone well cemented by calcium carbonate with some shaly siltstone. Locally it contains a few conglomerate lenses rich in shaly siltstone clasts (Witkind, 1988). The Kayenta Formation is a permeable aquifer. Salt-water disposal wells inject into this aquifer.

The Navajo Sandstone is an eolian deposit, and its rocks are typically light-brown to light-gray, thick-bedded to massive, fine-grained quartz sandstone, crossbedded in large trough sets, clean and friable. The Navajo contains a few thin (about 5 ft [1.5 m] thick), lenticular, light-gray limestone beds in the upper part (Witkind, 1988). The Navajo Sandstone is a permeable aquifer, and it will be discussed in greater detail later in this chapter. Salt-water disposal wells inject into this aquifer.

The middle Jurassic Carmel Formation is a marine deposit that consists of two members. The lower unit has a thickness ranging between 30 to 50 ft (9 and 15 m). Typical rocks of the lower unit are light-gray to brownish-gray (pale-green locally), thin-bedded, dense limestone. In places it passes laterally into a very fine-grained calcareous sandstone marked by ripple marks and other evidence of shallow-water deposition. The upper unit has a thickness of about 250 ft (75 m) and contains

reddish-brown, thin-bedded shaly siltstone with few a thin sandstone beds in the upper part. The upper unit also contains many small (2 to 5 ft [0.5 to 1.5 m] thick) intercalated lenses and beds of gypsum that are contorted in places and locally coalesce to form beds about 25 ft (8 m) thick (Witkind, 1988).

The middle Jurassic Entrada Sandstone is a near-shore eolian deposit, and its rocks are typically orangish-brown to reddish-brown and locally light-brown sandstone, medium- to thick-bedded, dominantly fine-grained (locally medium- to coarse-grained), faintly crossbedded and friable, containing interlayered lenses of shaly siltstone and mudstone (Witkind, 1988). The Entrada Sandstone is typically a permeable unit.

The middle Jurassic Curtis Formation is a marine deposit, and its rocks are light-gray to light-brown and greenish-gray, thin- to medium-bedded, locally crossbedded, fine- to medium-grained quartz sandstone with minor beds of siltstone, conglomeratic sandstone and conglomerate. The Curtis Formation is firmly cemented by calcium carbonate and forms ledges that act as a resistant cap (Witkind, 1988). The Curtis Formation is a barrier to the movement of water except where faulted or fractured; thus, it acts as a confining layer.

The middle Jurassic Summerville Formation is a tidal-flat deposit, and its rocks are a reddish-brown shaly siltstone and sandstone characterized by thin, even, continuous bedding. The Summerville Formation contains many interlayered seams and thin beds of gypsum. The Summerville Formation is also a barrier to the movement of water except where faulted or fractured (Witkind, 1988).

The Salt Wash Sandstone Member of the Morrison Formation is a fluvial deposit, and its rocks are a light-gray, thin- to medium-bedded, crossbedded, fine- to

coarse-grained, friable quartz sandstone, with lenticular beds of conglomeratic sandstone and conglomerate (Witkind, 1988). It is a slightly permeable unit.

Cretaceous Stratigraphy

There are five (geologic) units within the Cretaceous: 1) the Brushy Basin Member of the Morrison Formation, with a total thickness ranging from 150 to 250 ft (45 to 75 m); 2) the Cedar Mountain Formation, which ranges between 160 to 230 ft (50 and 70 m) thick; 3) the Dakota Sandstone, from a pinch-out to 30 ft (0 to 9 m) thick; 4) the Mancos Shale, 2,300 to 6,100 ft (700 to 1,860 m) thick; and 5) the Mesaverde Group (Hintze, 1988).

The Brushy Basin Member of the Morrison Formation contains bentonitic claystone and mudstone, and ranges in color from yellow to purple but is dominantly bluish-gray and gray. There are a few thin limestone and sandstone beds; limestone beds are locally gray and nodular (Witkind, 1988). The Brushy Basin Member has a very low permeability and is usually a barrier to the movement of groundwater except where faulted or fractured.

The lower Cretaceous Cedar Mountain Formation consists of two units. The lower unit is a gray, massive to thick-bedded, fluvial crossbedded conglomerate and conglomeratic sandstone. Clasts consist of well-rounded white quartz and black, brown and light-gray chert. The upper unit is dominantly massive to thick-bedded mudstone, variegated in shades of purple, red, gray and green, with few discontinuous sandstone lenses (Witkind, 1988). The lower conglomeratic unit is slightly permeable to permeable, while the upper unit has a very low permeability except where faulted or fractured.

The Dakota Sandstone is a beach to marginal-marine/deltaic deposit that is tan to light-brown, thin-bedded, crossbedded, fine- to medium-grained quartz sandstone with thin discontinuous carbonaceous seams (Witkind, 1988). It is a slightly permeable sandstone.

The middle Cretaceous Mancos Shale contains five members: 1) the Tununk Shale Member, which ranges in thickness from 400 to 650 ft (120 to 200 m); 2) the Ferron Sandstone Member, from 150 to 750 ft (50 to 230 m) thick; 3) the lower Blue Gate Shale Member, from 1,600 to 2,400 ft (490 to 730 m) thick; 4) the Emery Sandstone Member, from 50 to 800 ft (15 to 245 m) thick; and 5) the upper Blue Gate Shale Member, from 300 and 1,300 ft (90 and 400 m) thick (Hintze, 1988).

The rocks of the Mancos Shale were deposited into the Mancos Sea along the western margin of the interior Cretaceous seaway in response to the abundant supply of sediments shed from the thrust-faulted and uplifted Sevier orogenic belt located to the west in southeastern Nevada, western Utah, and southern Idaho between 89 and 90 million years ago (Garrison et al., 1997).

The Tununk Shale Member of the Mancos Shale is one of several eastward-thinning clastic wedges that prograded into the Mancos Sea. The rocks of the Tununk Shale are a light- to dark-gray, thin- to medium-bedded, even-bedded shale and shaly siltstone. It locally contains discontinuous lenses of silicified shale and a few sandstone concretions (Witkind, 1988). It has a very low permeability and is usually a barrier to the movement of groundwater except where faulted or fractured.

The Ferron Sandstone Member of the Mancos Shale is also an eastward-thinning clastic wedge that prograded into the Mancos Sea. The Ferron Sandstone consists of an upper and lower sandstone unit separated by a middle shale unit. The

upper and lower sandstone units are light-brown, thin- and even-bedded, crossbedded, very fine- to fine-grained sandstone. The middle shale unit is light- to dark-gray, thin- to medium-bedded, even-bedded shale and shaly siltstone (Witkind, 1988). CBM produced in the study area is sourced from coal beds found in the Ferron Sandstone. It is a fairly permeable unit, especially where faulted or fractured.

The lower Blue Gate Shale Member is a light-gray, bluish-gray, and gray, thin- to medium-bedded shale and shaly siltstone. It contains sparse interlayered thin sandstone beds and resembles the upper Blue Gate and the Tununk Shale Members (Witkind, 1988). The lower Blue Gate Shale Member has a very low permeability, and is usually a barrier to the movement of groundwater.

The Emery Sandstone Member consists of upper and lower sandstone units separated by a middle shale unit. The upper and lower sandstone units are light-brown, yellowish-brown, and grayish-brown, thin- to medium-bedded, locally crossbeded, very fine- to fine-grained quartz sandstone. The middle shale unit is a light-gray to gray, thin- and even-bedded shale and shaly siltstone, and is sandy locally (Witkind, 1988). It is a permeable unit, especially where faulted or fractured.

The upper Blue Gate Shale Member of the Mancos Shale is a light-gray, bluish-gray, and dark-gray, thin- to medium-bedded shale and shaly siltstone with few interlayered brown sandstone beds (Witkind, 1988).

The Mesaverde Group contains four formations: 1) the Star Point Sandstone and 2) the Blackhawk Formation, which together range in thickness from 700 ft (215 m) to about 1,000 ft (305 m); 3) the Castlegate Sandstone, at about 130 ft (40 m) thick; and 4) the Price River Formation, which includes the Bluecastle Sandstone and

Mudstone Members, which together range in thickness between 400 ft (120 m) to about 880 ft (270 m) (Hintze, 1988).

The upper Cretaceous Blackhawk Formation and Star Point Sandstone consist of dominantly light-gray, light-brown, and brownish-gray, thin- to medium-bedded, crossbedded, fine- to medium-grained quartz sandstone interlayered with shaly siltstone, shale, carbonaceous shale and coal (Witkind, 1988).

The Castlegate Sandstone is a fluvial deposit that is a light- to dark-gray, locally yellowish-brown to dark-brown, thick-bedded to massive, fine- to coarse-grained quartz sandstone (Witkind, 1988).

Throughout much of the Wasatch Plateau, the Price River Formation is divisible into an upper part and the Bluecastle Sandstone and Mudstone Members, both of which are underlain by the Castlegate Sandstone. The upper part of the Price River Formation consists of a series of conglomerates, conglomeratic sandstones and sandstones. The Bluecastle Sandstone Member is a fluvial deposit that is a light-gray to yellowish-brown, medium- to thick-bedded, fine- to medium-grained quartz sandstone, and the Mudstone Member is a fluvial and floodplain deposit that is a gray to dark-gray, thin- to medium-bedded mudstone interlayered with siltstone and sandstone (Witkind, 1988).

Ferron Sandstone CBM play

The Ferron Sandstone play is located along the western margin of the San Rafael Swell, a prominent Laramide (late Cretaceous-Eocene) uplift in central Utah. The play fairway is estimated to be 6 to 10 mi (10 to 16 km) wide and 20 to 60 mi (32 to 96 km) long (Montgomery et al., 2001).

The Ferron Sandstone can be divided into two distinct clastic wedges (Ryer, 1981) (Figure 4). The lower portion of the Ferron Sandstone is a thin, northerly derived storm- and wave-dominated shoreline/deltaic complex, informally called the Vernal deltaic complex (Garrison et al., 1997). The upper portion of the Ferron Sandstone is a younger, thicker, and more north-northeasterly prograding deltaic complex, informally called the Last Chance deltaic complex. The Ferron deltaic complex is composed of sediments deposited during a series of transgressions and regressions of the Cretaceous shoreline (Garrison et al., 1997).

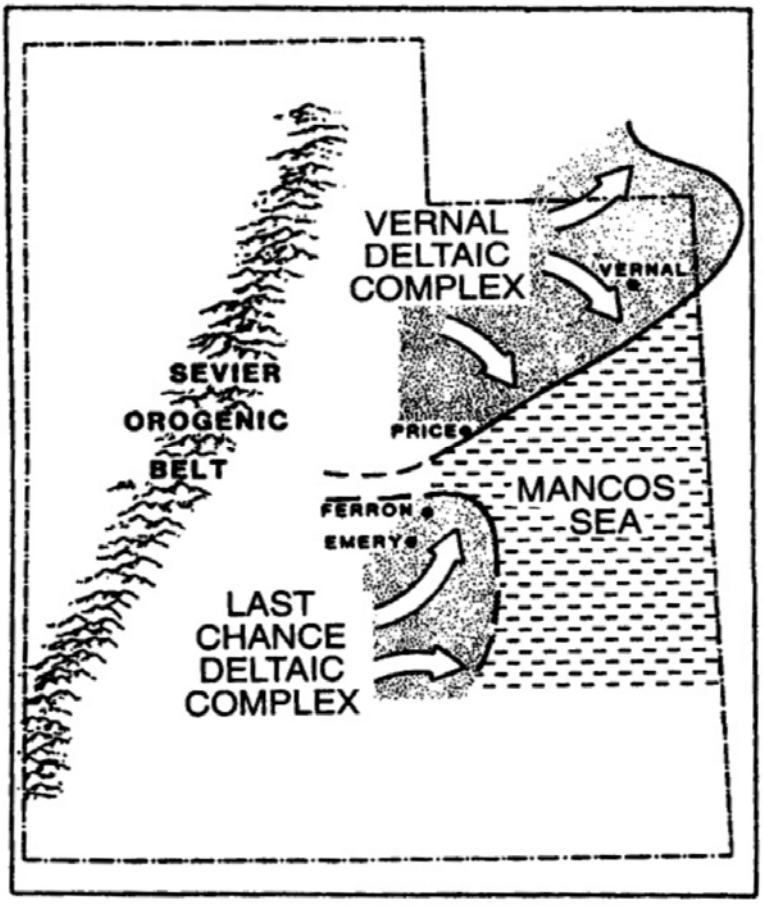

Figure 4: Interpreted regional extent of the two major delta systems, Vernal deltaic complex and Last Chance deltaic complex, within the Ferron Sandstone (modified from Ryer, 1981).

Major coal beds occur within the Ferron sandstone complex and generally mark the top of the deltaic events (Garrison et al., 1997).

Northern coals (coals of the Vernal deltaic complex) are unexposed, have very high gas contents, and appear to be over-pressured due to artesian conditions. Southern coals are exposed along an extensive outcrop belt, exhibit somewhat lower rank, and have significantly lower gas contents. Southern coals, however, are thicker, cover a much wider area, and are relatively unexplored. Thus, their ultimate potential is unknown but may be considerable, especially away from faults which may have partially stripped out the methane (Garrison et al., 1997).

Structural Geology of the Ferron Sandstone Play

Numerous folds and faults are present in the subsurface of the Ferron trend, but relatively few are exposed at the surface. Kneedy (2005) evaluated CBM production in two areas within the Drunkards Wash field (Figure 5). In Area B, vague northeast-trending, high-gas-production areas follow estimated fault trends. Several faults may also be present in Area A. If Area A does contain faults, fault-induced fractures and/or damage zones adjacent to the faults could create conduits that allow fluids to migrate from coal beds into adjacent sedimentary beds, and ultimately could even result in fluids escaping to the surface.

Drunkards Wash Gas Field

More than 600 wells are encompassed in the Drunkards Wash field (as of March 2007), and are producing methane from coal layers found in the Ferron Sandstone Member of the Mancos Shale. The CBM reservoirs in this field average 24 ft (7.2 m) in net thickness and occur at depths of 1,100 to 3,400 ft (330 to 1,030 m).

Production from Drunkards Wash began in 1999 and has been impressive (Montgomery et al., 2001). By November 1999, cumulative production for the unit exceeded 125.9 billion ft^3 (3.5 billion m^3) of gas (Montgomery et al., 2001).

In 2000, Chevron-Texaco and Phillips Petroleum acquired a major portion of the Drunkards Wash field and began drilling a large number of wells to exploit the methane.

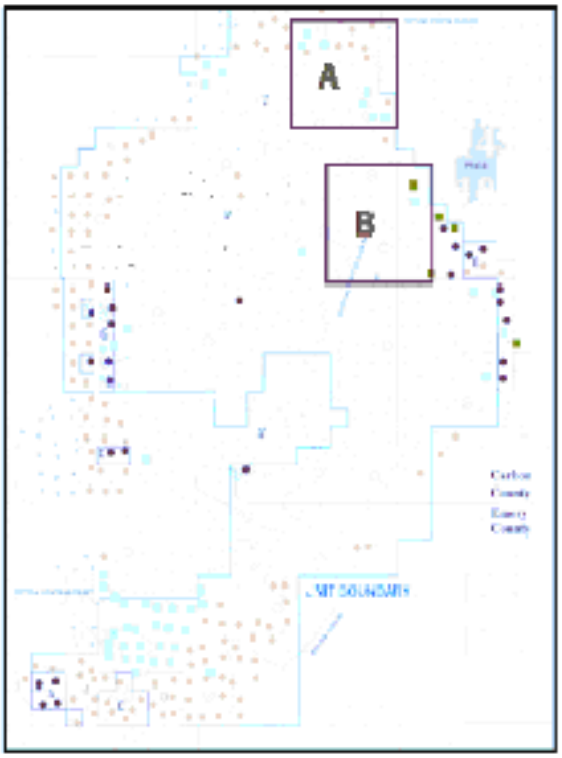

Figure 5: Drunkards Wash, central Utah. Area B contains northeast-trending high-gas production, which follow estimated fault trends (modified from Kneedy, 2005).

Anadarko and Marathon have junior interests in producing CBM. Average daily flow rates have increased steadily from less than 300 million ft^3 (mcf) (8.5 million m^3) to more than 620 mcf (17.5 million m^3), in part as a result of increased dewatering due to rapid growth in the number of producers. Currently, Drunkards

Wash is the largest gas field in Utah (Utah Division of Oil, Gas and Mining, 2007), and is the 42nd largest gas field in the U.S. (Energy Information Administration, 2002).

Hydrogeology

Hydrogeology of CBM

Because most CBM reservoirs are also deep aquifers and require dewatering for optimal gas production, analysis of hydrological conditions in a coalbed methane play is essential (Montgomery et al., 2001). In central Utah, mapping has helped establish flow gradients within the eastern, productive part of the CBM fairway (Tabet, 1998). Between Price and Castle Dale, groundwater flow is to the south and east, changing to the northeast in the southern area between Castle Dale and Emery (Montgomery et al., 2001). Recharge on a regional basis is from the Wasatch Plateau to the west; however, local patterns are almost certainly affected by structure and lithology (Figure 6). To the south, the prominent north-south Joe's Valley fault system likely supplies significant recharge to the area just north and south of Emery (Lines and Morrissey, 1983).

The composition of waters derived from Ferron coals provides another clue to differences within the overall fairway (Montgomery et al., 2001). As discussed by Rice (1999), produced water shows considerable differences amongst the Drunkards Wash, Helper and Buzzard Bench fields. The most recent data available indicate an average of 8,900 milligrams per liter (mg/L) total dissolved solids (TDS) for Drunkards Wash, increasing to 26,000 mg/L TDS only 6 mi (10 km) to the north in the Helper field. In Buzzard Bench to the south, water values average 11,000 mg/L

TDS, but range from higher than the values found at Drunkards Wash to less than 1,000 mg/L. Analyses of isotopic values of hydrogen and oxygen along with chloride concentrations also indicate that recharge waters are distinct from those at Drunkards Wash (Rice, 1999). The implication is that Ferron coalbed reservoirs are quite heterogeneous and possibly compartmentalized.

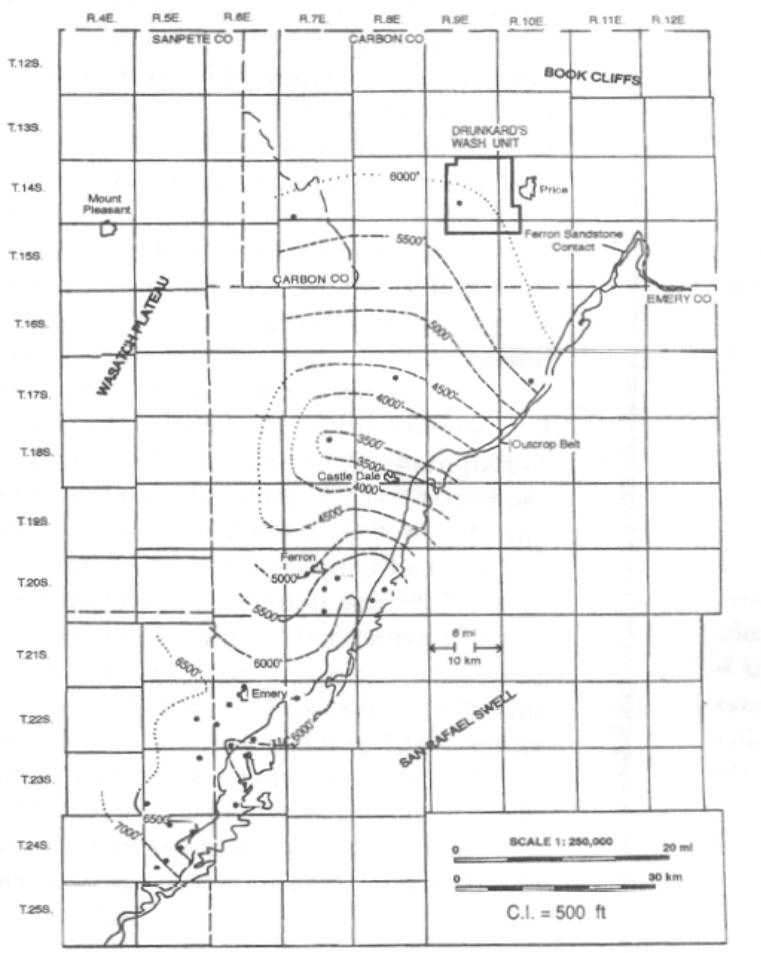

Figure 6: Potentiometric contour map within the vicinity of the Ferron CBM fairway, Emery and Carbon Counties, (modified from Tabet, 1998).

Previous Hydrogeologic Investigations

Hydrogeologic investigations were performed in the late 1970s by Waddell et al. (1978) and Sumsion (1979) in order to characterize the groundwater resources of the Wasatch Plateau/Book Cliffs area and the lowlands of Castle Valley. Both reports contain data relating to surface water quantity and quality, water discharged from mines, analyses of formation samples and, most important for this study, chemical analyses of water from selected water wells. Both investigations show that deep water wells (>400 ft [>130 m]) contain water of poor chemical quality, which typically worsens with depth. The shallow water-supply wells (<400 ft [<130 m]) contain water of suitable quality for human consumption (TDS <1,000 mg/L), with the exception of water from wells completed in the Blue Gate Member of the Mancos Shale, which are shallow wells and contain very poor quality water. A third investigation by Waddell et al. (1981) also reports data from fresh-water wells but is a reprint of Waddell et al. (1978).

The USGS, in cooperation with the U.S. Bureau of Land Management (BLM), conducted a reconnaissance from July 1975 to September 1977 which was designed to provide an assessment of the hydrology of the Wasatch Plateau-Book Cliffs coal-fields area in Utah. The U.S. Environmental Protection Agency (EPA) also supported the study by providing additional funds for enhancement of the water-quality effort (Waddell et al., 1981).

Water wells are the main source of subsurface information for the lowlands area of Castle Valley, and are reported in Waddell et al. (1978) in a series of tables separated according to the source/document which provided the data. Chemical

analyses for fresh-water wells drilled from 1946 to 1976 are shown in Table 1 (Waddell et al., 1978).

Utah Basic-Data Release No. 31 was prepared in cooperation with the BLM as a way to present a more detailed compilation of groundwater-related data that were collected and compiled during October 1976 to March 1978 (Sumsion, 1979). Only water-well data are presented in Table 2 (Sumsion, 1979).

In the lowlands area water wells are the source of most of the groundwater data gathered by Waddell et al. (1981) during the 1975-1977 hydrologic reconnaissance, including well yields, well logs, water-level measurements and chemical analyses. Most of the subsurface water in the lowlands contains more than 2,000 mg/L TDS, and the water is not suitable for public use. However, much of the water contains less than 35,000 mg/L TDS (Waddell et al., 1981).

The public supply for the city of Emery is obtained from a well developed in the lower part of the Ferron Sandstone. This well is pumped at rates of 150 to 250 gal/min (gpm) (0.6 to 1.0 m^3/min); the water contains about 790 mg/L TDS (Lines and Morrissey, 1983). The Kemmerer Coal Company drilled a well into the lower part of the Ferron about 1.5 mi (2.5 km) south of Emery. The water from this well is similar in chemical quality to the water from the Emery well in that it also contains less than 1,000 mg/L TDS (Lines and Morrissey, 1983).

Several test holes were drilled into the upper part of the Ferron Sandstone Member several miles southeast of Emery by Consolidated Coal Company. These test holes were not constructed to hydraulically separate the upper part of the Ferron from other possible overlying water-bearing zones. Water levels in the test holes are typically above the top of the Ferron and within several feet of the land surface. It is

Table 1: Select data from Waddell et al. (1978) (all values in mg/L unless otherwise specified).

Location	Year Constructed	Date sampled	Depth (ft)	Principal aquifer	Lithology of aquifer	Use of water	Temp (°C)	pH	Specific Conductance (umhos/cm)	Bicarbonate	Boron (ug/L)	Calcium	Chloride	Iron (ug/L)	Magnesium	Sodium	Potassium	Phosphorus	Sulfate	Silica	Strontium (ug/L)	Zinc (ug/L)	TDS
(D-12-7)3bcc-1	?	9/19/1975	100	Castlegate Ss.	ss	household				275	20	45	10	320		5.8	1.9	0.01	18	7.9		210	
(D-12-7)10bcd-1	1965	9/19/1975	137	Blackhawk Fm.	ss & shale	public, rec., household	9.5		650	313	30	91	27	20	21	9.1	1.5	0.01	45	7.9		110	**362**
(D-12-7)10dcb-1	1960	9/19/1975	102	Blackhawk Fm.	ss & shale	household				297	80	34	4.2	1300	22	19	4.6	0.01	6.8	7.1		30	**246**
(D-13-7)5cab-1	?	9/19/1975	?	Blackhawk Fm.	ss & shale	unused	8	7.1	510	337	30	64	6	620	24	8.4	2.7	0.01		7.9		40	**280**
(D-13-8)4bbb-1	1976	9/17/1976	160	Castlegate Ss.	ss. silty	unused	6	7.1	540	237	30	82	6.6	10	15	3.9	3.6	0	79	7.3	340	0	**315**
(D-13-9)25add-1	1971	9/24/1975	210	BlueGate(Mancos)	shale	unused	12.5	7.6	4000	102	610	240	35	49000	210	640	12	0.01	2800	3.3		40	**4040**
(D-13-9)25dcc-1	1956	9/18/1975	31	Alluvium	?	household	17.5		1270	248	210	84	17	80	71	52	7.6	0.01	400	15		90	**778**
(D-13-14)24dba-1	?	7/15/1966	?	?	?	unused		8.2	499	366		59	8		29	30	1		20				**327**
(D-15-13)2dad-2	1948	9/17/1975	76	Alluvium	sand, gravel	household	14	7.4		532	210	130	44	100	120	280	4.4	0.01	920	19		590	**1790**
(D-19-10)15bac-1	1946	10/21/1976	476	Carmel Fm.	sand, soft	stock/cattle	14	7.1	3700	105	1000	510	270	60	270	210	10	0	2200	13	11000	240	**3550**
(D-19-21)29dbc-1	1971	3/14/1972	4760	Entrada Ss.	sandstone	industrial use		7.1	9540	182	4100	300	1800	1600	27	1900	50		2600	31			**6810**
(D-22-6)4cab-1	1966	9/10/1975	1614	Ferron Ss.	sandstone	public supply	26.5	7.6	1080	270	200	36	20		20	200	4.2	0	330	15		30	**759**
(D-22-6)17abc-1	1973	9/10/1975	1543	Ferron Ss.	sandstone	unused		8.7	990	276	190	16	19		17	190	4	0	250	10		20	**652**
(D-22-6)31dab-1	1972	10/7/1976	406	Ferron Ss.	ss. silty	stock/cattle	13	7.9	1800	299	280	33	45	120	18	360	3.7	0	600	14	2300	10	**1230**

Table 2: Select data from Sumsion (1979) (all values in mg/L unless otherwise specified).

Location	Date Sampled	Interval Sampled (ft)	Geologic Unit	Temp (°C)	pH	Specific Conductance (umhos/cm)	Bicarbonate	Boron (ug/L)	Calcium	Chloride	Iron (ug/L)	Magnesium	Sodium	Potassium	Na + K	Sulfate	Silica	Strontium (ug/L)	Zinc (ug/L)	TDS
(D-13-8)17cdd-1	7/18/1955		alluvium		7.7	1100	393		102	18	1080	62			38	272	44			736
(D-13-9)8ccc-1	3/19/1941		Blackhawk Fm.		7.5	2260	425		147	50	0	139			64	559	12.4			1492
(D-18-14)9dcd-1	8/8/1958		alluvium		7.1	4620	408		563	185		235			449	2640	16			4290
(D-19-10)15bac-1	10/21/1976	445-465	Carmel Fm.	14	7.1	3700	105	1000	510	270	60	270	210	10		2200	13	11,000	240	3550
(D-20-14)31cbd-1	4/26/1978	150	Carmel Fm.	15	7.3	800														530
(D-20-16)17dab-1	8/8/1958		alluvium		7.7	1870	670		147	72		60			234	450	18			1310
(D-21-16)9aac-1	9/21/1960	8 to 12	alluvium		7.2	3840	561		377	95		150			472	1910	14			3290
(D-22-6)31dab-1	10/7/1976	360-402	Ferron Ss.	13	7.9	1800	299	280	33	45	120	18	360	3.7		600	14	2300	10	1230
	6/23/1977			13	7.9	1900														1300
	7/13/1977			13.5	7.8	1700														1160
	9/21/1977			13	7.8	1750														1200
	6/2/1978			13.5	7.9	1820														1240
(D-22-10)23cbc-1	12/27/1971	83	Wingate Ss.		7.7	645	295	680	68	8	0	31	11	18		73	7		0	360
(D-22-19)10cbb-1	2/9/1936	27-34	Mancos Shale			10600			139	158		218	108			3505				6964
(D-23-6)32bdd-1	9/29/1976	253-293	Ferron Ss.	17	8.4	1250	413	210	5.4	13	70	4.4	290	1.3		300	8.3	310	10	834
(D-23-9)2ccb-1	8/12/1971	576-690	Cutler Fm.		7.2	1650	700	150	216	14	250	112	10	8		412	9			1214
(D-23-10)12ddd-1	10/31/1958	199-214	Moenkopi Fm.	11	8.2	3650	465		238	81		400			204	2100	4.6			3260
(D-23-19)18ddd-1	3/20/1936	410-920	Dakota Ss., Burro Canyon Fm., & Morrison Fm.			2800			35	235		19	152			470				1850

not known whether the water levels in these test holes are representative of the potentiometric surface in the upper part of the Ferron or the water table in the overlying Blue Gate Member of the Mancos Shale (Lines and Morrissey, 1983).

The Ferrron Sandstone Member may lose water by seepage to streams and mines, but the quantities involved are unknown. Approximately 200 to 300 gpm (0.75 to 1.15 m^3/min) is discharged from the Emery (Browning) Mine, which is about 4 mi (6.5 km) south of Emery. Coal is mined from the upper part of the Ferron Sandstone, but some of the mine water is believed to be coming from the Blue Gate Member, which overlies the Ferron Sandstone. The TDS content of water from the Browning Mine was 5,100 mg/L on September 16, 1976 (Lines and Morrissey, 1983).

Samples from three wells believed to be representative of water in the Ferron Sandstone Member had TDS contents ranging from 652 to 1,230 mg/L; the principal constituents were sodium, sulfate, and bicarbonate. The water in the Ferron Sandstone, although of marginal chemical quality for public consumption, is probably the best obtainable from aquifers within depths of 2,000 ft (600 m) or less along the margins of the uplands (Sumsion, 1979).

Navajo Sandstone aquifer. Hood and Patterson (1984) studied the hydrogeology of the Navajo Sandstone. Of the three thick sandstone aquifers (Navajo, Entrada, and Wingate), more hydrogeologic data have been collected for the Navajo because it is the shallowest, the most permeable and, near the San Rafael Swell, it contains the freshest water (Hood and Patterson, 1984).

The permeability of the Navajo Sandstone in the northern San Rafael Swell area ranges from very low to moderate, but locally it may be high (Hood and Patterson, 1984). Measured hydraulic conductivity values for outcrop and core

samples range from 0.0037 to 5.1 ft/day (0.00112 to 1.55 m/day). Transmissivities derived from low discharge, short-term aquifer tests at the only wells in the San Rafael Swell area available for testing ranged from 27 to 642 ft^2/day (2.5 to 60 m^2/day) (Hood and Patterson, 1984).

The hydrostatic surface of the Navajo Sandstone was found for all three gas fields by converting the down-hole pressure from pounds per square inch (psi) to feet of water, by using a conversion factor of 1 psi equals 2.306 feet of water. The static bottom-hole pressure was measured at each SWD well during a step-rate test conducted to determine the necessary surface injection pressures by the respective energy companies. Nine SWD wells (43-007-30290, 43-007-30314, 43-007-30361, 43-007-30555, 43-007-30567, 43-015-30272, 43-015-30323, 43-015-30338, 43-015-30490) were calculated and are presented in Table 3.

The hydrostatic surface in the Navajo was found to be below the land surface for all nine wells, ranging from 401 to 1,543 feet (122 to 470 meters) below the ground elevation where each respective well was drilled. The bottom-hole pressure was found to range from 2,200 to 2,912 pounds per square inch (psi) (15,169 to 20,078 kPa).

Salt-water disposal well aquifer chemistry. Water quality data for the disposal wells (Navajo Sandstone, Kayenta Formation and the Wingate Sandstone) are available from the Utah Division of Oil, Gas and Mining (UDOGM, 2007) website (http://ogm.utah.gov). Only wells which were sampled as part of this study are presented in Table 3 for comparison between injected waters and native disposal-reservoir waters. Several of the wells were sampled using packers to target sampling from a specific formation and present values for the Navajo Sandstone, the Kayenta Formation or the Wingate Sandstone, or a composite of all three aquifers combined.

Table 3: Data from the disposal reservoirs (all values in mg/L unless otherwise specified).

API Well #	Well Name	Formation	Bicarbonate	Carbonate	Calcium	Chloride	Iron	Magnesium	Sodium	Sulfate	TDS	Static down hole pressure (psi)	Water Level above well bottom (ft)	Well Depth (ft)	Hydrostatic surface (fft below ground)	Well Elevation (ft above sea level)	Water Elevation (ft above sea level)
43-007-30290	D-3	composite	705	0	1,390	116,163	11	465	78,500	3,390	217,264	2351	5421	6510	1089	5691	4602
43-007-30314	D-4	Navajo	2,610	0	898	69,652		384	47,850	3,200	138,260	2490	5742	6474	732	5733	5001
43-007-30361	H-1	na	na	na	na	na	na	na	na	na	na	2287	5274	6489	1215	5965	4750
43-007-30555	F-2	Navajo	4,313	0	448	32,757	28	97	23,037	1,791	62,446	2485	5730	6155	425	5678	5253
43-007-30567	D-14	Navajo	1,010	<2	890	67,500	40	210	40,000	5,180	121,000	2200	5073	5474	401	5564	5163
		Wingate	4,180	<3	1,400	105,000	230	320	6,200	3,180	186,000						
43-015-30272	SWD-1	?	1,012	0	448	24,800	15	126	17,194	3,095	46,690	2690	6203	7746	1543	5988	4445
43-015-30323	SWD-2	na	na	na	na	na	na	na	na	na	na	2618	6037	7295	1258	6041	4783
43-015-30338	UT D7	na	na	na	na	na	na	na	na	na	na	2500	5765	6485	720	5827	5107
43-015-30490	SWD-4	?	3,172	0	1,224	35,000	14	83	23,550	2,646	68,026	2912	6715	7895	1180	5895	4715

Native waters in the disposal reservoir have low water quality and are exceptionally high in sodium and chloride. Values for sodium range from 6,200 to 78,500 mg/L, while the range for chloride is from 24,800 to 116,163 mg/L. The TDS values range from 46,690 to 217,264 mg/L. The TDS values increase as a function of depth, demonstrating that the Kayenta and Wingate contain higher concentrations of dissolved solids. The highest TDS value is from a composite sample, which also shows the highest values for sodium, chloride, and magnesium.

CO_2 Sequestration

Carbon dioxide (CO_2) sequestration consists of injecting CO_2 into geologic formations such as oil and gas reservoirs, unmineable coal seams, and deep saline aquifers. These are structures that have stored crude oil, natural gas, brine and CO_2 over millions of years. Research in CO_2 sequestration has been spurred by growing concern over the increasing amount of anthropogenic greenhouse gas emissions, specifically CO_2, and its influence on global climate change.

One of the options proposed is to collect CO_2 from point sources, such as fossil-fuel-fired electrical power plants, and inject it into deep aquifers. The aquifers most suitable for disposal of CO_2 are deep, saline aquifers (Bergman and Winter, 1995). Approximately 65% of CO_2 power-plant emissions come from plants situated directly above potential disposal aquifers (Bergman and Winter, 1995). It is possible that CO_2 could be injected directly into these deep, saline aquifers without the need for long pipelines (Bergman and Winter, 1995).

Sequestration of CO_2 into deep, confined aquifers may turn out to be a good long-term solution to storing it, rather than releasing it into the atmosphere. As explained by Holloway and van der Straaten (1995), the CO_2 could be injected into

the host formation, ideally an immature sandstone, in an area where it would move very slowly along a long flow path at approximately the speed of the natural groundwater flow. As it moves through the reservoir it would come into contact with uncarbonated formation water and reactive minerals. A proportion of it would dissolve in the water and a further proportion would be fixed by reactions with minerals in the host rock. If the flow path is long enough, the CO_2 might all dissolve or become fixed before it reached the basin margin. Furthermore, the rates of transport within the host formation might be so slow as to effectively trap the CO_2 for thousands, if not millions, of years.

The main issues with geologic sequestration are uncertainties in the volumes available for sequestration, the costs associated with CO_2 transport to the sequestration site, the sequestration operation itself, and especially the long-term integrity of the sequestration storage location (Herzog, 1997). The storage integrity of a reservoir depends on site-specific issues such as the lithology of the host rock, host-rock properties, presence of faults, effectiveness of cap-rock seals, fluid pressures in the reservoir, pore-water chemistries, and the ability of the target storage formation to sequester CO_2 through mineral trapping (Holloway and van der Straaten, 1995; Allis et al., 2001; Gale, 2002). Many of these issues will require a combination of experimental and theoretical research. However, volumetrically, deep aquifer sequestration may be a very viable approach to reducing emissions, especially for point sources of CO_2 gas such as fossil-fuel-fired power plants (Herzog, 1997).

Deep-aquifer sequestration is currently being demonstrated. In September 1996, Statoil of Norway began storing CO_2 from the Sleipner West gas field into a sandstone aquifer 3,280 ft (1,000 m) beneath the North Sea. The CO_2 is injected from

a floating rig through five pipes at a rate of 44 million lbs/week (20 million kg/week), corresponding to the rate of CO_2 produced from a 140-megawatt (MW), coal-fired power plant (Herzog, 1997). Another notable example of CO_2 sequestration into a deep aquifer is the plan by Exxon and Pertamina to inject about 140 trillion ft^3 (4 trillion m^3) of CO_2 into a deep aquifer 3,280 ft (1,000 m) below the South China Sea floor from their natural gas field at Natuna (Herzog, 1997).

Two-dimensional numerical modeling of a non-dome-shaped geological structure on the San Rafael Swell of the Colorado Plateau has been done to determine the amount of CO_2 that returns to the surface versus the amount sequestered. Ignoring water-rock reactions CO2 returns to the surface after about 250 years and about 40% remains sequestered after 1,000 years. However, coupling water-rock reactions shows significantly more CO2 is sequestered. All scenarios show some leakage to the surface but an estimated 70% remains permanently sequestered (White et al., 2003).

CHAPTER III

METHODS

Well Selection and Sampling

Shallow Water Supply Wells

Records from the Utah Division of Water Rights (2005) were searched and all water wells which might possibly be sampled were identified. Based on permit applications filed with the Utah Division of Water Rights, 24 shallow water-supply wells were initially identified as candidates for potential sampling (Table 4). Data associated with these water wells include water rights identification number, owner, location, date of water rights, right (quantity), depth of the well, and a few wells have drillers logs included.

Of the 24 wells identified only four were sampled (see Table 4 and Figure 7). As for the 20 wells which were not sampled, five could not be sampled, seven were permitted but never drilled, four were drilled but were not completed, and four were drilled and later destroyed (Table 4).

Field measurements of temperature, pH, electrical conductivity (EC) and alkalinity were made for all wells sampled at the time of the site visit. A YSI model 33 salinity, conductivity and temperature meter was used to measure those parameters, and pH was measured using an Orion model 230A pH meter. Alkalinity was measured in the field using a Hach Test Kit, Model AL-AP with an accuracy of 20 mg/L of $CaCO_3$. The titration was done using

Table 4: Sampling status for all shallow water-supply wells

Study ID no.	Water Rights ID No.	Owner	Location	Date filed	Right	Log?	Depth (ft)	Well Sampling Status
1	93-3720 (A19548)	Cottonwood Creek Consol. Irr. Co.; G.J. Curtis	NE 1/4, NE1/4,Sec15, T18S, R7E	12/1/95 (1877 Priority)	5.28 af	No	NA	**Sampled**
2	93-823 (A52547)	Emery Co. WCD	NW1/4,NW1/4,Sec15, T18S,R9E	1/9/1979	.45 cfs	No	NA	Not sampled
3	93-1566 (A54454)	P. Bishop	NW1/4,SW1/4,Sec25, T17S,R8E	4/4/1980	.015 cfs	No	NA	Never drilled
4	91-4194 (A52821)	J.O. & P.F. Hawkins	NE1/4,NW1/4,Sec1,T17S,R9E	3/23/1978	.015 cfs	No	NA	**Sampled**
5	91-4219 (A54310)	G.K. Horrocks	NE1/4,NW1/4,Sec1,T17S,R9E	2/26/1980	.015 cfs	Yes	131	Not sampled
6	91-4220 (A54311)	G.K. Horrocks	NE1/4,NW1/4,Sec1,T17S,R9E	2/26/1980	.015 cfs	Yes	142	Not sampled
7	91-4221 (A54312)	G.K. Horrocks	NW1/4,NE1/4,Sec1,T17S,R9E	2/26/1980	.015 cfs	Yes	110	Destroyed
8	91-5041 (A73119)	D. & J. Guymon	SE1/4,SE1/4,Sec12,T17S,R9E	9/13/2000	4.73 af	No	NA	Never drilled
9	93-767 (A50571)	L. McMullin	NW1/4,SW1/4,Sec12,T17S,R9E	11/28/1977	.015 cfs	No	NA	Destroyed
10	91-4204,5,6 (A53663,77,78)	A.S. Larson	SW1/4,NW1/4,Sec14,T17S,R9E	8/21/1979	.015 cfs	No	NA	Not completed
11	91-4207,8 (A53679,80)	A.S. Larson	NW1/4,NW1/4,Sec14,T17S,R9E	8/21/1979	.015 cfs	No	NA	Not completed
12	91-4259 (A56033)	C.W. Corbin	SE1/4,NE1/4,Sec16,T17S,R9E	3/26/1981	.015 cfs	No	NA	Never drilled
13	91-4180 (A52429)	A. & D. Christensen	SW1/4,NE1/4,Sec23,T17S,R9E	12/8/1978	.015 cfs	Yes	180	Destroyed
14	91-4193 (A52826)	J.B. Jarvis	SW1/4,SW1/4,Sec36,T16S,R9E	3/20/1979	.015 cfs	Yes	120	Not sampled
15	91-4214 (A53898)	F. Jones	NW1/4,NE1/4,Sec19,T16S,R10E	9/15/1979	.015 cfs	No	NA	Never drilled
16	91-4198 (A53119)	R.J. Alger	NW1/4,SE1/4,Sec20,T16S,R10E	5/16/1978	.015 cfs	No	NA	Destroyed
17	91-4127 (A44153)	Emery Co. WCD	NW1/4,SE1/4,Sec28,T16S,R10E	8/20/1974	1.0 cfs	No	NA	Never drilled
18	91-4197 (A53118)	R.L. Lundy	NW1/4,SW1/4,Sec30,T16S,R10E	5/15/1979	.015 cfs	Yes	194	Not completed
19	91-4199 (A53184)	A. & G.L. Hansen	SW1/4,SE1/4,Sec30,T16S,R10E	5/29/1979	.015 cfs	No	NA	Not completed
20	91-4264 (A56345)	G.W. Irvine	NW1/4,NW1/4,Sec31,T16S,R10E	5/6/1981	.015 cfs	Yes	225	**Sampled**
21	91-4181 (A51960)	M.A. Coonrood II	SW1/4,SW1/4,Sec33,T16S,R10E	8/21/1978	.015 cfs	No	NA	Never drilled
22	91-4164 (A49858)	Beaver Creek Coal Co.	NE1/4,NW1/4,Sec2,T15S,R10E	7/22/1977	.25 cfs	Yes	21	Not sampled
23	91-5081 (A75213)	R. Erwin; C. Hunt	NE1/4,Se1/4,Sec3,T15S,R10E	12/23/2003	.95 af	No	NA	Never drilled
24	91-4210,13 (A53772,841)	C. Grames	SW1/4,SW1/4,Sec22,T14S,R10E	9/17/1979	0.015 cfs	Yes	192	**Sampled**

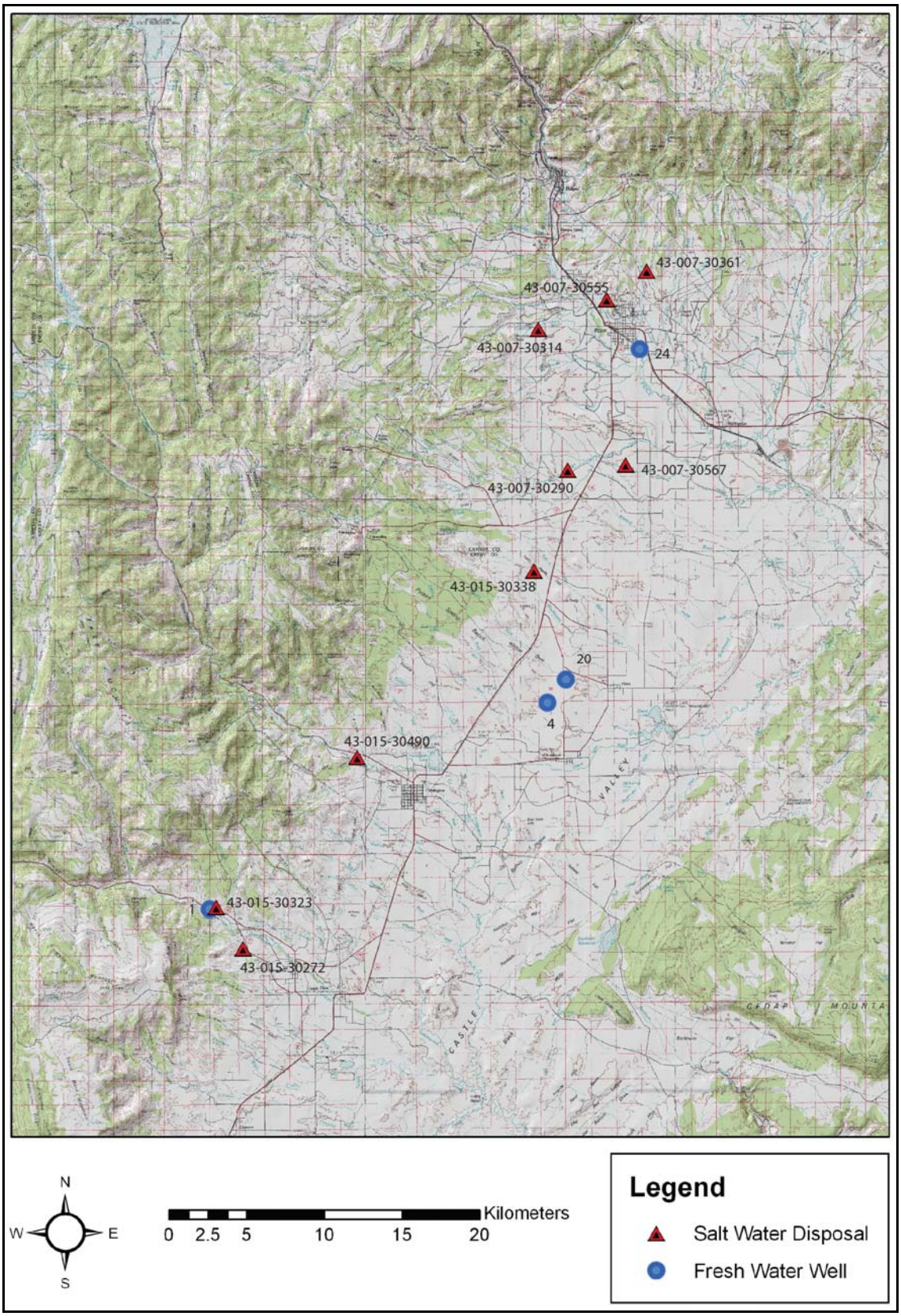

Figure 7: Locations of the four shallow water-supply wells and nine SWD wells sampled.

Bromcresol Green-Red indicator powder and sulfuric acid added to the water that had been filtered through a 0.45-micron (μm) filter.

Three samples were collected from each of the four wells to be analyzed for: 1) major and minor ions and trace metals, including boron, barium, calcium, chloride, copper, iron, potassium, magnesium, manganese, sodium, nickel, phosphorus, sulfate, silica, strontium, and zinc; 2) the stable isotope ratios of deuterium (^{2}H) to hydrogen (D/H) and oxygen-18 to oxygen-16 ($^{18}O/^{16}O$); and 3) the stable isotope ratio of carbon-13 to carbon-12 ($^{13}C/^{12}C$). Once the sample bottles were filled leaving no head space they were cooled to 5°C, and sent to their three respective laboratories: 1) the Utah State University analytical laboratory for the major and minor ions and trace metals; 2) the Stable Isotope Ratio Facility for Environmental Research at the University of Utah for the hydrogen and oxygen isotopes; and 3) Geochron Laboratories, a division of Krueger Enterprises, Inc., in Cambridge, Massachusetts, for the carbon isotopes.

Well Site Investigations

Well site investigations were conducted from July 19, 2005 to October 13, 2005. Well locations were identified and marked on 30- x 60-minute (1:100,000 scale) metric topographic maps of Price, Huntington, and Manti, Utah, based on township and range coordinates obtained from the Utah Division of Water Rights (2005). Wells are identified using the study identification number in the first column of Table 4. In general, wells are discussed in the order in which they were encountered in the field and not in numerical order according to the study ID number. The first well visited in the field is in Price, where field work began, as it was the northernmost well identified for

this study. Once a well was located and sampled or it was determined that no sample could be taken, the next well south was located and visited.

Well 24 is owned by Clyde Grames and is located in a pump house/storage shed next to his home. The well has a 4-in (10-cm) diameter casing inside a 6-in (15-cm) diameter surface casing. The water level could not be measured due to a 4-in (10-cm) cap bolted onto the casing; however, the owner mentioned that the water level has remained constant at about 22 ft (6.7 m) since the well was drilled.

Well 22 is found between the Price River and a set of railroad tracks. The drillers log indicates that the well is only 21 ft (6.4 m) deep. It was determined in the field that sampling this well would be useless as the water is likely river water and would not be representative of the ground water.

Wells 3, 8, 12, 15, 17, 21 and 23 appear to have never been drilled.

Well 16 has been destroyed. As of July 2005 the homeowner had only lived at that residence for two months and commented that before she moved in there had been a well located behind the home that the previous owner did not use and covered over before selling the home.

Well 20 is owned by Gregory W. Irvine and is located behind his residence. Mr. Irvine was very accommodating and allowed his well to be sampled after purging the well for several minutes so that a representative sample could be obtained from the aquifer and not water that had been sitting in the well casing for an unknown amount of time.

Well 18 was located with the assistance and knowledge of long-time local resident Arvel Hansen, who indicated that a well was drilled but not completed because water was never encountered. Arvel Hansen also indicated that Well 19 was drilled, but

no casing was installed. The spot where the well was drilled seeped water for some time after drilling was attempted, but is now dry.

Wells 10 and 11 were drilled, but not completed because no water was found.

Well 9 was drilled and was not used for years. A local rancher who farms in the field where the well was located indicated that it had not been used for quite a long time and was eventually plowed over.

Well 5 was found but was blocked by debris at 21 feet (6.4 m). Well 6 was dry to a depth of 49 feet (14.9 m).

Well 4 was found and is currently not being used for any purpose. This well has a removable rubber cap flush with the ground surface and has no pump in it. The outer casing is 6-in (15-cm) diameter PVC, while the inner casing is 4-in (10-cm) diameter PVC. The static water level was 22.5 ft (6.86 m) below the land surface (July 29, 2005), and the total depth at present is about 101 to 102 ft (30.8 to 31.1 m), as soft sediment has accumulated on the bottom. As there is no pump in this well it was necessary to rent a portable, submersible pump in order to collect a water sample. When the well was sampled on October 13, 2005, the static water level was 21.44 ft (6.535 m) below the land surface. The well was purged of over 100 gallons (380 L) of water before a sample was taken, which is equal to approximately 3.5 wellbore volumes.

Well 1 is owned by Gary Curtis and is located in Straight Canyon east of Orangeville. The well is located in a pump house/storage shed next to the owner's home. The water level could not be measured due to the well being capped; however, the owner commented that he believes the water level fluctuates between 8 and 10 ft (2.4 and 3.0 m) below the land surface.

Well 7 was never found. It is assumed that it has been destroyed or plowed over, as the coordinates place it in an alfalfa field.

Well 13 is owned by Doris Christensen and was located behind her home. At the time of the July well-site visit the well was available for sampling, but no pump was in the well. When the well was revisited in October with a portable submersible pump, the well had since been destroyed; thus, it was no longer available for sampling.

Well 14 is owned by Bonida Jarvis and is located inside a pump house next to her home. Upon investigating the condition of the well, the pump was not functioning and inhibited any sort of sampling equipment from being used to sample the well; thus, it could not be sampled.

Well 2 belongs to the Emery County Water Conservancy district and is unsamplable as no permission could be obtained to sample the well.

Salt-Water Disposal Wells

There are 20 salt-water disposal (SWD) wells in the Drunkards Wash, Helper, and Buzzard Bench CBM gas fields. Eleven of these SWD wells were identified as candidates for chemical sampling based on their proximity to the shallow water-supply wells. It was determined that the other nine SWD wells were located so far to the northwest of the shallow water-supply wells that it is unlikely that the salt water being injected into these nine wells would travel to the shallow water-supply wells faster than the water injected into the eleven SWD wells which were chosen for chemical sampling.

Samples were taken from nine of the 11 SWD wells originally identified as candidates for sampling (Table 5). The other two SWD wells are no longer operating. A representative from each of the companies, Anadarko Petroleum, ConocoPhillips and

Table 5: Relevant information for SWD wells, including sampling information.

API Well Number	Well Name	Owner	Total Depth	Injection Interval	Injection Formations	Date Sampled	pH	Temp °C	EC (uS)	Alkalinity (mg/L)
43-007-30290	Utah D-3	Phillips	6510	5561-6058	Navajo, Wingate	8/3/2005	7.9	21.7	3450	na
43-007-30314	Utah D-4	Phillips	6580	6095-6474	Navajo, Wingate	8/3/2005	7.57	23.4	3020	na
43-007-30361	Helper State SWD #1	Anadarko	6489	5920-6320	Navajo, Wingate	8/2/2005	7.48	28.7	4400	na
43-007-30555	Federal F-2 SWD	Anadarko	6200	5649-6155	Navajo, Kayenta, Wingate	8/2/2005	7.08	25	4310	4200
43-007-30567	Sampinos D-14	Phillips	5474	4558-5281	Navajo, Kayenta, Wingate	8/3/2005	7.53	21.7	4200	na
43-015-30272	SWD -1	XTO	7760	6582-7586	Navajo, Shinarump	10/13/2005	7.76	20	2960	na
43-015-30323	SWD -2	XTO	7590	7078-7296	Navajo	10/13/2005	7.64	16	3465	na
43-015-30338	Utah D-7	Phillips	6573	5665-6485	Navajo, Kayenta, Wingate	8/3/2005	7.68	20.8	7340	na
43-015-30490	SWD -4	XTO	8001	6548-7190	Navajo, Wingate	10/13/2005	7.67	15.4	3500	na

XTO Energy, provided access to the facilities, aided in collecting the samples and insured that all safety regulations were followed.

Field measurements of temperature, pH, and electrical conductivity (EC) were made for all nine SWD wells sampled at the time of the site visit. Alkalinity was measured for one of the SWD wells (43-007-30555), but not for the other eight SWD wells due to the large amount of acid required to complete the in-field titration. All samples taken at the nine SWD wells were analyzed for the same chemical constituents as the shallow water-supply wells; major and minor ions and trace metals, D/H, $^{18}O/^{16}O$ and $^{13}C/^{12}C$.

Hydrochemistry

Water samples have been collected and analyzed to compare SWD well samples with shallow water-supply well samples. Using the concentrations of major and minor ions and trace metals, D/H, $^{18}O/^{16}O$ and $^{13}C/^{12}C$ it should be possible to determine if mixing is occurring between disposal aquifers and fresh-water aquifer(s). Different ratios of D/H, $^{18}O/^{16}O$ or $^{13}C/^{12}C$, or elevated levels of sodium or chloride, may also indicate that a particular water sample contains some water that was injected into one or more disposal wells.

Major and Minor Ions and Trace Metals

The brine injected into the SWD wells has high TDS concentrations, while water from the shallow, water-supply wells have much lower TDS concentrations. Major ion concentrations will be plotted on a trilinear diagram (Piper, 1944). It will also be useful to compare TDS concentrations in the shallow aquifer(s) from this study with published chemical results from shallow water-supply wells and springs throughout Castle Valley

from Waddell et al. (1978) and Sumsion (1979) (see Tables 1 and 2) as a way of comparing water samples from before injection began to the present, as salt-water injection is taking place. If the samples collected from the shallow water-supply wells for this study reveal significantly higher concentrations of major or minor ions or trace metals on either a local or regional scale, then mixing may be inferred, as the salt water being injected at depth may have migrated to the shallow, fresh-water aquifer(s).

Stable Isotopes

Stable isotopes help determine the source of the groundwater and will aid in determining if any mixing is occurring between aquifers. Isotopic data can be used in this way due to the phenomenon of isotopic fractionation. Isotopic fractionation refers to the change in the relative abundance of isotopes of a particular element. It takes place as a result of differences in the properties of isotopes of differing masses.

Isotopic data for an element in a sample is typically given using the delta (δ) notation, which represents the comparison of the ratios of heavy-to-light isotopes in a sample to the heavy-to-light isotope ratio in a standard. This is seen in Equation 1 (Faure, 1986):

$$\delta\ (‰) = ((R\ sample/R\ standard)-1)x1{,}000 \qquad \text{(Equation 1)}$$

where R is the ratio of heavy-to-light isotopes in the sample or standard. A sample yielding a positive δ value is enriched in heavy isotopes relative to the standard. A sample with a negative value is isotopically light or depleted in heavy isotopes.

δD and $\delta^{18}O$. As stated by Brownlow (1996), water has two independent isotopic ratios, D/H and $^{18}O/^{16}O$. Values for δD and $\delta^{18}O$ are reported in units of parts per thousand (‰) or per mil. The oxygen and hydrogen isotopes are graphed in relation to

the global meteoric water line (GMWL) (Craig, 1961), and is an indicator of the source of groundwater. By using the stable isotopes of hydrogen and oxygen, a graph of the $^{18}O/^{16}O$ ratio (x-axis) and the D/H ratio (y-axis) relative to standard mean ocean water (SMOW) may reveal that the two sets of samples plot in separate, distinct portions of the graph. However, mixing may be inferred if any fresh-water production well sample(s) plot in between the salt-water samples and fresh-water samples.

There is a linear relationship between δD and $\delta^{18}O$ for present-day meteoric waters known as the global meteoric water line (GMWL) as represented by Equation 2 and illustrated in Figure 8 (Brownlow, 1996):

$$\delta D = 8 \delta\, ^{18}O + 10 \qquad \text{(Equation 2)}$$

Each local area has its own local meteoric water line that differs somewhat from the GMWL. As shown in Figure 8 waters that have experienced evaporation typically plot away from the GMWL on evaporation trajectories with slopes of ~ 5 (Faure, 1986).

Sheppard (1986) points out that the mean isotopic compositions of meteoric waters at a specific locality are determined by many factors: temperature, latitude, altitude, distance from coasts, intensity of precipitation, local climate, and local topography. Brownlow (1996) also points out that while the mean and range of isotopic compositions of present-day seawater and of meteoric waters are known, we can only approximate these values for other natural waters.

In a graph of δD versus $\delta^{18}O$, the source and history of a groundwater determines where it plots in relation to the GMWL. Shallow groundwater derived from a meteoric source will reflect the isotopic composition of the precipitation and plot very near the GMWL, unless the precipitation has undergone excessive evaporation prior to infiltration

(Sheppard, 1986). Modern groundwater is generally assumed to have the same isotopic compositions as those of the local precipitation unless modified by surface evaporation.

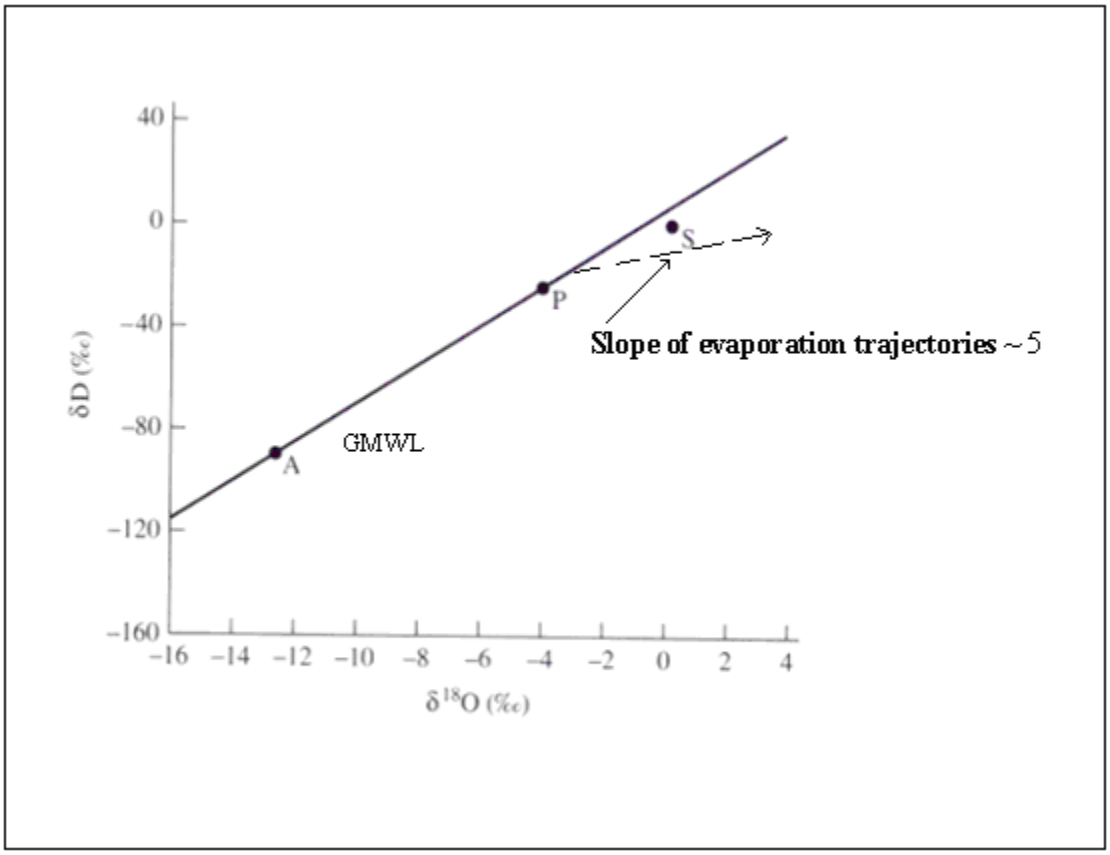

Figure 8: Variation in δD and $\delta^{18}O$ in the hydrologic cycle. S = surface ocean water; P = mean precipitation over the oceans; A = mean atmospheric water vapor over the oceans (after Brownlow, 1996).

A graph of the $\delta^{18}O$ relative to SMOW on the x-axis versus δD relative to SMOW on the y-axis may well reveal that the fresh-water and salt-water samples plot in distinctly different portions, with the salt-water samples plotting far to the right of the fresh-water samples. Any samples from shallow, water-supply wells that plot in between the other fresh-water samples and the salt-water samples may contain some water that has been injected into one or more disposal wells.

$\delta^{13}C$. Carbon-13 is an indicator of the carbon source and will also be useful in determining if mixing is occurring. Carbon-13 is used to identify sources of carbon and

is particularly valuable for distinguishing between carbon derived from CO_2 in the atmosphere or organic matter in the soil (isotopically light) and carbon derived from carbonate minerals (isotopically heavy) (Drever, 1997). Drever (1997) also notes that there are several possible sources of carbon: 1) dissolution of calcite, aragonite or dolomite from limestones or dolostones, which introduces relatively heavy carbon; 2) oxidation of organic matter, which introduces relatively light carbon; and 3) transport of CO_2 gas from the soil or atmosphere, which also introduces relatively light carbon. A sample yielding a positive $\delta^{13}C$ value is enriched in heavy isotopes relative to the standard PDB (PeeDee belemnite). A sample with a negative value is isotopically light or depleted in ^{13}C.

Structural Analysis

The purpose in conducting the structural analysis for this study is to identify any potential faults that displace rocks in the subsurface but are not visible on the surface. Subsurface faults may not displace rocks at the surface due to the ductile deformation of shales versus the brittle deformation of sandstones. Faults of this nature and fault-induced fractures and/or damage zones adjacent to the faults could create conduits that allow fluids to migrate from the disposal formations into overlying sedimentary beds, and ultimately could result in fluids infiltrating to the shallow fresh-water aquifers.

Several tools were used to identify the locations of faults, including construction of structural cross sections from gas well logs from the Drunkards Wash gas field. Gas production data, as well as water production data from wells in the Drunkards Wash gas field, may be helpful in identifying or confirming locations of interpreted faults, as faults create a more dense fracture network in the damage zone, allowing for higher gas and

water production through the seismically created fractures. A stratigraphic analysis will aid in understanding the geologic materials comprising both fresh-water and SWD aquifers.

The structural analysis was accomplished using the digital well logs from 479 wells (see Figure 9) of the more than 600 wells in the Drunkards Wash CBM gas field. These well logs were provided by ConocoPhillips, and are compatible for use in the geoPLUS computer program PETRA (geoPLUS Corporation, 1996-2005). Digital well logs for the Helper and Buzzard Bench CBM gas fields were not made available for this study from Anadarko Petroleum and XTO Energy, respectively.

The information that was provided for each well includes: unique well identification (UWI), total depth of the well, latitude, longitude and elevation at the land surface where the well was drilled, measured depths (MD) from the land surface, and sub-sea (SS) depths (feet above mean sea level, reported as a negative number) for the following geologic units: Blue Gate top, Ferron top, top coal, base coal, and coal thickness. Several obvious errors were found in the dataset for 14 wells. Suspected erroneous data were found in the measured depths and sub-sea depths, which reported that the formation tops were encountered anywhere between 1,000 to 4,000 ft (300 to 1,200 m) shallower than surrounding wells only a few miles away. Upon investigating the information reported for each well that was filed with UDOGM (2007), on the

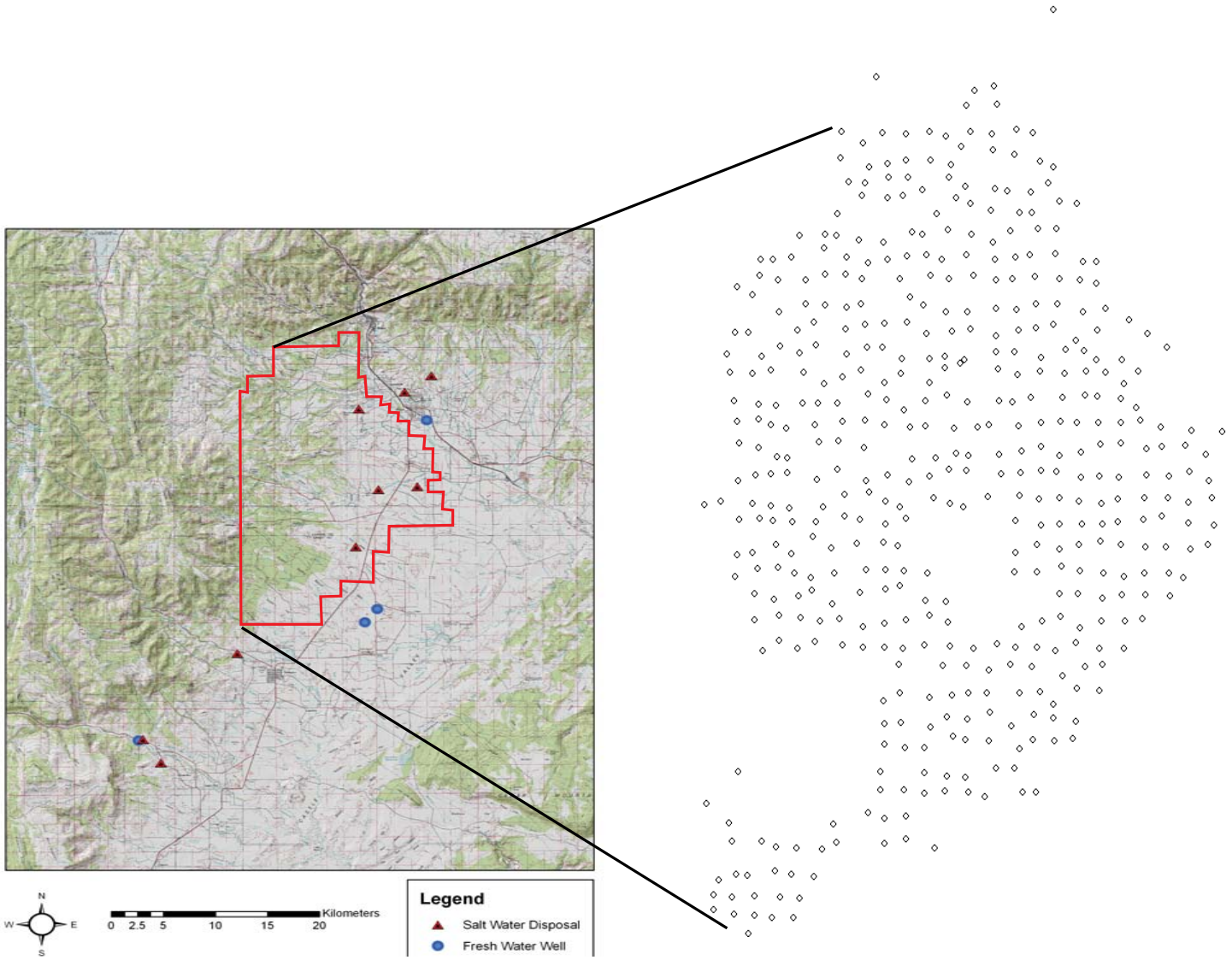

Figure 9: Map showing locations of the 479 wells in the Drunkards Wash gas field used in the structural analysis, including contouring and cross sections (data provided by ConocoPhillips).

UDOGM website (http://ogm.utah.gov), the measured depths to each formation were found in the drilling records and compared to the digital database provided by ConocoPhillips. Errors in the database for these 14 wells were due to omission of the first number reported (input error) for the drilled depth. For example, if the measured depth to the Ferron top was 1,250 ft, the erroneous data would report the measured depth to be 250 ft from the land surface. All wells which appeared to have erroneous data were checked against the records available on the UDOGM website. This mistake was found to be consistent in all 14 wells, and easily corrected in the database

Sixty-one of the 479 wells from ConocoPhillips were unusable, either because the wells were not included as part of the dataset or the data files were corrupted. The two areas where the data are missing are visible as two "holes," one in the middle of the map shown in Figure 9 (17 missing), and the other in the lower left portion of the map (44 missing). Several of these missing wells were identified, and can be found on the UDOGM website. Several of these wells were identified by their UWI, and an attempt was made to find the information in the UDOGM website well-file information regarding their location, including latitude, longitude, elevation and measured depths to formation tops. Latitude, longitude and elevation were successfully found; however, the data for measured depths to formation tops were either unavailable or appeared to be inaccurate, so no attempt was made to restore/correct the database in PETRA.

Computer-Based Contouring

There are seven different methods/options for contouring subsurface data using the computer-based contouring program PETRA (geoPLUS Corporation, 1996-2005).

Each method determines the shape and characteristics of the gridded surface by applying different mathematical functions to the original data.

1) Highly connected features - This is the default gridding style and works best for most data. A least-squares algorithm is employed and tends to produce connected features (i.e., cross sections) as opposed to disconnected features.

2) Disconnected features - This technique, also referred to as linear projection, tends to produce closed-off features. Slope information at each control point is used to project estimated Z values onto the grid node location based on regional slopes at each control point. The weighting function varies at each grid node based on the farthest control point used in the estimate. It can sometimes be used for isopach data to produce a more closed-off appearance.

3) Simple weighting with slopes - This technique applies a simple weighted average using the inverse of the distance to the control point. Slope information at each control point is used to project estimated Z values onto the grid-node location based on regional slopes at each control point.

4) Simple weighting without slopes - This technique applies a simple moving average using the inverse of the squared distance to the control point. No slope information is used. This option is useful for very dense control such as 3D seismic bin locations.

5) Distance grid - This option merely produces a grid showing distances around and radiating away from each control point. It can be used to illustrate drainage radii.

6) Closest point - This option simply sets each grid node to the value of the closest data point. It is best used with very dense data such as 3D seismic coverage.

7) Minimum curvature (no faults) - This option produces a surface with "minimum curvature." The smoothness of the surface can be controlled by a "tension" factor located on the “Advanced” tab. Due to the nature of this method's implementation, it cannot be used with faults. However, the minimum-curvature algorithm is also used with surface "flexing," so the highly connected method can be used with faults, then the flex option can be added.

Contour maps were created for each of the geologic contacts available in the digital well files: Blue Gate Member top, Ferron Sandstone. top, top coal, and base coal. An interval isopach map was created for the coal thickness. Seven methods were discussed as options for subsurface contouring in PETRA, all of which were tested and only one, the first method, the “highly connected features” method, was found to be the most useful for this application.

Structural Cross Sections

Various data can be used to construct a vertical cross section. It can be based on surface data (dips), electric well log data (markers, unit tops and bases, dips, and faults), seismic data, or entirely from completed subsurface maps (Tearpock and Bischke, 2003).

Tearpock and Bischke (2003) recommend that structural cross sections be drawn with the same horizontal and vertical scales whenever possible. With the same scales, the

cross sections are prepared true to scale with no vertical exaggeration. At times, however, exaggeration is required to permit legible vertical detail.

Electric well logs or well-log sticks can be used in the construction of structural cross sections. A stick is defined as a vertical or deviated line that represents an electric log. A stick section has several advantages over the electric log section, including simplicity, clarity, and ease of construction. Since sticks do not show any correlation data (stratigraphic correlations or faults), it is necessary to record the depths of all pertinent correlations and faults obtained from the actual electric logs. Stick sections are often used to solve structural problems because of their simplicity and lack of clutter (Tearpock and Bischeke, 2003).

Thirty-one east-west cross sections (Figure 10) and 20 north-south cross sections (Figure 11) were created in PETRA using the data from the 479 wells in the Drunkards Wash CBM gas field. East-west cross sections are labeled alphabetically (i.e., A – A') starting in the north and moving south. Once cross section Z – Z' was assigned, the labeling continued as cross section A1 – A2' and continued alphabetically ending on the southern boundary with cross section E1 – E2' (Figure 10). North-south cross sections are labeled numerically starting on the western boundary with cross section 1 – 2' and ending with cross section 20 – 21' on the eastern boundary (Figure 11).

Cross sections were created and used in conjunction with the structure contour maps for the purpose of identifying subsurface faults which are not visible on the land surface. Once a faulted area has been identified, it will be possible to measure the amount of fault throw based on the offset amount of beds. Net shale thickness will be used along with the fault throw to calculate a first-order approximation of the fault seal potential for these faulted areas.

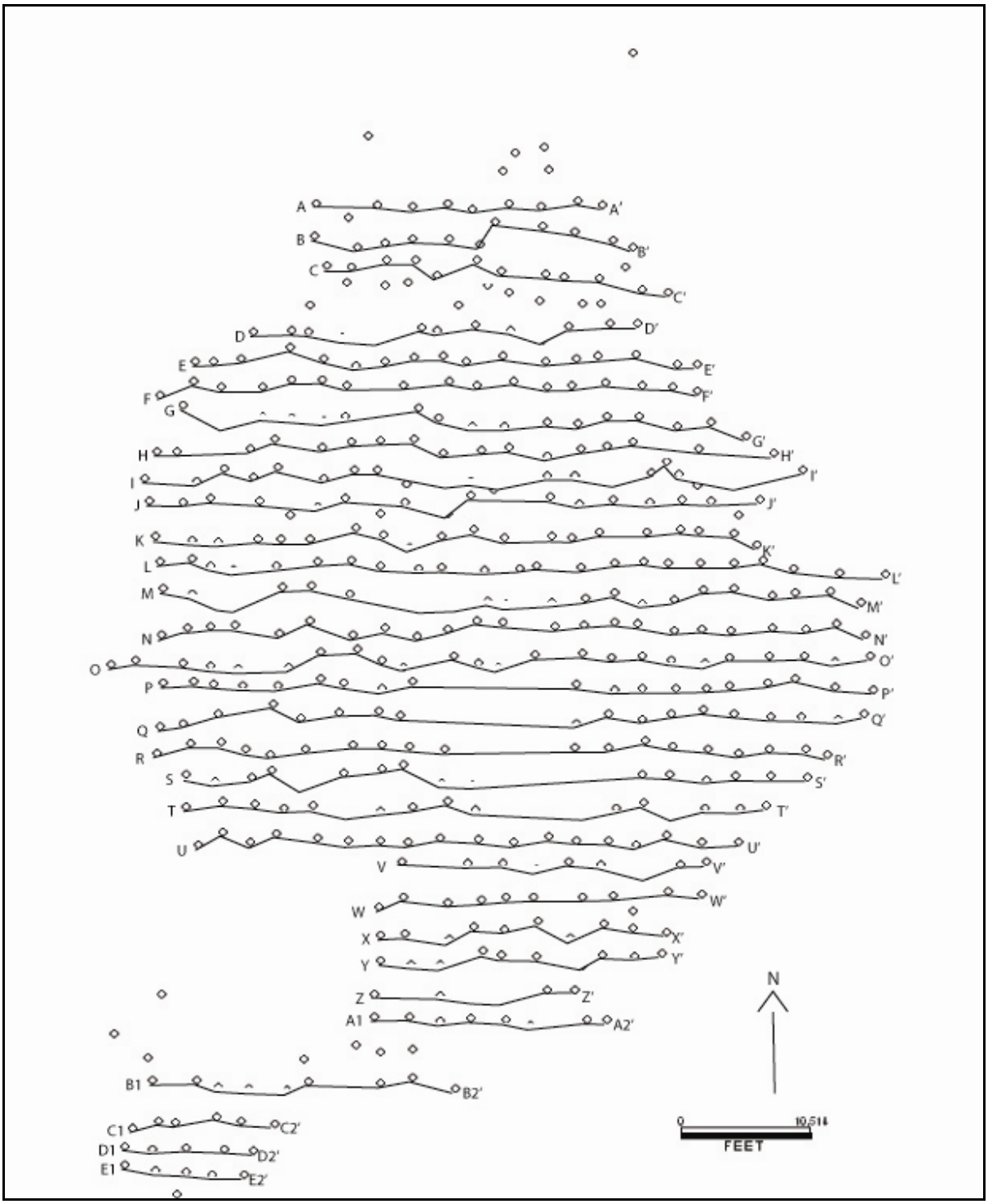

Figure 10: East-west cross sections created using digital well logs and PETRA in the Drunkards Wash CBM gas field, (for proximity to physical features see Figure 9).

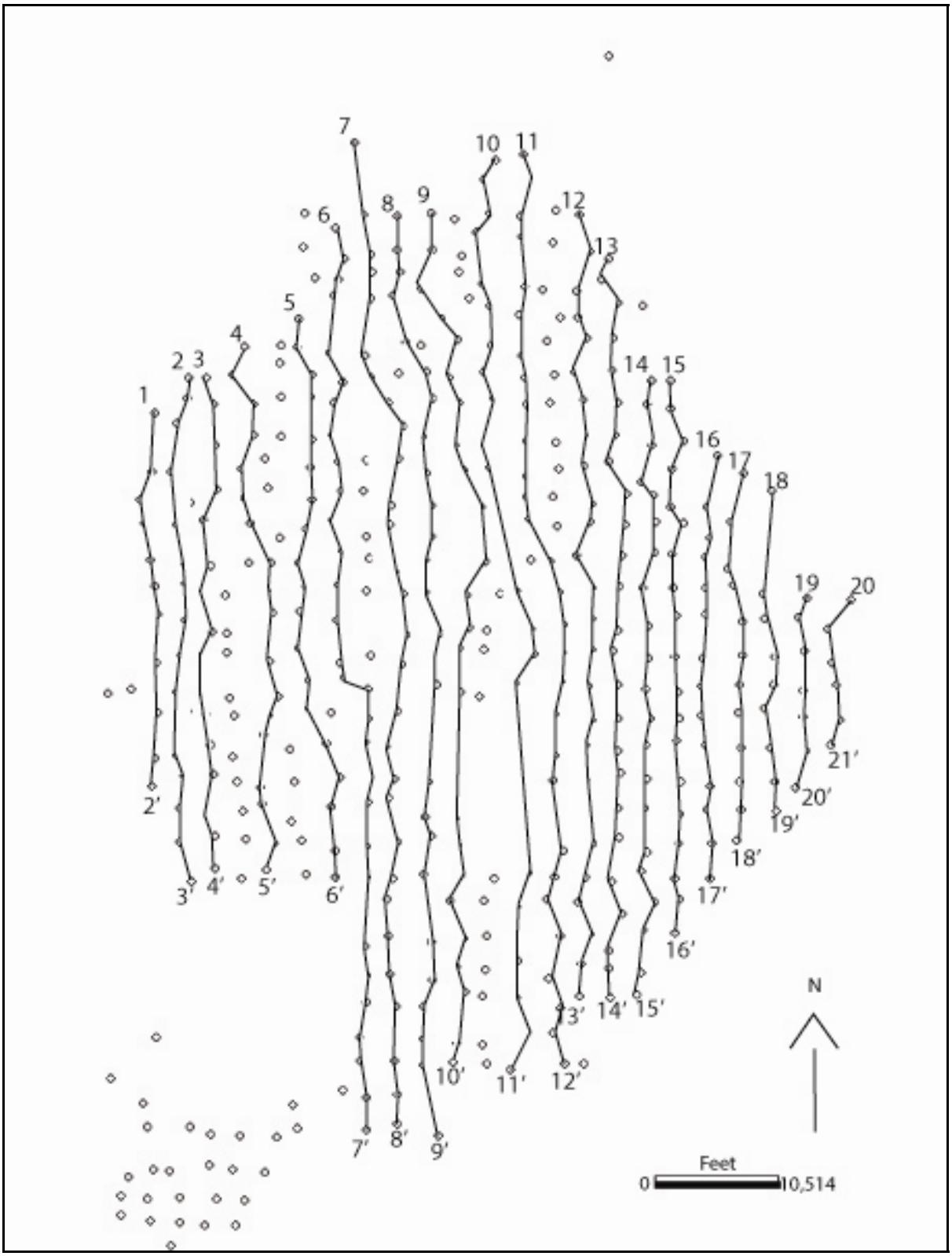

Figure 11: North-south cross sections created using digital well logs and PETRA in the Drunkards Wash CBM gas field, (for proximity to physical features see Figure 9).

Gas production from faulted areas will be compared with gas production from areas where faults are thought not to exist as a qualitative estimate of the relative amount of fracturing in the rocks. During the production of CBM, the gas is desorbed from the micropores of the coal, which then travels as a gas through coal fractures to the wellbore. It is assumed that a higher fracture density would result in: 1) greater gas production, 2) increased rate of maximum gas production, and/or 3) reaching maximum water production more quickly when compared to an area of lower fracture density.

Fault Seal Analysis

A fault seal is a body of rock or soil having pore throats too small and too poorly connected to allow the passage of hydrocarbons (Knipe, 1992) or other fluids. Fault seals generally form where a low-permeability layer is offset by a fault with a throw greater than the vertical thickness of that layer (Lindsay et al., 1993). While different groups use slightly different nomenclatures, in general, fault seals can be divided into the following types and subtypes (Knipe, 1992):

1) Fault zone seals (senso stricto) - The fault zone materials themselves form the seal.
2) Juxtaposition seals - The fault is a planar feature that places rocks of different permeabilities adjacent to one another.

According to Knipe (1992), the mechanisms that form these two main types of seals include: 1) porosity reduction by disaggregation, mixing, and grain boundary sliding without large-scale cataclasis; 2) dissolution, transport, and precipitation; 3) cataclasis; 4) cementation; and 5) clay smearing. The majority of recent work shows the

most effective seals are evaporites, fine-grained clastics and organic-rich rocks (Knipe, 1992).

*Gamma-ray logs***.** Gamma ray logs measure the natural radioactivity in formations. Shale-free sandstones and carbonates have small amounts of radioactive material and give low gamma ray readings. As the shale content increases, the gamma ray log response increases because of the concentration of radioactive material in shale (Asquith and Krygowski, 2004).

The gamma-ray log is usually displayed in the left track (track 1) of a standard log display, commonly with a caliper curve. Tracks 2 and 3 usually contain porosity or resistivity curves (Asquith and Krygowski, 2004).

Clay smear algorithms. Several factors control the potential for clay and/or shale smearing: 1) thicker shale source beds can produce thicker clay smears; 2) shear-type smears decrease in thickness with increasing distance from the source layer; 3) abrasion-type smears decrease in thickness with increasing throw: and 4) multiple source beds displaced past a particular point on the fault plane can give a combined continuous smear (Bouvier et al., 1989; Yielding et al., 1997). These observations imply that the fault-seal potential of a particular fault can be quantified using algorithms and the related factors of bed thickness, distance from source bed and fault throw.

Lindsay et al. (1993) developed an algorithm called the shale smear factor (SSF), which is defined as the ratio of fault displacement to the apparent thickness of a shale layer. SSF is calculated by dividing the fault throw by the thickness of the clay/shale bed. Incomplete smears have SSF values greater than 7, whereas smaller SSF values suggest continuous smears and/or sealing. High clay smear potential (CSP) values correspond to SSF values of 4 to 5 (Lindsay et al., 1993). This equation estimates the

relative likelihood of clay smear being developed in the fault-gouge zone as a first order approximation. To fully understand the sealing capacity of reservoir-scale fault zones, well and seismic data are necessary (Yielding et al., 1997).

CHAPTER IV

RESULTS

Hydrochemistry

Shallow, Water-Supply Wells

Tables 6 and 7 present the temperature, pH, electrical conductivity (EC), alkalinity, major and minor ion and trace metal concentrations, and δD, $\delta^{18}O$ and $\delta^{13}C$ values for the four shallow water-supply and nine SWD wells sampled, respectively. Temperatures range from 11.4 to 14°C. The fresh-water samples are essentially neutral, ranging in pH from 6.87 to 7.26. Electrical conductivity ranges from 629 to 1,120 µS, and alkalinity ranges from 280 to 460 mg/L. Three of the four samples have TDS concentrations within the expected range of water-supply wells, ranging from 843 mg/L to 1,595 mg/L. The sodium (Na) and chloride (Cl) concentrations for these three samples range from 117.4 to 224.7 mg/L and 69.1 to 94.6 mg/L, respectively.

The close grouping of the three shallow water-supply wells and their separation from Well 4 is obvious in Figure 12. Well 4 has a TDS concentration of 11,337 mg/L, which is seven times higher than the next highest well. The Na (3,382 mg/L) and Cl (7,619 mg/L) concentrations are also much higher than those for the three other wells. Well 4 has the highest concentrations of boron, barium, copper, potassium, and strontium when compared with the three other wells (Table 6), but also has the lowest concentrations of calcium, magnesium and sulfate. The iron, manganese, silica, and zinc concentrations for Well 4 lie within the range found for the other three wells. The concentrations of nickel and phosphorus did not exceed their respective detection limits (< 0.01 mg/L) for any of the four samples.

Table 6: Chemical data from the shallow water-supply wells (all values in mg/L).

Water Rights ID No.	Well	Date Sampled	Temp °C	pH	EC (uS)	Alkalinity	B	Ba	Ca	Cl	Cu	Fe	K	Mg	Mn	Na	Ni	P	SO_4	Si	Sr	Zn	TDS	δ13C	δD	δ18O
93-3720 (A19548)	1	7/29/2005	11.4	7.22	629	280	0.19	0.03	187.1	94.6	0.02	0.01	6.55	96.82	<	117.4	<	<	893	40.43	1.81	0.02	842.6	-8.1	-117	-14.7
91-4194 (A52821)	4	10/13/2005	12.6	7.26	1,120	460	2.22	0.83	69.8	7,619	0.05	0.18	42.73	59.68	0.04	3,382	<	<	305	48.63	9.94	0.02	11,336.9	-7.5	-111	-14.3
91-4264 (A56345)	20	7/29/2005	11.8	7.23	800	400	0.5	0.03	376.9	69.1	0.01	1.84	12.46	138.3	0.79	224.7	<	<	2101	65.31	4.26	0.1	1,594.5	-3	-117	-15.1
91-4210,13 (A53772,841)	29	7/29/2005	14	6.87	900	400	0.38	0.07	311.9	77.6	0.01	0.02	8.66	108.5	0.68	193	<	<	1592	64.2	3.24	0.02	1,298.8	-11.3	-109	-13.8

Table 7: Chemical data from the SWD wells (all values in mg/L).

API Well Number	Well Name	Date Sampled	Temp °C	pH	EC (uS)	Alkalinity	B	Ba	Ca	Cl	Cu	Fe	K	Mg	Mn	Na	Ni	P	SO_4	Si	Sr	Zn	TDS	δ13C	δD	δ18O
43-007-30290	D-3	8/3/2005	21.7	7.9	3,450	NA	3.86	16.88	26.35	3,525	<	0.76	30.07	20.9	0.03	2,684	<	0.26	2.37	50.94	6.81	0.03	6,366.7	19.7	-83	-8.9
43-007-30314	D-4	8/3/2005	23.4	7.57	3,020	NA	3.13	11.63	21.97	2,422	<	0.36	25.17	13.99	0.02	2,400	<	0.22	1.65	51.44	4.44	0.03	4,955.0	19.1	-90	-9.9
43-007-30361	H-1	8/2/2005	28.7	7.48	4,400	NA	3.57	95.7	73.31	1,117	<	1.73	58.16	62.31	0.04	4,106	<	0.3	1.11	46.49	21.71	0.03	5,586.7	26.3	-40	-1.3
43-007-30555	F-2	8/2/2005	25	7.08	4,310	4,200	3.89	64.9	65.99	8,347	0.02	0.58	44.88	54.21	0.05	3,720	<	0.14	3.33	49.26	18.1	0.03	12,370.2	28.3	-44	-2
43-007-30567	D-14	8/3/2005	21.7	7.53	4,200	NA	5.47	16.1	28.02	3,789	<	0.57	27.86	22.45	0.02	2,960	<	<	0.63	40.07	8.05	0.02	6,897.8	25.2	-77	-7.6
43-015-30272	SWD-1	10/13/2005	20	7.76	3,330	NA	2.12	10.85	19.3	1,535	<	0.18	25.34	11.13	0	2,609	0.01	0.34	0.9	60.33	4.2	0.02	4,278.1	15	-79	-8.3
43-015-30323	SWD-2	10/13/2005	16	7.64	3,465	NA	2.06	12.31	16.27	1,575	<	0.15	27.79	12.04	0	2,588	<	0.25	0.75	59.32	4.47	0.01	4,297.9	14.2	-76	-7.7
43-015-30338	D-7	8/3/2005	20.8	7.68	7.95 mS	NA	2.13	37.44	31.27	9,974	<	0.78	56.27	42.93	0.02	4,037	<	0.23	1.71	46.02	15.43	0.02	14,244.1	25.2	-50	-3.8
43-015-30490	SWD-4	10/13/2005	15.4	7.67	3,500	NA	2.33	23.69	22.41	3,287	<	0.23	38.02	20.54	0.02	3,133	0.01	0.22	1.02	57.09	8.11	0.01	6,593.0	15.7	-51	-3.8

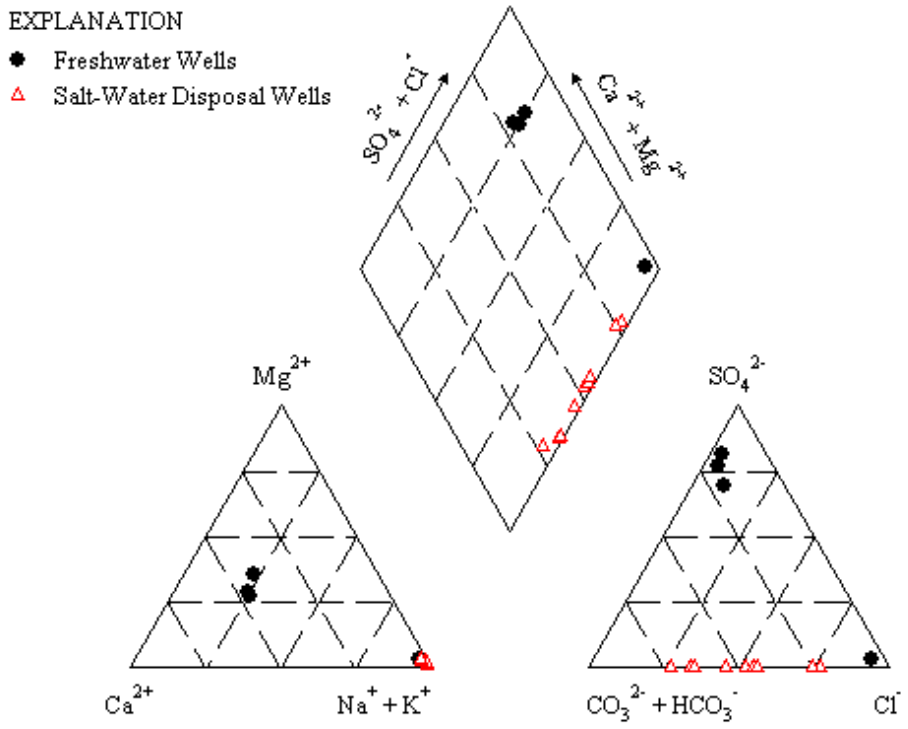

Figure 12: Trilinear (Piper, 1944) diagram of well samples generated using GW_Chart Version 1.3.1.0.

Delta D and $\delta^{18}O$ values for all four wells range from -109 to -117 and -13.8 to -15.1 per mil, respectively. These four samples lie very near the GMWL (Figure 13), indicating that local precipitation probably is the source of recharge to these wells.

All four shallow water-supply well samples have negative values of $\delta^{13}C$ (Table 6), ranging from -3 to -11.3 per mil, indicating that the source of the carbon is likely from organic matter or from CO_2 gas in the soil or atmosphere, both of which introduce relatively light carbon.

Like the shallow, water-supply wells, the SWD well samples are relatively neutral, with a pH range from 7.08 to 7.9. Temperatures for all the SWD wells are

higher than the shallow water-supply wells, ranging from 15.4 to 28.7 °C. Higher temperatures can be explained by the great depths of the production wells and the

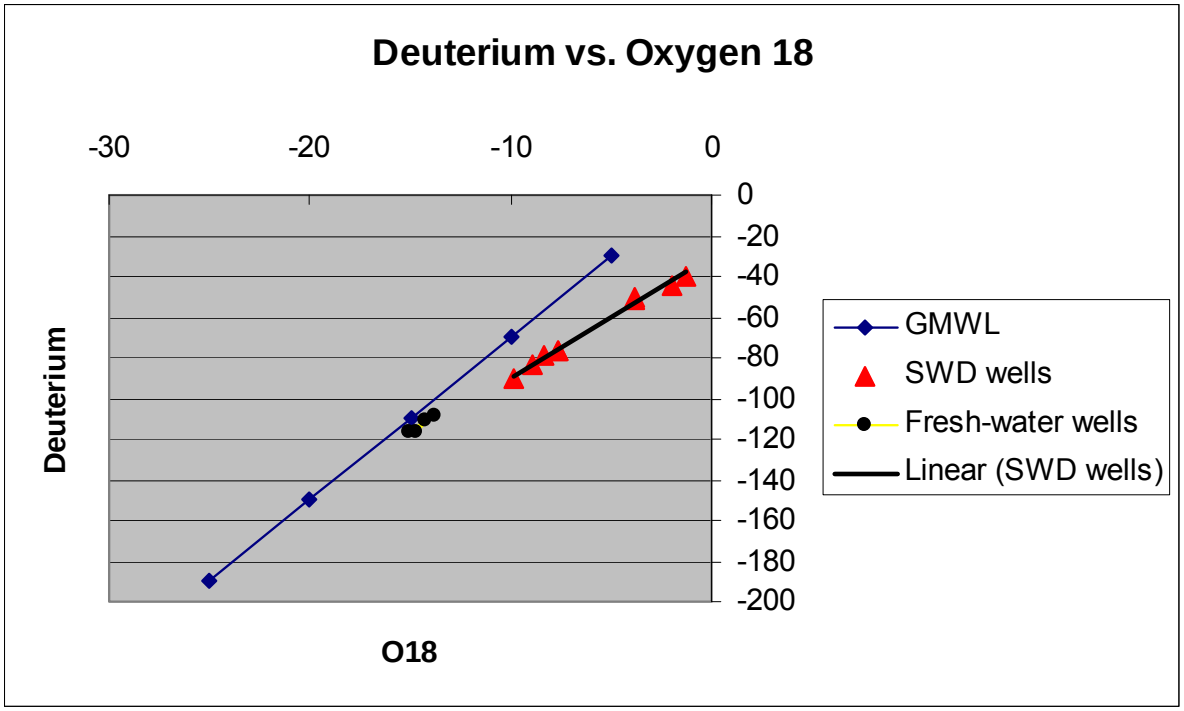

Figure 13: Delta D and $\delta^{18}O$ from shallow, water-supply wells and SWD wells plotted with the GMWL (all values in per mil).

geothermal gradient in this area. Electrical conductivity is at least three times higher than the highest shallow water-supply well (Well 4).

Well 43-007-30555 (F-2) is the only well where the alkalinity or acid neutralizing capacity was measured. Two-hundred ten drops of sulfuric acid were required to complete the titration, which equals 4,200 mg/L alkalinity, and is approximately ten times the amount of acid required on any of the shallow water-supply wells.

Figure 12 is a trilinear diagram (Piper, 1944) that includes the SWD well samples plotted along with the shallow, water-supply well samples. Alkalinity was measured for one of the SWD wells (43-007-30555), but not for the other eight SWD

wells due to the large amount of acid required to complete the in-field titration. As an alkalinity value is required for the program to create a reasonable diagram the value of 4,200 mg/L was used for all the SWD wells as using a value of zero would be far less representative than using the one measured value applied to all nine SWD wells.

The TDS concentrations for the SWD wells are significantly higher than that for the water-supply wells, with the exception of Well 4, which range from 4,278 to 14,244 mg/L. Sodium and Cl concentrations are very high, as expected, ranging from 2,400 to 4,106 mg/L and 1,117 to 9,974 mg/L, respectively. Concentration ranges for barium, calcium, chloride, iron, magnesium, chloride, sulfate, and strontium have great variability, with a range of values from 3 to 10 times higher than the lowest concentration, respectively. Concentration ranges for boron, copper, potassium, sodium manganese, nickel, phosphorus, silica, and zinc show significantly less variability, with concentrations ranging from nearly identical to less than three times higher, respectively. The great variability seen in these wells may be due to the heterogeneity of the Ferron Sandstone aquifer, or water may be migrating downward from overlying aquifers (i.e., Upper Blue Gate Shale member of the Mancos Shale) from dewatering during CBM gas production.

Delta D and $\delta^{18}O$ values are much less negative in the deep water injection wells than those for the shallow, water-supply wells, ranging from -40 to -90, and from -1.3 to -9.9, respectively (Table 7). The SWD wells also plot far from the GMWL (Figure 13). I infer that the source of the water from the SWD wells is not from recent precipitation, but is likely older and displaying an evaporative signature (Figure 13).

All nine SWD wells have positive $\delta^{13}C$ values (Table 7), ranging from 14.2 to 28.3 per mil, indicating that the samples are isotopically heavy and are enriched in ^{13}C. The source of the carbon is likely from the dissolution of calcium minerals such as calcite, aragonite, or dolomite from limestones or dolostones, as noted by Drever (1997).

Structural Analysis

Cross Sections

Three subsurface, north-south trending downward to the west normal faults have been identified in the study area from structural cross sections using the 479 digital well logs from the Drunkards Wash gas field (Figure 14). The three faults were identified using the east-west cross sections. The north-south cross sections do not reveal the presence of any structures; thus, results from the north-south cross sections are not presented.

One fault is in the north and the other two are in the central part of the gas field near the eastern and western flanks of the gas field. An anticline has also been located on the southern boundary of the gas field north of Huntington, Utah.

Fault throws range from as much as 130 ft (40 m) to as little as 10 ft (3 m) (Table 8). Average fault throw is roughly 75 ft (23 m), which was found to be fairly consistent between all three faults zones. Interpreted cross sections are located in Appendix A; uninterpreted cross sections can be found in Appendix B. Cross sections are presented with vertical exaggeration, which is computed automatically by PETRA (geoPLUS Corporation, 1996-2005) based on the length of the cross section.

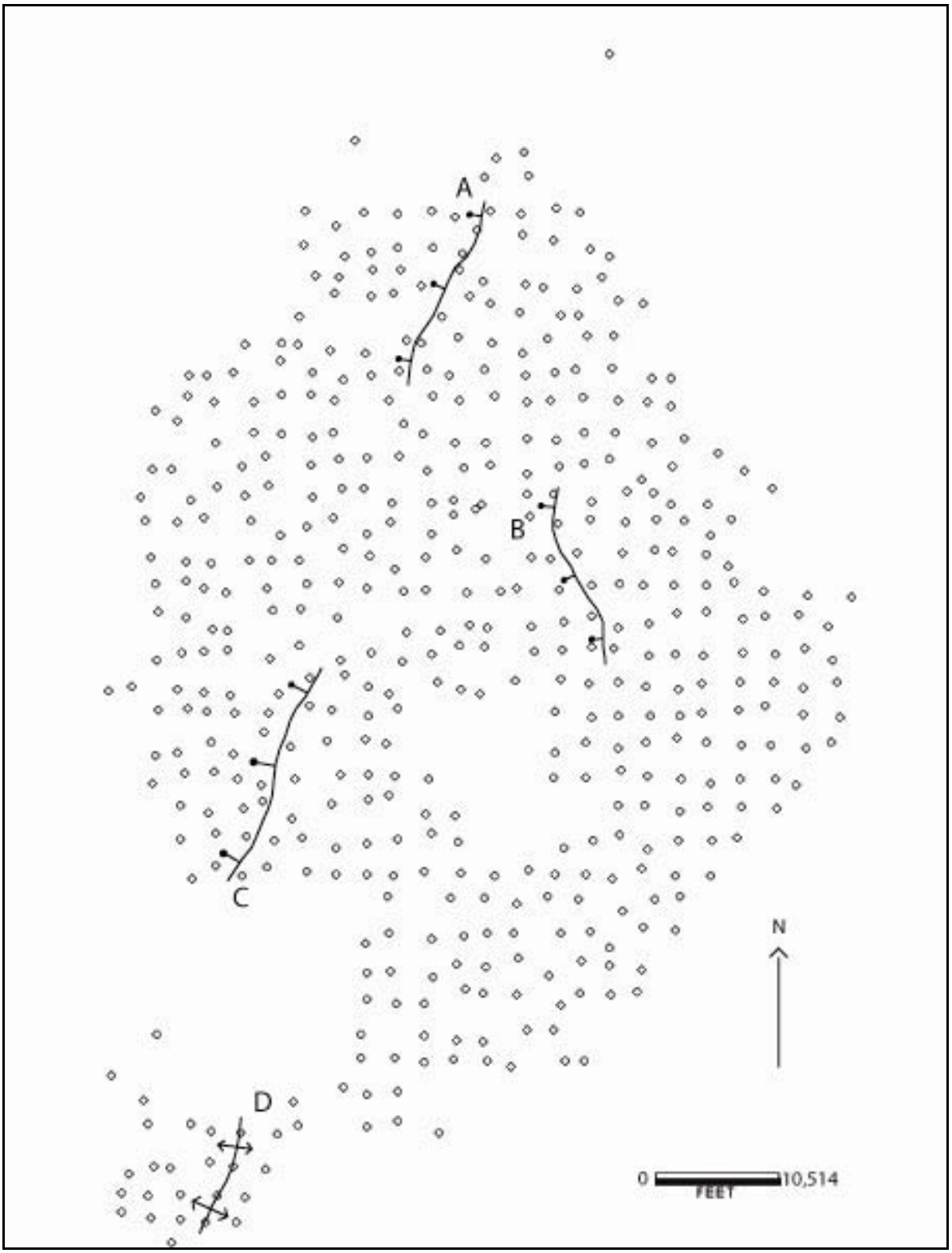

Figure 14: North-south trending faults and anticline identified in the Drunkards Wash CBM gas field, (for proximity to physical features see Figure 9).

Table 8: Fault throws from areas A, B and C.

Area	Cross Section	Fault Throw (ft)
A	B-B'	107
	C-C'	32
	D-D'	76
	E-E'	16
B	I-I'	54
	J-J'	35
	K-K'	10
	L-L'	67
	M-M'	130
	N-N'	101
C	O-O'	13
	P-P'	46
	Q-Q'	106
	R-R'	108
	S-S'	119
	T-T'	107
	U-U'	51

For presentation purposes the four structural features have been labeled alphabetically, starting with the fault found on the northern end of the gas field and moving south. The fault identified in the north has been labeled fault A, fault B is the next fault south, which lies in the center of the gas field on the eastern flank. Fault C is in the center of the gas field on the western flank, while the anticline found at the southern end of the gas field is labeled D.

Four cross sections have been used to locate fault A in the northern part of the gas field. Cross section B-B' is the northernmost cross section where a fault is visible, followed by cross sections C-C', D-D' and E-E'.

Formation tops were identified by ConocoPhillips prior to receiving the data set. A comparison was made between the formation tops in the data set and the records available on the UDOGM website and was found to be very accurate, with the exception of the erroneous data previously discussed, which were later corrected.

Cross section E-E' has the least amount of throw for this fault at 16 ft (5 m). Being the furthest cross section to the south, the small amount of throw implies that the fault likely terminates completely before encountering cross section F-F'.

Five cross sections have been used to locate fault B: cross sections I-I', J-J', K-K', L-L', M-M' and N-N'. The fault is most visible in cross sections M-M' and N-N', as fault throw is greatest along the southern half. Cross section M-M' shows the greatest fault throw for the entire Drunkards Wash gas field at 130 ft (40 m).

Seven cross sections have been used to locate fault C: cross sections O-O', P-P', Q-Q', R-R', S-S', T-T' and U-U'. The fault is most noticeable along its southern length using cross sections Q-Q' through T-T'. Cross section O-O' has the least amount of throw at 13 ft (4m), yet it is still sufficient to easily identify the fault, especially since the location is in line with the trend of the fault interpreted along its southern length.

The four southernmost cross sections reveal a north-south trending anticline just north of Huntington, Utah. The cross sections used to identify this anticline are cross sections B1-B2', C1-C2', D1-D2' and E1-E2'. It is unknown how far this anticline extends as it cannot be traced because 44 of the wells in this area are missing from the data set. This anticline has also been mapped on the geologic map by Witkind (1988).

Contour Maps

Contour maps for the Blue Gate top, the Ferron top and the top and base of the coal have been made to aide in identifying faults and seeing the subsurface contours, as these are the formation tops available as part of the well log dataset provided by ConocoPhillips. Contour maps are located in Appendix C. The contour intervals

displayed are the only intervals which PETRA will allow for each particular formation. An attempt was made to display consistent contour intervals between figures, but the program was unable to adjust appropriately.

Each contour map shows the rocks in the eastern part of the gas field dip to the west, the dips are horizontal or nearly so in the center of the field, and the rocks dip gently to the east in the western part of the gas field. Taking into account the major regional structural features, this is expected, as the westward-dipping San Rafael Swell is located to the east of the gas field. While to the west of the Drunkards Wash gas field is the Wasatch Plateau, with rocks that dip gently to the east.

Gas and Water Production

The amount of fracturing associated with the faults identified can be qualitatively estimated in a first order approximation by comparing gas and water production in areas where faults have been identified to areas where no faults are thought to exist. CBM is produced by the desorbtion of methane from the coal micropores and then travels as a free gas through the coal fractures into the wellbore as the water is pumped out. It is assumed that a higher fracture density would result in either: 1) greater overall (total and maximum) gas production, 2) increased rate of maximum gas production, or 3) reaching maximum water production more quickly than an area of lower fracture density.

Using several of the CBM production wells surrounding the identified faults and anticline, areas have been designated using the same labeling system (i.e., area A) which can be compared to a control area adjacent to each faulted area where no faults are thought to exist (Figure 15). Control areas are labeled A-control, B-control, C-control and D-control to easily identify which faulted area the control area is

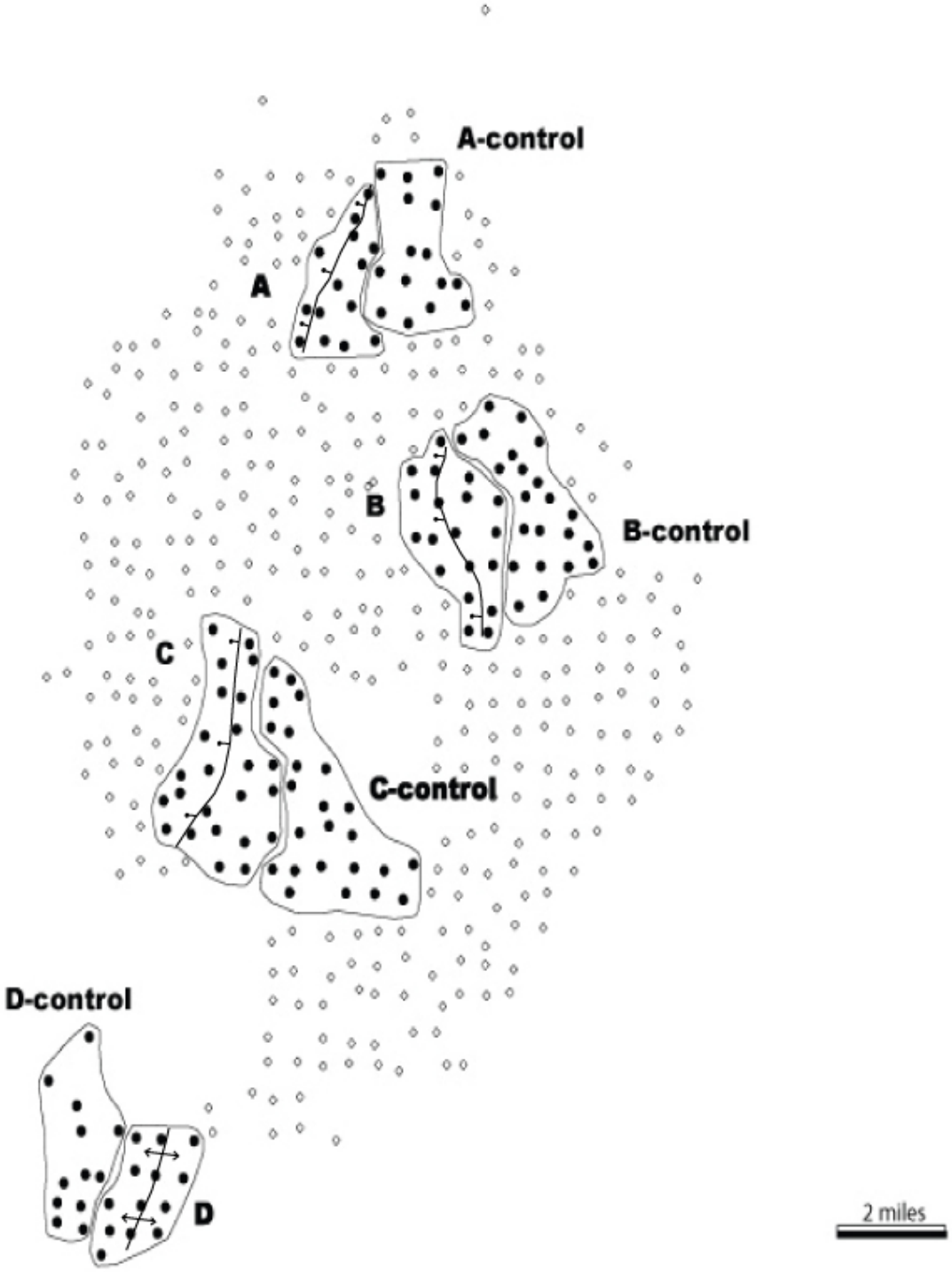

Figure 15: Faulted areas (A, B, C and D) and associated control areas for gas and water production, (for proximity to physical features see Figure 9).

associated with. It is assumed that the areas which are faulted would have a higher fracture density than their respective control areas; thus, they potentially should have higher gas and water production.

Gas production data were obtained from the UDOGM (2007) website (http://ogm.utah.gov). Data are reported once monthly as a cumulative production in mcf. Gas production data for wells from the areas designated in Figure 15 were downloaded into an Excel spreadsheet and compared at 24 months of production, then compiled into a bar graph for each separate area.

Water production data were also included in the spreadsheet downloaded from the UDOGM website. Maximum water production for each well was found, and the average has been calculated for both the faulted and control areas. Also, the maximum water production for the well with the highest production has been presented for each area. Cumulative water production for up to 24 months from each well was used to calculate the average over each area. Volumes of water are reported in barrels (1 barrel = 42 gallons [159 L]).

The 24^{th}-month average gas production per well, and maximum gas production of the single best producing well are shown in Table 9. Also included in Table 9 is the average maximum water production per well and maximum water production for the well with the highest production, to easily compare differences between faulted areas and control areas.

Table 9: Summary of gas and water production statistics for faulted and control areas.

Area	Number of Wells	Average Gas Production/Well (24^{th} month)	Maximum Gas Production of Single Well (24th month)	Maximum Water Production from Single Well	Average Maximum Water Production/Well	Average Cumulative Water Production (24 months)
		mcf		barrels		
A	14	14,515	36,195	119,033	25,632	305,396
A-control	15	2,333	7,289	22,730	4,746	33,872
B	19	24,171	48,846	63,086	18,653	186,501
B-control	20	6,175	18,226	39,659	7,808	57,558
C	24	20,747	34,576	40,945	17,825	207,346
C-control	24	9,296	19,594	16,338	5,131	33,839
D	13	2,488	5,850	12,151	2,948	17,764
D-control	12	2,163	5,067	7,831	2,631	15,181

Area A. Area A contains 14 wells and the associated control area (A-control) has 15 wells (Table 9). The following gas wells were chosen for area A: 43-007-30779, 30490, 30499, 30455, 30497, 30428, 30419, 30320, 30321, 30422, 30325, 30322, 30319, and 30323. The following gas wells were chosen for area A-control:

43-007-30607, 30608, 30627, 30628, 30498, 30500, 30211, 30335, 30340, 30345, 30404, 30450, 30423, 30509, and 30415 (Figure 16).

Area A shows higher gas production than A-control. There are seven wells in area A that have production greater than 10,000 mcf (283 million m^3), while none of the wells in area A-control have gas production greater than 10,000 mcf. Average gas production for the 24th month in area A is 14,515 mcf (411 million m^3), and the average for area A-control is 2,333 mcf (66 million m^3). The highest gas production for the 24th month in area A is 36,195 mcf (1,025 million m^3), while the greatest production in area A-control is 7,289 mcf (206 million m^3). The average maximum water production per well for area A is 25,632 barrels (4,075,162 L), while the average maximum water production for area A-control is 4,746 barrels (754,553 L). The average 24-month cumulative water production for area A is 305,396 barrels (48,554,083 L), and for area A-control is 33,872 barrels (5,385,217 L). Maximum water production from a single well for area A is 119,033 barrels (18,924,734 L), while area A-control is only 22,730 barrels (3,613,781 L).

Area B. Areas B and B-control have 19 and 20 wells (Table 9), respectively. The wells used in area B are: 43-007-30186, 30204, 30181, 30196, 30203, 30180, 30142, 30195, 30198, 30197, 30184, 30221, 30224, 30225, 30226, 30222, 30232, 30228, and 30202. The wells used in area B-control are: 43-007-30205, 30208, 30206, 30156, 30130, 30185, 30143, 30305, 30253, 30183, 30144, 30178, 30218, 30217, 30254, 30179, 30192, 30220, 30223, and 30157 (Figure 17).

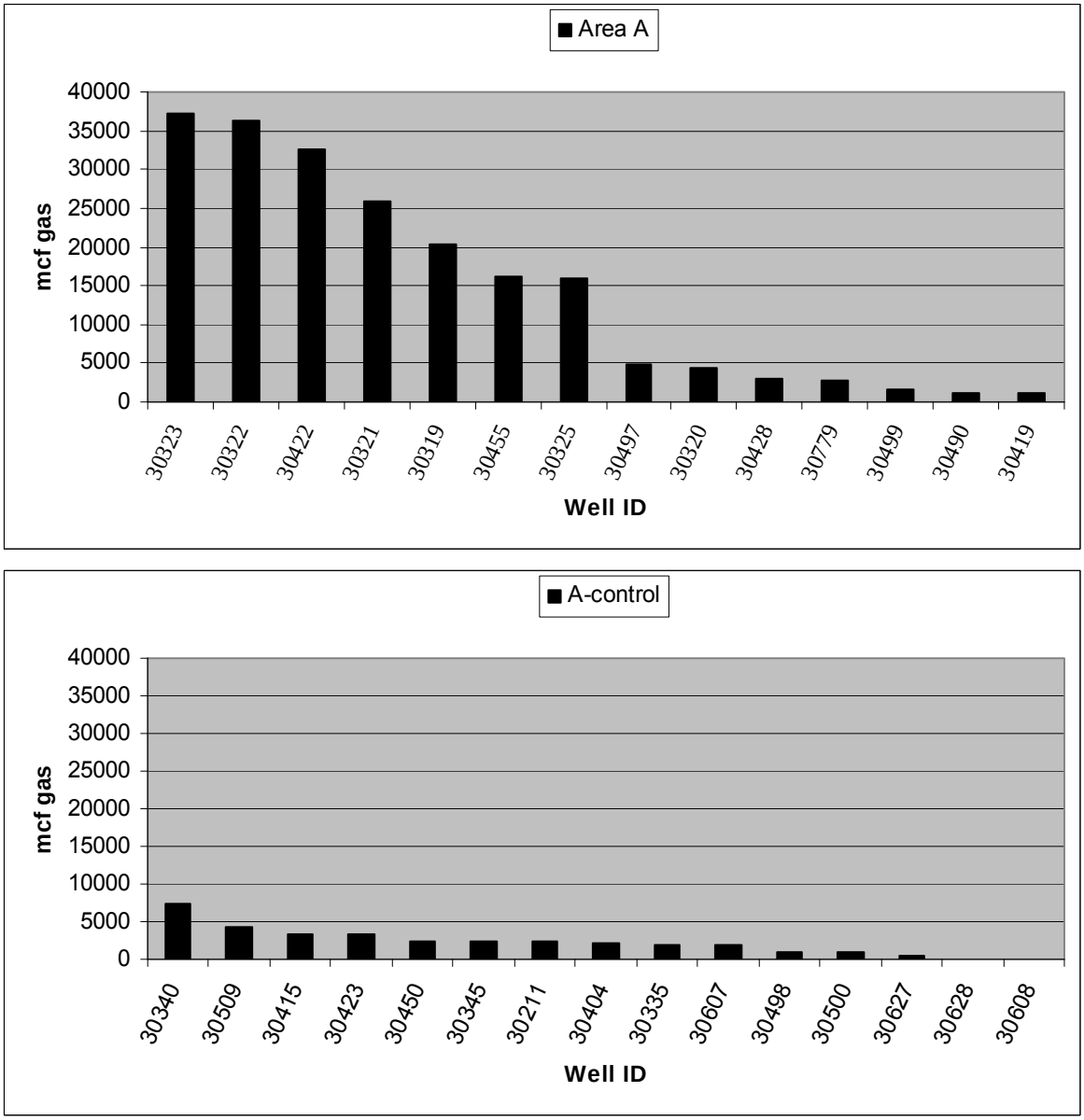

Figure 16: Gas production for areas A (upper) and A-control (lower).

Area B shows higher gas production than B-control for the 24th month of production. The average gas production for area B is 24,171 mcf (684 million m^3) compared to area B-control, which is 6,175 mcf (174 million m^3). In area B there are eleven wells with monthly production over 20,000 mcf (566 million m^3) and in B-control there are no wells over 20,000 mcf. The highest gas production for the 24th month in area B is 48,846 mcf (1,383 million m^3), and that of area B-control is 18,226 mcf (516 million m^3). The average maximum water production per well for area B is

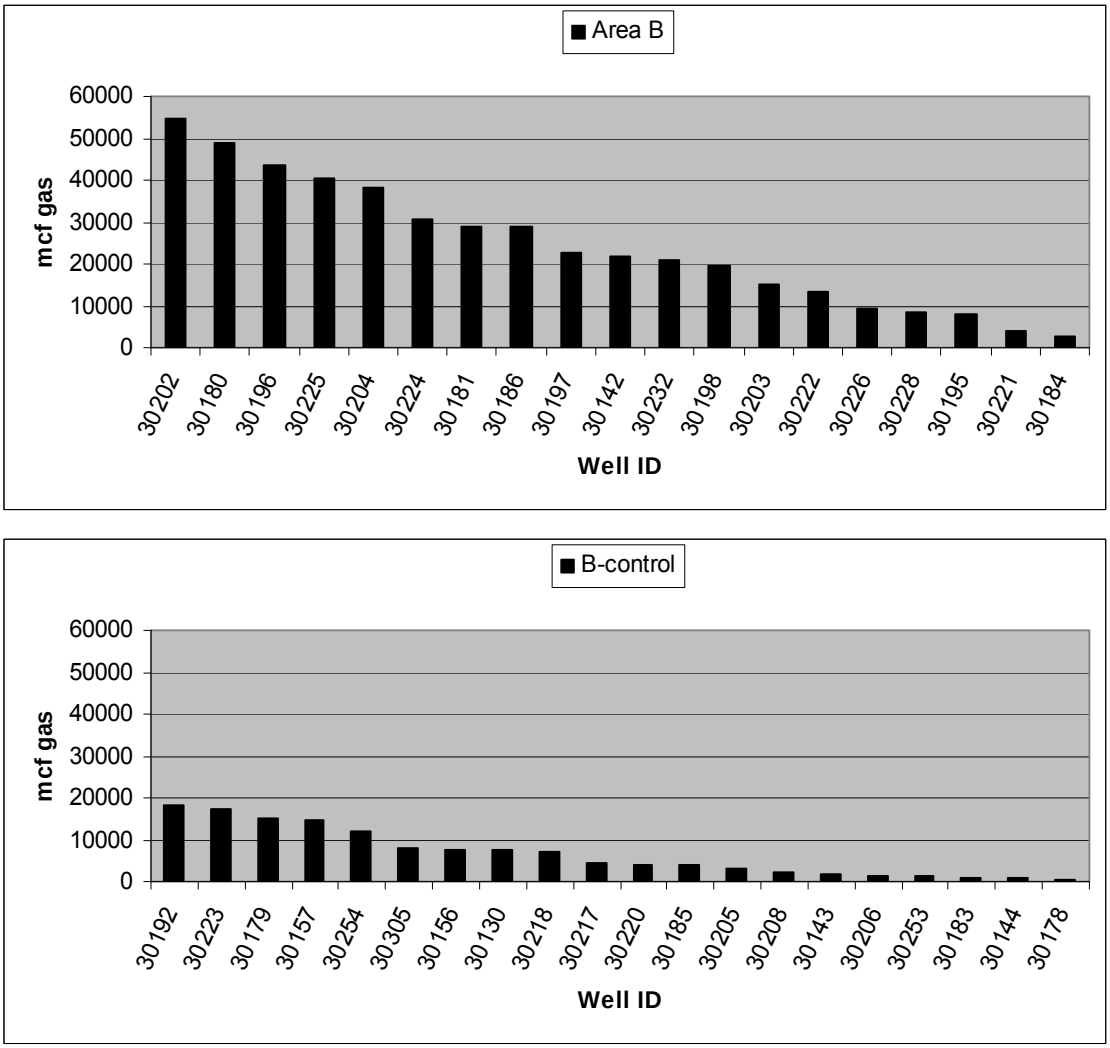

Figure 17: Gas production for areas B (upper) and B-control (lower).

18,653 barrels (2,956,827 L), while the average maximum water production for area B-control is 7,808 barrels (1,241,372 L). The average 24-month cumulative water production for area B is 186,501 barrels (29,651,289 L) and for area B-control is 57,558 barrels (9,150,990 L). Maximum water production from a single well for area B is 63,086 barrels (10,029,872 L0), while area B-control is 39,659 barrels (6,305,277 L).

Area C. Twenty-four wells have been used in each of areas C and C-control (Table 9). The wells in area C are: 43-007-30487, 30409, 30421, 30258, 30720,

30459, 30485, 30729, 30730, 30651, 30652, 30705, 30747, 30505, 30751, 30731, 30753, 30752, 30750, 30740, 30626, 30624, 30623, and 30625. The wells used in area C-control are the following: 43-007-30741, 30742, 30669, 30551, 30513, 30512, 30744, 30653, 30743, 30559, 30518, 30560, 30257, 30502, 30457, 30347, 30739, 30738, 30514, 30515, 30511, 30510, 30488, and 30412 (Figure 18).

Area C also has a higher gas production than area C-control. Average gas production for the 24 wells in area C is 20,747 mcf (587 million m^3) for the 24th month. The average gas production for C-control is 9,296 mcf (263 million m^3). Twelve of the 24 wells in area C have production exceeding 20,000 mcf (566 million m^3), whereas in area C-control there are two wells with gas production exceeding 20,000 mcf. The highest gas production for the 24th month in area C is 34,576 mcf (979 million m^3), while the highest gas production in C-control is 19,594 mcf (555 million m^3). The average maximum water production per well for area C is 17,825 barrels (2,833,948 L), while the average maximum water production for area C-control is 5,131 barrels (815,763 L). The average 24-month cumulative water production for area C is 207,346 barrels (32,965,379 L) and for area C-control is 33,839 barrels (5,379,971 L). Maximum water production from a single well for area C is 40,945 barrels (6,509,734 L), while area C-control is only 16,338 barrels (2,597,534 L).

Area D. Thirteen wells have been used in area D and 12 wells have been used in area D-control (see Table 9). The wells used in area D are: 43-015-30493, 30301, 30330, 30335, 30491, 30514, 30516, 30517, 30513, 30542, 30541, 30519, and 30544.

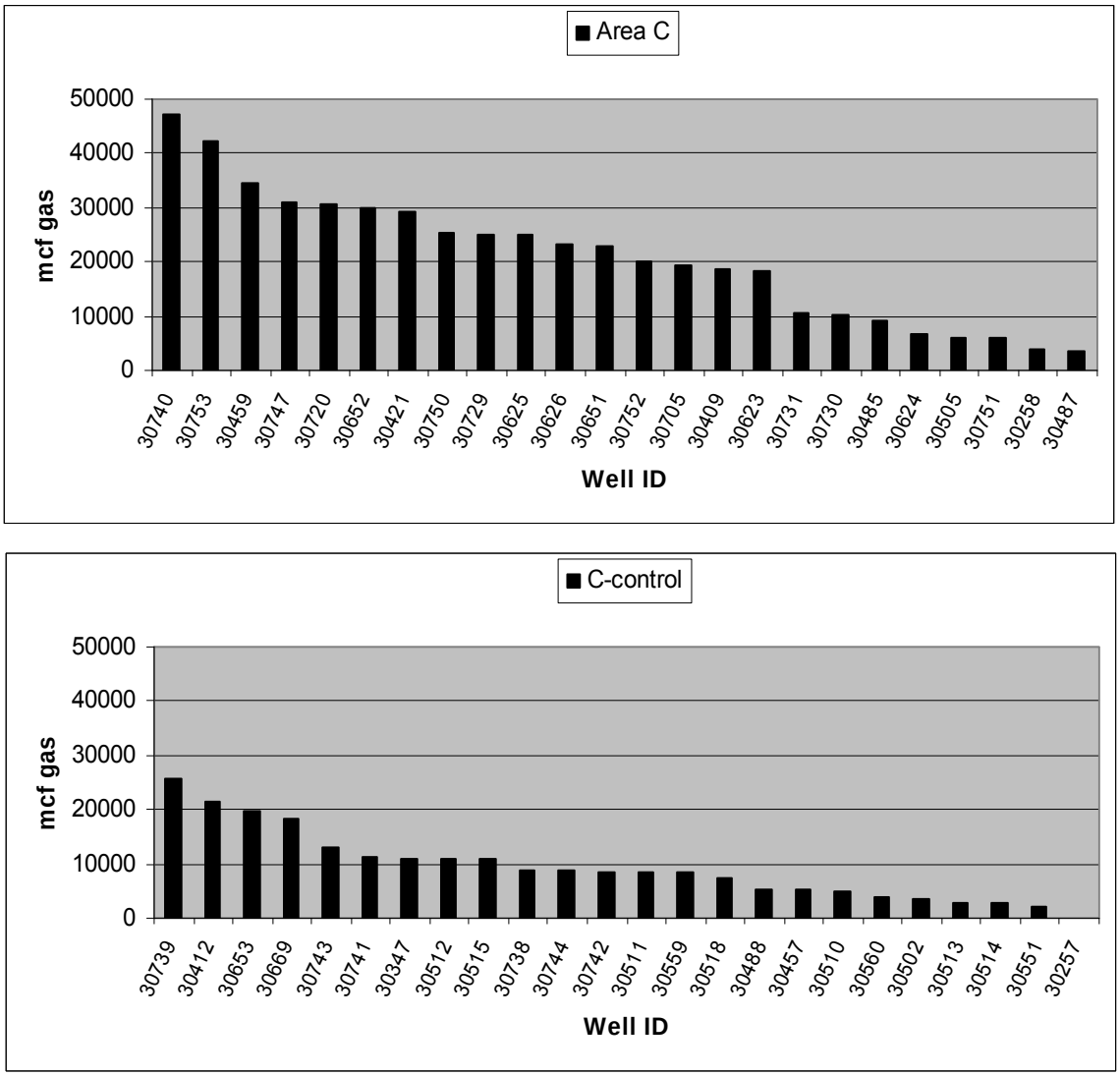

Figure 18: Gas production for areas C (upper) and C-control (lower).

The wells used in area D-control are: 43-015-30391, 30279, 30494, 30334, 30331, 30538, 30534, 30535, 30537, 30536, 30545, and 30546 (Figure 19).

There does not appear to be any difference in gas production between area D and area D-control. The average gas production in area D is 2,488 mcf (70 million m^3), and the gas production in area D-control is 2,163 mcf (61 million m^3). The

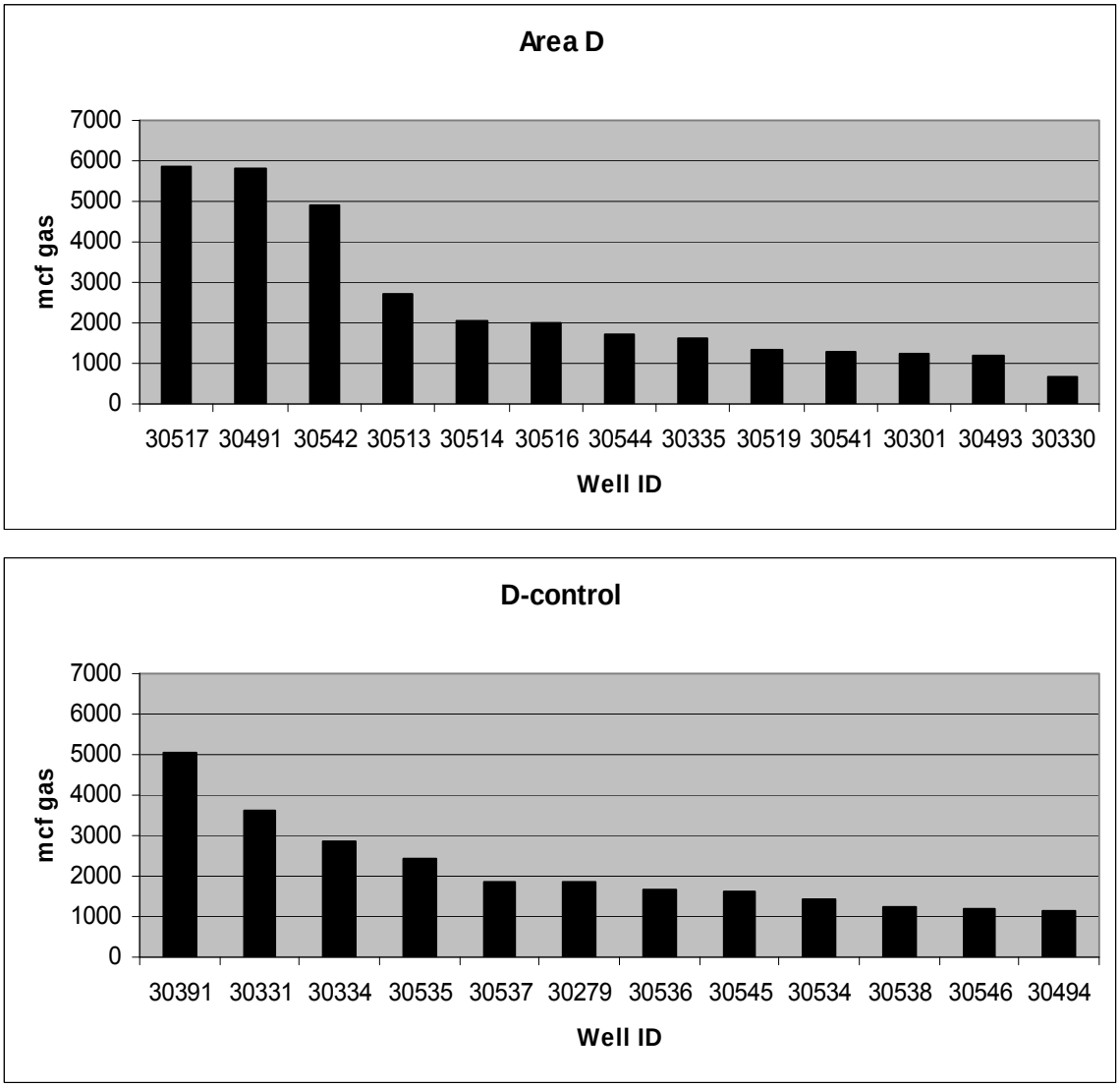

Figure 19: Gas production for areas D (upper) and D-control (lower).

highest gas production for the 24th month in area D is 5,850 mcf (166 million m^3), and that of area D-control is 5,067 mcf (143 million m^3). The average maximum water production does not appear to show any significant difference between area D and the associated control area. The average maximum water production for area D is 2,948 barrels (468,732 L), while the average maximum water production for area D-control is 2,631 barrels (418,329 L). The average 24-month cumulative water production for area D is 17,764 barrels (2,824,476 L) and for area D-control is 15,181 barrels (2,413,779 L). Maximum water production from a single well for area D is

12,151 barrels (1,931,854 L), while area D-control is only 7,831 barrels (1,245,029 L).

Faulted areas and control areas are compared using a Mann-Whitney statistical test in order to check for equivalence of the medians of the two sample sets. The Mann-Whitney test is the nonparametric equivalent of the parametric t-test (Davis, 2002). Using the Mann-Whitney test, U is found as shown in Equation 3. Then U is used in Equation 4 to find U':

$$U = n_1 \cdot n_2 + \frac{n_1(n_1 + 1)}{2} - R1 \quad \text{(Equation 3)}$$

$$U' = n_1 \cdot n_2 - U \quad \text{(Equation 4)}$$

where n_1 and n_2 (faulted and control areas, respectively) are the number of samples from each population. R1 is the sum of the ranks from each sample set, which is determined by ranking from highest to lowest the values when comparing the two populations (with the highest value receiving the highest rank), of which R1 is the sum of the ranks from the n_1 population. U' is then compared with tables which determine the probability of the two sample sets being statistically different. Kneedy (2005) did a similar analysis to verify that the age difference did not create an apparent production difference. Kneedy concluded that age does not account for the production differences he saw; hence, there must be some geologic explanation.

Table 10 shows the values calculated as part of the Mann-Whitney test, as well as the probability of significance between the two compared populations. Based on the results of the Mann-Whitney test, Areas A, B and C show a significant difference between faulted and control areas for both gas and water production (Table

10). The probability of exceedence is found to be between <0.003 and <0.0001 for gas production, whereas water production ranges between <0.05 to <0.0001. Areas D and D-control both show a probability of exceedence of <0.1. Thus Areas A, B and C are quite different statistically when compared to their associated control areas for both gas and water production, while D and D-control are not as statistically different from each other.

Table 10: Statistical analysis using the Mann-Whitney nonparametric test.

	Area	n_1	n_2	R1	U	U'	p
Gas	A	14	16	283	46	178	<0.003
	B	19	20	524	46	334	<0.0001
	C	24	24	750	126	450	<0.001
	D	13	12	171	76	80	<0.1
Water	A	14	16	251	78	146	<0.05
	B	19	20	505	65	315	<0.0001
	C	24	24	732	144	432	<0.003
	D	13	12	180	67	89	<0.1

Fault Seal Analysis

Three wells logs, one from each faulted area (Areas A, B and C), were selected to identify the net shale thickness surrounding the fault. Well 43-007-30428 was used for area A, well 43-007-30224 for area B, and well 43-007-30731 for area C. These three wells were selected based on their proximity to the three respective faults. The well log intervals chosen for interpretation were selected specifically to see the rocks above, below and within the Ferron Sandstone. Well logs were obtained from the UDOGM (2007) website (http://www.ogm.utah.gov) under the well log scans section of the oil and gas program. The standard well log suite is presented, including caliper, gamma ray, resistivity, neutron porosity (% porosity) and density porosity (% porosity); however, the log of interest is the gamma ray log as it

measures the higher radioactivity in shales and reveals a lower response for sandstone formations of lower radioactivity.

From area A the log for well 43-007-30428 from 2,200 ft to 2,800 ft (670 to 850 m) (measured depth) has 250 ft (76 m) that has been identified as a single “shale packet” at the top of the log, with interbedded sand and shale in the middle which becomes finer near the bottom (Figure 20). Thus, a shale thickness of 250 ft (76 m) has been interpreted from this log.

Well 43-007-30224 from area B from 1,700 to 2,200 ft (520 to 670 m) (measured depth) (Figure 21) shows 115 ft (35 m) of shales with a single, small sandstone lense found in this shale packet 15 ft (4.6 m) below the top of the section. Below this shale packet there are sands and shales interbedded with likely coal seams which remain undifferentiated. Fines are found on the bottom 75 ft (23 m) of the well log and are likely shales. Thus, a shale thickness of 190 ft (58 m) has been interpreted.

Well 43-007-30731 from area C from 2,850 to 3,500 ft (870 to 1,070 m) (measured depth) (Figure 22) appears to be almost exclusively shales in the top 380 ft (116 m), below which the interbedded sands and shales with likely coals (undifferentiated) can be found to the bottom of the well log. Thus, a shale thickness of 380 ft (116 m) has been interpreted.

Values for the maximum fault throw will be used in the clay smear algorithm as a conservative estimate, as larger throws tend to erode the shale veneer in the fault (Yielding et al., 1997). Fault throw as identified in the structural cross sections range from as much as 130 ft (40 m) in area B to as little as 13 ft (4 m) in area C (Table 8).

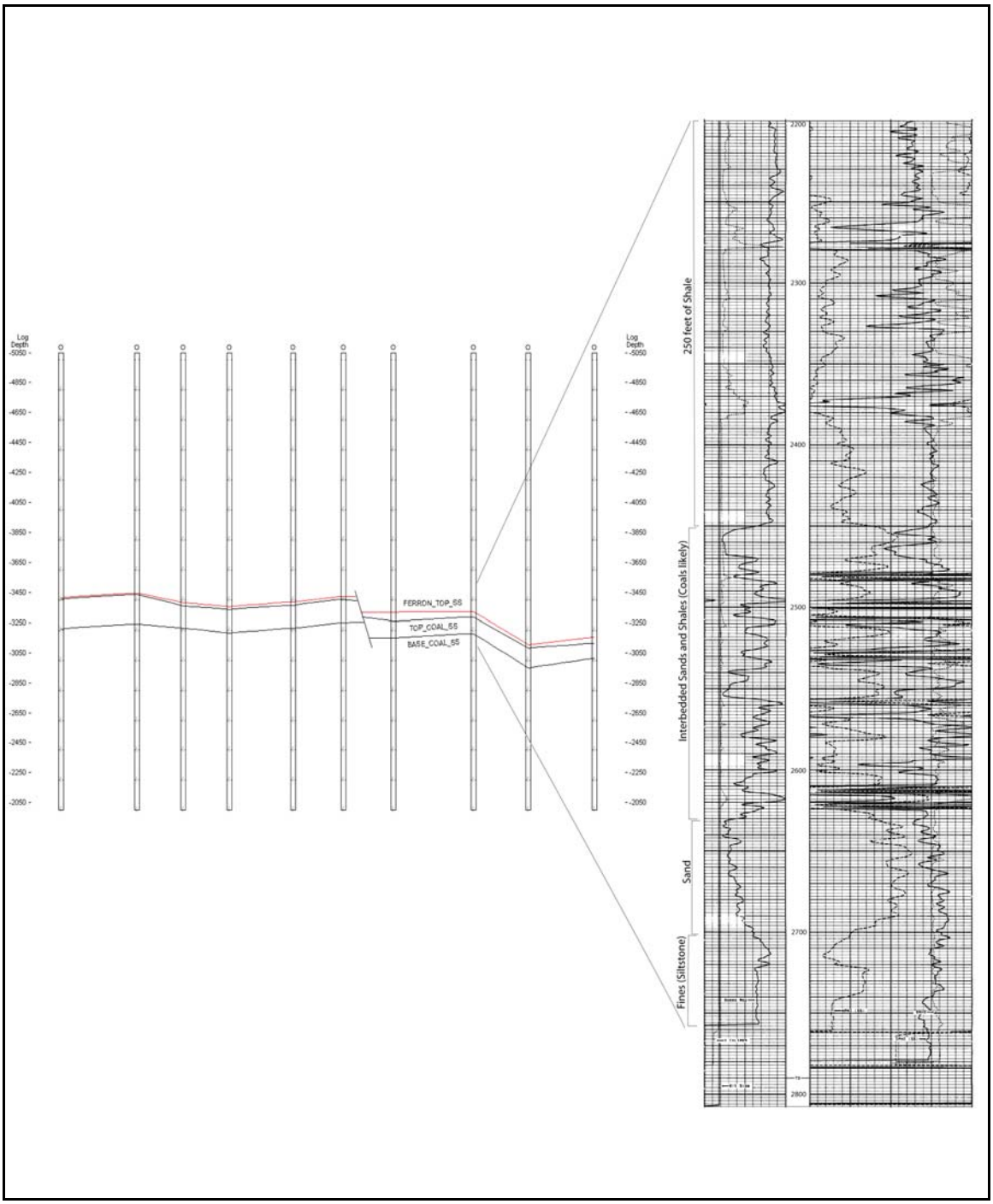

Figure 20: Interpreted log for well 43-007-30428 from area A

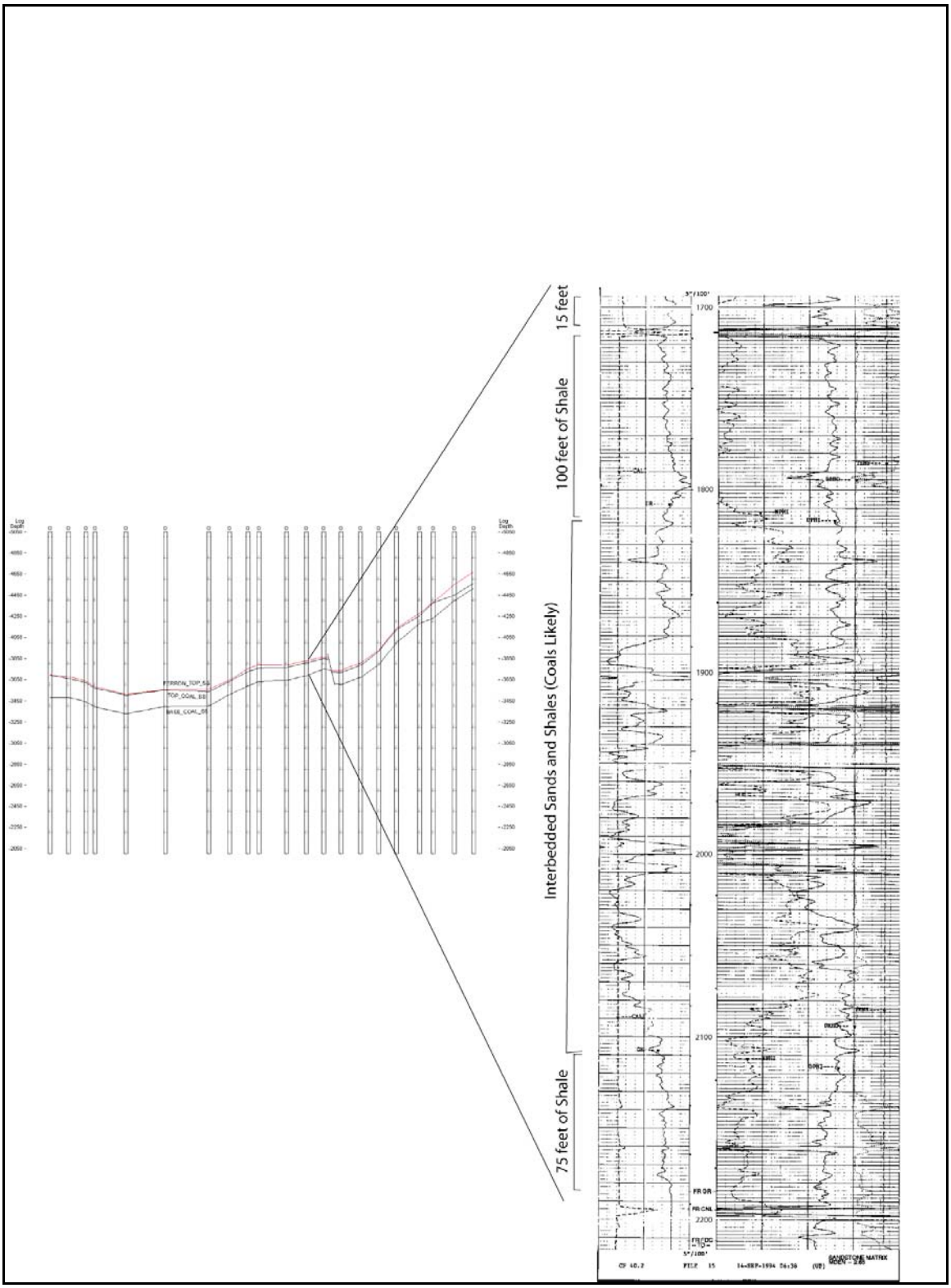

Figure 21: Interpreted log for well 43-007-30224 from area B.

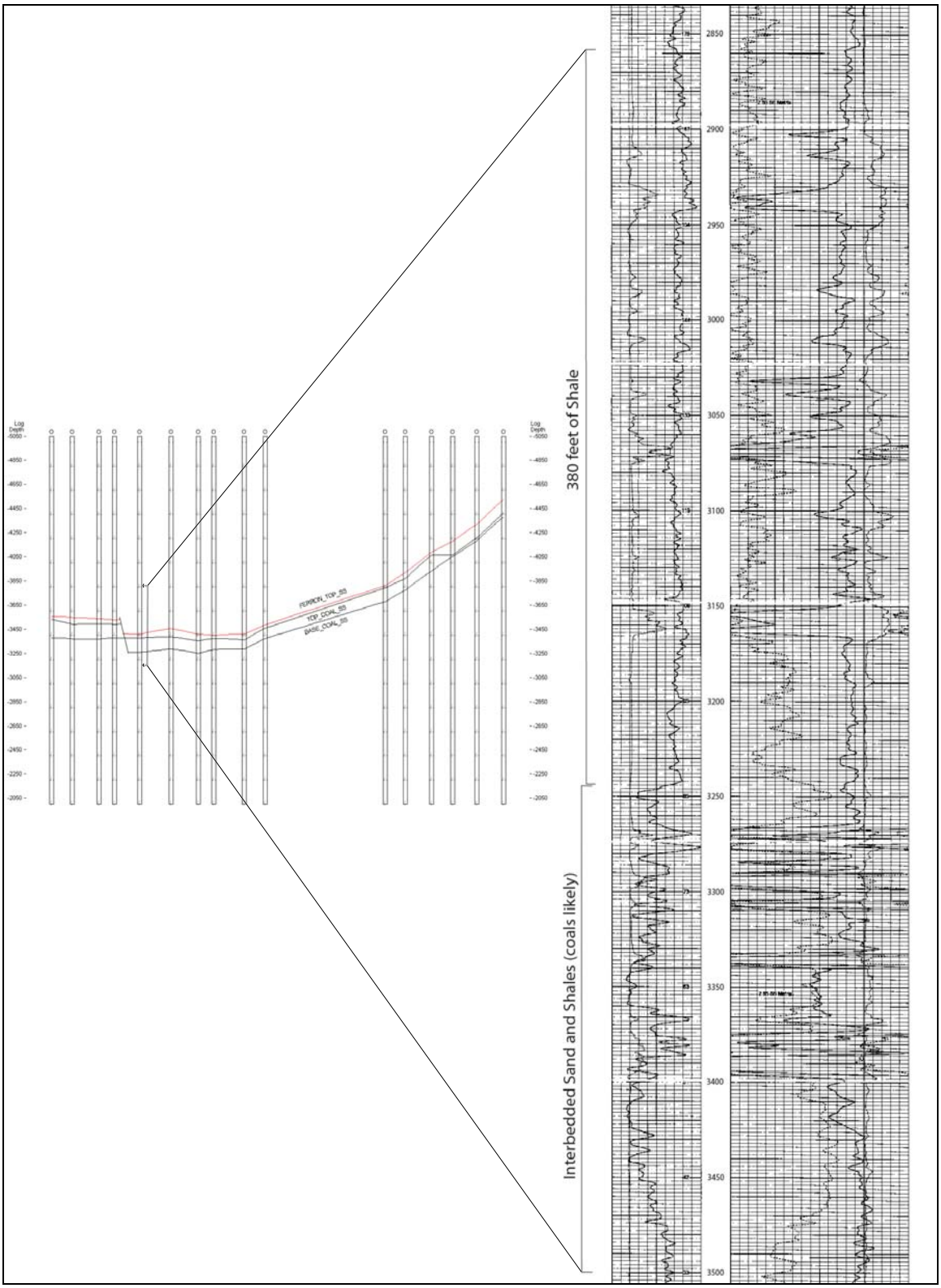

Figure 22: Interpreted log for well 43-007-30731 from area C.

The maximum fault throw in area A has been identified at 107 ft (33 m) in cross section B-B'. The maximum fault throw in area B is 130 ft (40 m) in cross section M-M', which is the largest fault throw identified in the Drunkards Wash gas field. The maximum fault throw in area C is 119 ft (36 m) in cross section S-S'.

Table 11 shows the SSF calculation using the maximum fault throw and shale thickness from each faulted area. Values for SSF from areas A, B and C are found to be less than one for all three faulted areas; thus, it can be presumed that the likelihood of fault sealing is quite high.

Table 11: Shale smear factor calculations

Area	Net Shale Thickness (ft)	Max Fault Throw (ft)	SSF
A	250	107	0.43
B	190	130	0.68
C	380	119	0.31

CHAPTER V

SUMMARY AND DISCUSSION

Hydrochemistry

Major and Minor Ions

With the exception of one shallow water-supply well (Well 4) the SWD wells and the shallow water-supply wells show dramatic differences in TDS and the concentrations of sodium and chloride. There are two possibilities to explain why Well 4 has such a high TDS concentration when compared to the other shallow water-supply wells: 1) deep disposal aquifers are hydraulically connected to the shallow aquifer in which Well 4 is completed, and mixing between aquifers is occurring as disposal waters are migrating through a preferential pathway of migration (e.g., faults or fracture zones), or 2) the geologic formation in which Well 4 is completed contains soluble salts and the dissolution of those salts is the source of the high TDS concentration.

I believe that the high TDS concentration found in Well 4 can be explained by the formation in which the well is completed, which is the Upper Blue Gate Shale Member of the Mancos Shale. Lines and Morrissey (1983) also demonstrated that water quality was poor from shales in the Mancos Shale, which contain large quantities of soluble sodium-sulfate minerals such as mirabilite and thenardite. They also state that TDS concentrations generally increase with increased time that water is in storage in the aquifer and in contact with the shales. In 1979 water in the Blue Gate contained about 20,000 mg/L of dissolved solids (Lines and Morrissey, 1983).

Historical records of chemical analyses for shallow, water-supply wells are presented in Tables 1 and 2, and show several wells with high TDS concentrations. Two

of those wells are identified as being completed in the Mancos Shale or the Blue Gate Member of the Mancos Shale. One of these wells, the location of which is identified as (D-13-9)25add-1 (Table 1) and is completed in the Blue Gate Member of the Mancos Shale, has a TDS concentration of 4,040 mg/L, with high sulfate, sodium and iron concentrations. The other well, the location of which is identified as (D-22-19)10cbb-1 (Table 2), is completed in the Mancos Shale, has a shallow sampling interval of 27 to 34 ft (8 to 10 m), and has high TDS of 6,964 mg/L and sulfate concentration of 3,505 mg/L (only concentrations of Ca, Cl, Mg, Na, and SO_4 are reported).

As for the other two wells, one, the location of which is identified as (D-19-21)29dbc-1 (Table 1), is exceptionally deep (4,760 feet [1,450 m]) and is completed in the Entrada Sandstone. This well has a TDS concentration of 6,810 mg/L, and is likely sampling old water thousands of feet below the Ferron Sandstone. Little is known about the other well, the location of which is identified as (D-18-14)9dcd-1 (Table 2), as it was sampled August 8, 1958 and is listed as being completed in alluvium and reports a TDS concentration of 4,290 mg/L and a sulfate concentration of 2,640 mg/L.

Major and minor ion and trace metal concentrations for the SWD wells (Table 7) are much higher for barium, boron, chloride, potassium, sodium, chloride, and phosphorus when compared to shallow, water-supply wells (Table 6). Concentrations for calcium, magnesium, manganese and sulfate are found to be higher for the shallow, water-supply wells, while the concentrations of copper, iron, nickel, silicon, strontium, and zinc show little differences between the two sets of wells.

The SWD wells have a high variability in concentrations for boron, barium, calcium, chloride, iron, magnesium, potassium, sodium, sulfate, silicon, strontium, and

TDS (Table 7). The high variability may be attributed to the varying amounts of water seeping in from rock units surrounding the Ferron Sandstone. As demonstrated by water production statistics, the areas around faults have a higher fracture density which allows for greater water production and increased water seepage into rock units with lower head. The variability seen in these wells may be due to the heterogeneity of the Ferron Sandstone aquifer, or water may be migrating downward from the overlying Upper Blue Gate Shale member of the Mancos Shale due to dewatering during CBM production. Water seeping in from overlying units may have higher concentrations of dissolved solids as the surrounding rocks are shales; thus, units with high rates of seepage may have high TDS concentrations, while units with little seepage may have lower TDS concentrations.

Stable Isotopes

Isotope data for D, ^{18}O and ^{13}C are more powerful tools than solute chemistry in determining if mixing between aquifers is occurring. Isotope data for D and ^{18}O are unambiguously distinct for the two types of water samples, as can be seen in Figure 12. Samples from shallow, water-supply wells plot very near the GMWL and have a range of -109 to -117 for δD and -13.8 to -15.1 for $\delta^{18}O$. Salt-water disposal well samples range from -40 to -90 for δD and -1.3 to -9.9 for $\delta^{18}O$. The source of recharge for the shallow, water-supply wells is likely local precipitation, while the water produced from the Ferron Sandstone (disposal waters) is likely old water from the overlying Upper Blue Gate Shale member of the Mancos Shale.

Values of $\delta^{13}C$ for the shallow, water-supply wells range from -3 to -11.3, and values for the SWD wells range from 14.2 to 28.3. The negative values for the shallow, water-supply wells indicate that the samples are isotopically light and are depleted in ^{13}C.

The source of the carbon is likely from the oxidation of organic matter or from the transport of CO_2 gas from the soil or atmosphere, both of which introduce relatively light carbon.

The SWD samples are all very high positive values indicating that they are abnormally heavy. Expected values range between -20 to -30 for coal relative to the PeeDee belemnite standard which is assigned a value of zero (Hunt, 1996). Dr. Dana Krueger of Geochron Laboratories was contacted to determine if there was an error in reporting the data without the negative sign. Dr. Krueger indicated that all equipment was checked previous to running the tests and that two samples were analyzed twice to confirm the results; thus, all results were reported correctly.

Dr. Krueger offered a possible explanation that if the SWD samples contained large amounts of carbon species (hydrocarbons), there might have been some interference in the measurement. For example, the cryogenic cleanup of CO_2 from groundwaters involves passing through a dry ice trap to remove water, then freezing it in liquid nitrogen and pumping off non-condensibles. The vapor pressure of propane is such that it might pass the first trap and be substantially retained in the second. Because the mass ratio 45/44 of propane is equivalent to approximately +2000‰ if calculated as δ13C of CO_2, the recovered CO_2 would only have to contain 1-2% propane to produce a 20-40‰ positive swing. However, propane does not naturally occur in a methane field. In order for propane to have caused such a large positive swing in the data the propane would have had to form elsewhere and migrated in from a different system.

Isotope studies of coalbed gases from the Drunkards Wash unit were performed to help determine the origin of the gas (Lamarre and Burns, 1997). The resulting data

suggest that a significant component of this gas has a biogenic source. Analyses of Drunkards Wash coalbed gases show δ13C values ranging from -45.59‰ to -50.07‰ for methane and +15‰ to +20‰ for carbon dioxide. These data imply mixing of biogenic and thermogenic gases in Ferron coals (Lamarre and Burns, 1997).

The isotope data provide additional evidence that the Upper Blue Gate Shale is the most likely source of the high TDS concentrations in Well 4. If the source of the high TDS in the water from Well 4 was from the migration of disposal waters, isotope data would necessarily show ratios that were more similar to values seen in the SWD wells, and would be outliers when compared with the other three shallow, water-supply wells, which is not the case (see Tables 6 and 7).

Structural Analysis

Cross Sections

The three faults identified using structural cross sections in the Drunkards Wash gas field are isolated in the subsurface and do not displace rocks at the surface, as no faults are identified in this area on a geologic map. The identification of these faults is important to this study, as faults would likely be the preferential pathway for the migration of fluids, specifically the disposal waters.

Fault A in the northern part of the Drunkards Wash gas field is identified in four cross sections with the maximum throw (107 ft [33 m]) in the northernmost cross section with a slight undulation in the middle of the fault which then tapers off to the south (Table 8).

Fault B is identified using six cross sections in the east-central portion of the Drunkards Wash gas field, which undulates slightly in the northern half, reaching a maximum displacement of 130 ft (40 m), then tapers off to the south.

Fault C is identified using seven cross sections in the west-central portion of the Drunkards Wash gas field with the least amount of displacement in the northern cross section (13 ft [4 m]), which increases consistently from one cross section to the next until reaching the maximum displacement of 119 ft (36 m) in cross section S-S' and then tapers off in the southern portion of the fault (Table 8). This fault likely continues to the south but is unidentifiable as the southern-most cross section represents the boundary of the Drunkards Wash gas field and can no longer be followed.

Gas and Water Production

Wells in all three faulted areas consistently show a statistically significant higher average 24th-month gas production when compared to wells in their respective control areas where no faults are thought to exist. This dramatic difference in gas production between faulted areas and control areas can be attributed to one or a combination of both of two factors: 1) fault-induced fractures and/or damage zones adjacent to the faults create a fracture network large enough to account for higher gas production, as CBM migrates through fractures to the wellbore once it is released from the coal micropores; or 2) the coal/gas content and the types of coal vary spatially in the gas field and the high productivity areas are a result of the variations in depositional environments. As no data are currently available regarding the coal/gas content or the types of coal and how either of these might vary throughout the Drunkards Wash gas field, it is necessary to rely on water production data to help determine which of these two options is most important. If

the amount of water produced from wells in the faulted areas and the control areas is similar, it would indicate that the coal types and/or gas content are controlling the observed differences in gas production between faulted and control areas.

Water production data reveal equally dramatic differences between wells in faulted areas and wells in their associated control areas. Cumulative 24-month water production for wells in faulted areas is three to nine times greater than for wells in the adjacent control areas (Table 9). The likely cause for these differences in gas and water production is that the faulted areas do in fact have associated fault-induced fractures and/or damage zones adjacent to them through which gas and water are being produced at greater quantities and higher rates.

Gas and water production from areas D and D-control are very similar to one another. Two possible explanations for this are: 1) little fracturing, if any, has occurred in area D from the deformation that produced the Huntington anticline, or 2) fracturing from the folding of the strata in the anticline is equally distributed between the areas D and D-control. However, when a comparison is made between the quantities of gas and water that are produced from both areas D and D-control and areas A, B and C, the quantities are much less in areas D and D-control, which likely indicates that little, if any, fracturing has occurred in area D.

Fault Sealing

The fault seal analysis performed for this study only took into account the shales within the Ferron Sandstone and slightly above the Ferron top and below the Ferron coals; thus, it represents a very conservative estimate, as it only accounts for a fraction of the shales present in the study area. The fault in area B has the greatest throw (40 m [130

ft]) of any fault in the Drunkards Wash gas field (see Table 8) and also uses the thinnest shale bed thickness (190 ft [58 m]) of any of the faulted areas as part of the SSF calculation (see Table 10) and still yields a value of 0.68, which implies a high likelihood of fault sealing.

The Upper Blue Gate Shale Member of the Mancos Shale, with a thickness ranging from 1,600 to 2,400 ft (490 to 730 m), overlies the Ferron Sandstone. This is an enormous thickness of shale compared to the thicknesses used in the SSF calculation. Underlying the Ferron Sandstone is the Tununk Shale Member of the Mancos Shale, with a thickness ranging from 400 to 650 ft (120 to 200 m). The possibility of disposal waters migrating through such a thick sequence of shale seems highly unlikely.

Conceptual Model

The four shallow water-supply wells which were sampled as part of this study are completed in materials ranging from alluvium to the Upper Blue Gate Shale Member of the Mancos Shale, and range in depth from tens of feet to 225 feet (Table 4). The source of recharge to the shallow, fresh-water aquifer(s) is likely from local precipitation on the lowlands area of Castle Valley and from higher topography such as the Wasatch Plateau (see Figure 23) and the San Rafael Swell. Rocks in the western portion of the study area, as well as to the west of the study area, are dipping gently to the east, which correlates with the dip of rocks found in the Wasatch Plateau. As described by Montgomerey et al. (2001), between Price and Castle Dale, groundwater flow is to the south, southwest (see Figure 6). Shallow groundwater discharges into Huntington Creek either directly or indirectly through springs. However, the amount of discharge, like the amount of

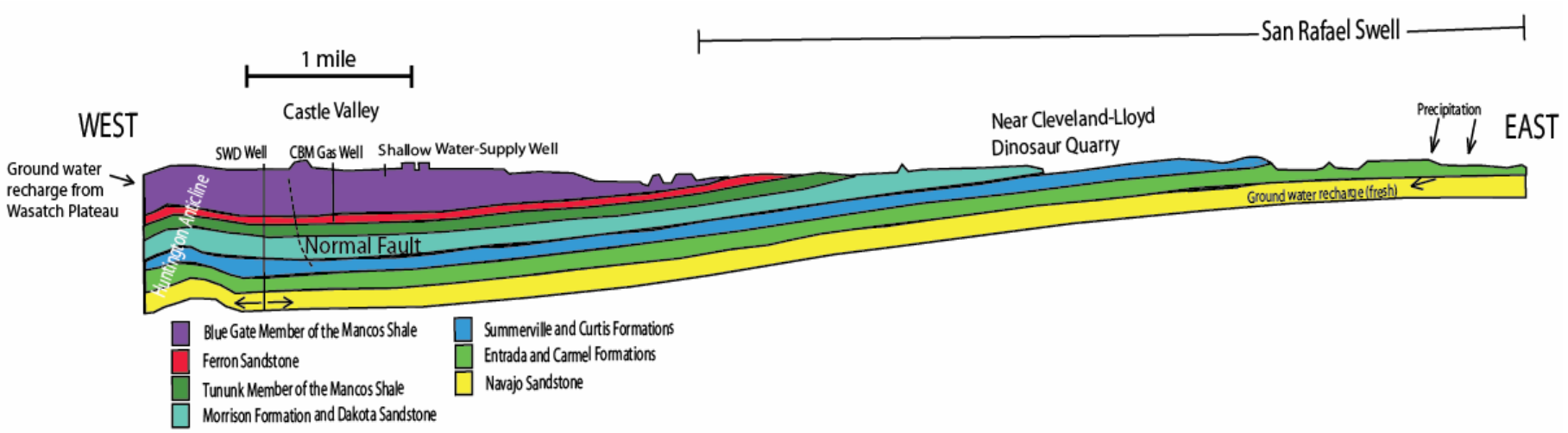

Figure 23: Conceptual model showing the shallow water-supply wells in the Upper Blue Gate Shale Member of the Mancos Shale, the deep SWD wells in the Navajo Sandstone and CBM producing zone in the Ferron Sandston, along with major structural features, including the San Rafael Swell to the east and the Huntington Anticline to the west.

recharge, is probably small, and most of the groundwater remains in storage due to the low hydraulic conductivity of the Upper Blue Gate Shale member of the Mancos Shale.

Rocks of the Mancos Shale (including the Ferron Sandstone) and the Navajo Sandstone (and presumably the Wingate Formation and Kayenta Sandstone) dip to the west in the eastern portion of the study area as a result of the deformation which formed the San Rafael Swell (Hood and Patterson, 1984). The source of recharge for water in the Navajo Sandstone is from the San Rafael Swell; however, the native water in the Navajo Sandstone in the study area is exceptionally high in TDS ranging from 46,690 to 217,264 mg/L (Table 3).

In the center of the study area the rocks are horizontal or nearly so, which represents the transition zone between the two major structural features, the Wasatch Plateau and the San Rafael Swell. The groundwater in the Navajo Sandstone in this portion of the study area has a hydrostatic surface ranging from 401 to 1,543 feet below land surface (Table 3), as discussed in Chapter II. The horizontal hydraulic gradient is likely very small compared to the vertical hydraulic gradient; thus, the groundwater appears to be stagnant and the Navajo Sandstone is simply storing water at depth with no apparent discharge to any surface water sources. The natural vertical hydraulic gradient is downward, as the water levels of the shallow water-supply wells range between 8 and 22 feet below the land surface (5,343 to 5,987 feet above sea level) while the original water levels in the Navajo Sandstone range from 401 to 1,543 feet below land surface (4,445 to 5253 feet above sea level) before injection began. The shallow water-supply wells have a higher head than that of the Navajo Sandstone and thus groundwater is migrating downward (albeit very slowly), and is likely dissolving soluble minerals during

this migration which is increasing the TDS as a function of depth, which eventually reaches a maximum as seen in the Navajo Sandstone (Table 3).

Injection of CBM disposal water into the disposal aquifers is reversing the vertical hydraulic gradient from downward to upward due to the injection pressures required to dispose of the saline waters. Injection pressures range from 1,350 to 2,000 psi (9,310 to 13,790 kPa) at the well heads of the nine salt-water disposal wells tested for this study (Table 12). Any sort of injection pressure at the surface results in an increased down-hole pressure felt at the bottom of the well, which would likewise result in a new hydrostatic surface for the Navajo Sandstone and a reversal in the direction of the vertical hydraulic gradient.

Table 12: Changes in water levels for SWD wells due to injection.

API Well Number	Max injection pressure at surface (psi)	Well Elevation (ft above sea level)	Water Elevation (ft above sea level)
43-007-30290	1,700	5,691	9,611
43-007-30314	1,350	5,733	8,846
43-007-30361	1,350	5,965	9,078
43-007-30555	1,350	5,678	8,791
43-007-30567	2,000	5,564	10,176
43-015-30272	1,750	5,988	10,023.5
43-015-30323	1,750	6,041	10,076.5
43-015-30338	1,700	5,827	9,747
43-015-30490	1,750	5,895	9,930.5

The new water-level elevations for the Navajo Sandstone range from 8,791 to 10,176 feet (2,679 to 3,102 meters) above sea level for the nine respective wells. The well with the highest water-level elevation is SWD well 43-007-30567 at 10,176 feet (3,102 meters) above mean sea level (Table 12). Likewise, SWD well 43-007-30555 has the lowest water-level elevation at 8,791 feet (2,679 meters) above mean sea level. The highest water-level elevation for any of the shallow water-supply wells is 5,752 feet (1,960 meters) above mean sea level in Well 4 (Table 13). Thus, the lowest water-level

elevation in the Navajo Sandstone is 3,039 feet (926 meters) higher than that in the highest shallow water-supply well (Figure 24). As the water levels in the Navajo Sandstone are significantly higher now that saline disposal waters are being injected into it, there exists a possibility that the reversal of the vertical hydraulic gradient may result in the disposal water eventually migrating upward into the shallow water-supply wells.

Table 13: Freshwater well elevations and depths to water.

Well Name	Well Elevation (ft above sea level)	Depth to Water (ft)	Water Level Elevation (ft above sea level)
1	5520	8	5512
4	5774	22.5	5751.5
20	5724	10	5714
24	5504	24	5480

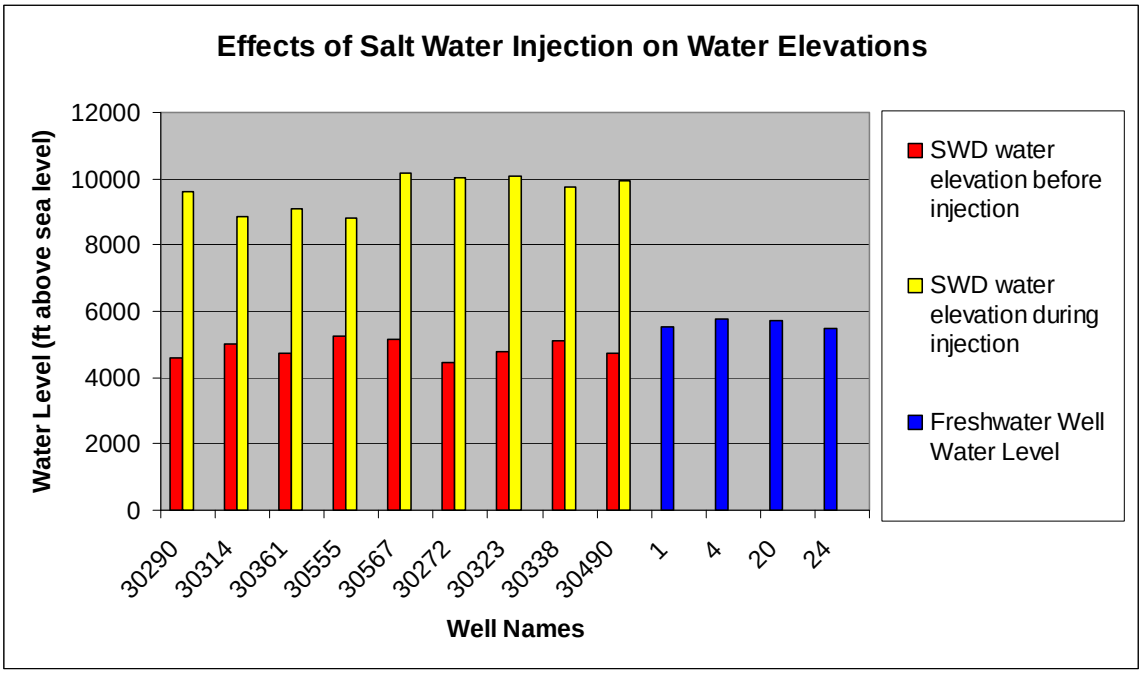

Figure 24: Effects of salt water injection on water level elevations.

By calculating the overall vertical hydraulic conductivity of the strata separating the disposal aquifers and the Upper Blue Gate Shale member of the Mancos Shale (surficial unit), an estimate can be made for the amount of time that could be expected for

the disposal water to migrate to the surface. The overall vertical hydraulic conductivity was conservatively estimated as 1.6 *10-5 meters/day using Equation 5 (Fetter, 2001):

$$K_v(avg) = \frac{b}{\sum(b_m/K_{vm})} \quad \text{(Equation 5)}$$

where $K_v(avg)$ is the overall vertical hydraulic conductivity, K_{vm} is the vertical hydraulic conductivity of the mth layer, b_m is he thickness of the mth layer and b is the total stratigraphic thickness. Table 14 shows the hydraulic conductivity values and thicknesses for each geologic unit that were used in estimating the overall vertical hydraulic conductivity. The hydraulic conductivity values were obtained from Driscoll (1986).

Table 14: Hydraulic conductivity and stratigraphic thickness approximations.

UNIT	K (m/day)	Thickness (ft)	Thickness (m)	Denominator
UBG SH	0.00001	1000	305	30,480,000
EMERY	1	600	183	183
LBG SH	0.00001	2000	610	60,960,000
FERRON	0.1	150	46	457
TUNUNK	0.00001	650	198	19,812,000
DAKOTA	0.01	15	5	457
CEDAR	0.0001	250	76	762,000
MORRISON	0.0001	400	122	1,219,200
SUMMER	0.0001	200	61	609,600
CURTIS	0.001	200	61	60,960
ENTRADA	0.1	250	76	762
CARMEL	0.0001	300	91	914,400
Sum		**6,015**	**1,833**	**114,820,019**

The overall vertical hydraulic conductivity is applied to Equation 6 (Fetter, 2001) to determine the groundwater velocity (v):

$$v = \frac{K(\Delta h/L)}{n_e} \quad \text{(Equation 6)}$$

where K is the overall vertical hydraulic conductivity and L is the distance separating the two aquifers; 6,015 feet (1,833 m) is used for this calculation. Delta h is the difference in

head between the maximum water level (3,102 m) of the injection wells during injection and the minimum water level elevation (1,670 m) for the freshwater wells. The minimum effective porosity (n_e) of the shale found in the study area is conservatively estimated as 0.005 as found in Driscoll (1986). Solving for time (t) is done by dividing the distance separating the two aquifers (L) by the velocity (v) calculated in Equation 3. Thus, the time can be estimated as 735,000 days or approximately 2,000 years. This amount of time required to push the disposal waters to the surface is much longer than the productive life of the CBM field.

Three faults and one anticline have been identified in the Drunkards Wash gas field from structural cross sections. These faults are the most likely potential conduits for the vertical migration of fluids in the study area and would be the only way in which the injection waters could migrate relatively quickly from the deep disposal aquifers to the shallow, fresh-water aquifers now that the vertical hydraulic gradient has been reversed. These faults were identified in the Ferron Sandstone member of the Mancos Shale; however, they do not displace rocks at the surface. It is unknown how high stratigraphically these faults extend upward. Likewise it is not known to what depth below the Ferron Sandstone these faults penetrate.

Between the shallow aquifers and the Ferron Sandstone are several thick packages of shale and sandstone contained in the Mancos Shale, which is exposed at the surface (see Figure 3). Between the Ferron Sandstone and the disposal aquifers are also several thick packages of shale as well as some clastic rocks (Figure 3). Based on the stratigraphy above and below the Ferron Sandstone, it is known that these three faults cut through several thick packages of shale, including the overlying Upper and Lower Blue

Gate Shale Members of the Mancos Shale as well as the underlying Tununk Shale, all of which will likely seal and retain their cap-like characteristics when faulted as was demonstrated using the shale smear factor (SSF) calculations in the fault seal analysis portion of this study.

CHAPTER VI

CONCLUSIONS, IMPLICATIONS AND RECOMMENDATIONS

Conclusions

Three of the four shallow, water-supply wells have low TDS concentrations, demonstrating that no mixing is occurring. As for Well 4, its high TDS concentration can be explained by the dissolution of soluble minerals found in the Upper Blue Gate Shale Member of the Mancos Shale (Lines and Morrissey, 1983), the formation in which the well is completed.

Based on the hydrochemical data, there are at least two separate aquifer systems. The shallow, water-supply wells are separated from the deep, disposal aquifer system by thousands of feet of sedimentary rocks including, but not limited to sandstone, coal, shale, limestone and siltstone. The hydrochemical data show that water from the shallow, water-supply wells and water produced from the Ferron Sandstone and injected into the Navajo, Wingate and/or Kayenta are from different sources and that no mixing appears to be occurring between the shallow, fresh-water aquifer(s) and the disposal aquifers.

Delta-deuterium and $\delta^{18}O$ values, when plotted in comparison with the GMWL, show a noticeable difference between the shallow, water-supply wells and the SWD wells. The shallow, water-supply wells plot very near the GMWL, implying local precipitation is the likely source of recharge. However, the SWD wells plot far from the GMWL, implying that the source of recharge is likely not from recent precipitation, but is likely old water as can be seen from the evaporative trend (Figure 13).

It is unfortunate that a more robust data set could not be gathered for the shallow, water-supply wells. Having only four wells from a study area of this size does not

provide the desired coverage that was originally sought after. However, on the positive side, the four shallow, water-supply wells cover a wide area, as one well was sampled in the northern part of the study area, two were sampled in the middle, and one was sampled near the southwestern boundary. Caution should be exercised when drawing any conclusions based exclusively on chemistry data with such a limited data set such as this. However, the structural analysis combined with the implications of the chemical data provide strong evidence that the disposal waters have not yet migrated to the shallow, fresh-water aquifers, yet with the reversal of the vertical hydraulic gradient it may be possible in the future to see evidence of migration occurring between the two aquifer systems.

Three north-south trending faults which are not visible at the surface were discovered within the Drunkards Wash gas field from structural cross sections prepared from digital well logs for 479 wells. These three faults appear to have associated damage zones which allow much greater production of gas and water when compared to control areas nearby which lack faults. A hydraulic connection between the shallow, water-supply wells and the deep, disposal aquifer is highly unlikely as the three faults show a high likelihood of sealing. The faulted rocks are sandstone, coal and, most important for fault sealing, thick sequences of shale. Fault seal calculations indicate that large amounts of shale should be entrained in the fault zone, creating high entry pressures and effectively sealing the faults.

Fault seal calculations were done using relatively small amounts of shale when compared to the overall amount of shale found in the stratigraphic section. The Lower Blue Gate Shale Member of the Mancos Shale, which overlies the Ferron Sandstone,

varies in thickness between 1,600 and 2,400 ft (490 and 730 m). The Tununk Shale Member of the Mancos Shale, below the Ferron Sandstone, varies in thickness between 200 and 300 ft (120 and 180 m). The likelihood of fluids migrating through shale sequences of these thicknesses is highly unlikely, based on the comparatively small values used for shale thickness in the fault seal calculations.

Comparison of the chemical results from the shallow, water-supply wells and the SWD wells, indicates that it is unlikely any mixing has yet occurred between the disposal aquifers and the shallow aquifer(s). However, due to the pressures required to inject the disposal waters into the Navajo Sandstone it is possible that mixing may eventually occur, as the vertical hydraulic gradient has changed from downward to upward. The change in vertical hydraulic gradient implies that the disposal waters are being pushed upward, even through the confining layers, and given sufficient time, could be pushed to the surface.

Implications

Implications for this study include:

1) Based on the data obtained to date, the deep disposal aquifers and the shallow, fresh-water aquifer(s) are not hydraulically connected either directly or through non-sealing faults.
2) Given sufficient time the disposal waters could be pushed through the geologic materials which separate the disposal aquifers and the shallow water-supply wells, including the confining shale layers. However, based on calculations shown above the amount of time required (2,000 years) to force the disposal waters up through thousands of feet of sedimentary rocks is beyond the productive life of the CBM

field, and thus the chance of disposal waters reaching the surface due to the reversal of the vertical hydraulic gradient is highly improbable.

3) The methods currently being utilized by Anadarko Corporation, ConocoPhillips, and XTO Energy to dispose of the class II UIC waters appear to be safe and to date have not proven to leak disposal waters to the shallow aquifers utilized for water-supply wells.
4) The injection of waters produced from the Ferron Sandstone into the disposal reservoirs is likely resulting in a slight dilution of the more saline waters present in the injection zones.
5) Sequestering CO_2 along with the disposal waters in the Navajo Sandstone may be feasible, as CO_2 is very likely to be contained in these aquifers based on the thicknesses of shale which overlies the disposal aquifers. Further investigation of this is recommended, as the cap rock properties are one of several factors to consider when sequestering CO_2.

Recommendations for Further Work

This study suggests that the disposal waters being injected into the Navajo Sandstone are in fact being contained at depth and that there is little likelihood that they will be migrating out of the Navajo, Kayenta and Wingate disposal aquifers at any point in the foreseeable future. Based on this conclusion, it is unnecessary to spend more time attempting to identify other shallow, water-supply wells in the area to sample (if any others even exist). Likewise, a re-evaluation of the geologic investigation performed herein would not be useful, unless new geologic information, such as seismic data collected by the energy companies, were to become available. The chances of that

happening are very remote, as the fields are well established and the cost of gathering this type of data is too expensive to justify its collection in a CBM gas field.

Future work to be performed in this study area should include investigations into the feasibility of using the Navajo Sandstone for the sequestration of CO_2 as a way of mitigating the amount of greenhouse gases emitted into the atmosphere. Three tasks should be performed in the order presented below:

1) Chemical modeling - A mixing model should be created in which a computer simulation evaluates the compatibility of the injected Ferron Sandstone disposal water and/or the Navajo, Kayenta, and Wingate Sandstone brines with respect to CO_2 saturation. This simulation should take into account the potential for mineral precipitation as the native disposal waters and the native groundwaters are mixed in various ratios under assumed downhole conditions (i.e., temperatures and pressures).

In 1998, the Utah Geological Survey (UGS) performed computer simulations using PHRQPITZ™ to evaluate the mixing between disposal waters and the waters found in the Navajo Sandstone (Gwynn, 1998). Ferron Sandstone water samples were collected from the open evaporation pond and analyzed after they had been cooled, aerated and degassed. Carbonate-mineral precipitation may have taken place as well. Therefore, the chemistry of the samples used in the UGS study is probably different from that of samples collected immediately after emerging from the well or the water-gas separator (Gwynn, 1998). The predictions made using the UGS data are questionable for this reason. Likewise, other geochemical computer programs, such as SOLMINEQ-88™, may model the brine-mixing scenario better than PHRQPITZ™ (Gwynn, 1998).

2) Laboratory experiments on the Navajo Sandstone - Using representative rock and water samples of the Navajo Sandstone, laboratory experiments should be performed in which a mixture of CO_2, disposal water, and native Navajo Sandstone water are all combined in a cylinder which can withstand simulated downhole pressures and temperatures. After letting the briney mixture "cook" for a reasonable amount of time (perhaps weeks to months), thin sections of the Navajo Sandstone can be made and analyzed for mineral precipitation. Of course this would require a before and after comparison, as thin sections will also need to be made before beginning the laboratory experiment. Another possible way of analyzing the potential mineral precipitates is to use X-ray diffraction (XRD) of the Navajo Sandstone before and after the proposed laboratory experiment.

3) Drill one or two CO_2-sequestration test well(s) in the Drunkards Wash gas field - Based on favorable results from the chemical modeling and laboratory precipitation experiment, one or two test wells should be drilled for the purpose of testing the suitability of the Navajo Sandstone for CO_2 sequestration. Upon injection of CO_2, or any other easily detectable gas, into the disposal aquifers, regular monitoring of shallow wells surrounding the test well should be performed to determine if CO_2 is leaking to the surface via faults. One or more monitoring wells may need to be installed as part of this experiment, as the number of shallow, water-supply wells available is limited.

Three options exist regarding where to place the CO_2 sequestration test wells: 1) the test well should be located near one of the faults identified in this study; 2) the test well should be located far away from all of the faults identified in this study, but still in

the study area so as to not drill next to a fault which could not be identified as part of this study; 3) two test wells should be drilled, one near a fault and one far away.

Locating the test well near one of the faults would be done in order to test the reservoir for its storage integrity as an engineering failure study. The ideal location for this test well would be near fault B, somewhere between cross sections M-M' and N-N', as they have the maximum fault throw identified in the study area; thus, they have the greatest likelihood of leaking CO_2 in the near future. However, if it were not possible to drill into fault B, then drilling close to the areas of maximum fault throw for faults A or C would also be suitable locations to test the sealing capacity of one of these faults.

Locating the test well far away from the faults would be done in order to avoid, as much as possible, the possibility of failure. The ideal location for this purpose would be near the crest of the anticline, as this structure is most likely to contain the CO_2 for long periods of time, assuming no migration to faulted areas occurs.

I believe the ideal situation would be to drill two wells, one well near a fault and the other far away from faulted areas. However, if that is not economically possible, and only one well can be drilled, I believe the ideal test would be to drill near a fault and test the reservoir for its storage integrity as an engineering failure study. This would demonstrate the reservoirs' integrity if CO_2 is shown to not leak.

REFERENCES CITED

Allis, R., Chidsey, T., Gwynn, J., Morgan, C., White, S., Adams, M. and Moore, J. (2001) Natural CO_2 reservoirs on the Colorado Plateau and southern Rocky Mountains: candidates for CO_2 sequestration. First National Conference on Carbon Sequestration, U.S. Department of Energy, National Energy Technology Laboratory, Washington, D.C., pp.19.

Armstrong, R.L. (1968) Sevier orogenic belt in Nevada and Utah. Geol. Soc. of Am. Bull. **79**, 429-458.

Asquith, G. and Krygowski, D. (2004) Basic Well Log Analysis. AAPG Methods in Exploration Series, No. 16. American Association of Petroleum Geologists, Tulsa.

Bergman, P.D. and Winter, E.M. (1995) Disposal of carbon dioxide in aquifers in the U.S. Energy and Conv. Man. **36**, 523-526.

Bouvier, J.D., Kaars-Sijpesteijn, C.H., Kluesner, D.F., Oneyejekwe, C.C. and Van Der Pal, R.C. (1989) Three-dimensional seismic interpretation and fault sealing investigations, Nun River Field, Nigeria. Am. Assoc. of Pet. Geol. Bull. **73** (11), 1397-1414.

Brownlow, A.H. (1996) Geochemistry. Prentice Hall, Upper Saddle River.

Craig, H. (1961) Isotopic variation in meteoric waters. Science **133**, 1702-1703.

Davis, J.C. (2002) Statistics and Data Analysis in Geology. John Wiley & Sons, New York.

Drever, J.I. (1997) The Geochemistry of Natural Waters: Surface and Groundwater Environments. Prentice Hall, Upper Saddle River.

Driscoll, F.G. (1986) Groundwater and Wells. Johnson Filtration Systems, Inc., St. Paul.

Energy Information Administration (2002) U.S. crude oil, natural gas liquid reserves. Annual Report, Appendix B. U.S. Department of Energy, Washington, D.C. Available from: <http://www.eia.doe.gov/pub/oil_gas/data/publications/crude>.

Faure, G. (1986) Principles of Isotope Geology. John Wiley & Sons, New York.

Fetter, C.W. (2001) Applied Hydrogeology. Prentice Hall, Upper Saddle River.

Gale, J. (2002) Geological storage of CO_2: what's known, where are the gaps and what more needs to be done. 6th International Conference on Greenhouse Gas Technologies, Kyoto. Available from <http://www.ieagreen.org.uk/ghgt6%20papers/GHGT61.pdf>.

Garrison, J.R., Jr., Van Den Bergh, T.C.V., Barker, C. and Tabet, D.E. (1997) Depositional sequence stratigraphy and architecture of the Cretaceous Ferron Sandstone: Implications for coal and coalbed methane resoureces-A field excursion. BYU Geol. Stud. **42** (II), 155-200.

geoPLUS Corporation (1996-2005) PETRA Computer Contouring and Structural Cross-Sections.

Gwynn, J.W. (1998) Potential mineral precipitation and water compatibilities related to the Drunkards Wash Project, Carbon, County, Utah. Report of Inv. 241. Utah Geological Survey, Salt Lake City.

Hawley, C.C., Robeck, R.C. and Dyer, H.B. (1968) Geology, altered rocks, and ore deposits of the San Rafael Swell, Emery County, Utah. USGS Bull. 1239. U.S. Geological Survey, Washington, D.C.

Herzog, H. (1997) CO_2 capture, reuse, and storage technologies for mitigating global climate change. White Paper Final Report, DOE Order No. DE-AF22-96PC01257. U.S. Department of Energy, Washington, D.C.

Hintze, L. F. (1988) Geologic History of Utah, A field guide to Utah's rocks. BYU Geol. Stud., Spec. Pub. 7. Brigham Young University, Provo, pp. 169-170.

Holloway, S. and van der Straaten, R. (1995) The Joule II project: The underground disposal of carbon dioxide. Energy and Conv. Man. **36**, 519-522.

Hood, J.W. and Patterson, D. J. (1984) Bedrock aquifers in the northern San Rafael Swell area, Utah, with special emphasis on the Navajo Sandstone. Tech. Pub. No. 78. Utah Department of Natural Resources, Salt Lake City.

Hunt, C.B. (1956) Cenozoic geology of the Colorado Plateau. USGS Prof. Paper 279. U.S. Geological Survey, Washington, D.C.

Hunt, J.M. (1996) Petroleum Geochemistry and Geology. W.H. Freeman and Company, New York.

Kneedy, J.L. (2005) Stratigraphic and structural analysis of coal in the Ferron Sandstone member of the Mancos Shale and Fruitland Formation: Relationship to coal reservoir permeability and coalbed methane production. M.Sc. Thesis, Utah State University, Logan, Utah.

Knipe, R.J. (1992) Faulting processes and fault seal. In Structural and Tectonic Modeling and its Application to Petroleum Geology (eds. R.M. Larsen, H. Brekke, B.T. Larsen and E. Talleras). Elsevier, Amsterdam, pp. 325-342.

Lamarre, R.A. and Burns, T.D. (1997) Drunkards Wash project: coalbed methane production from Ferron coals in east-central Utah. In Innovative Applications of Petroleum Technology in the Rocky Mountain Area (eds. E.B. Coalson, J.C. Osmond and E.T. Williams). Rocky Mountain Association of Geologists, Denver, pp. 47-559.

Lindsay, N.G., Murphy, F.C., Walsh, J.J. and Watterson, J. (1993) Outcrop studies of shale smears on fault surfaces. In Spec. Pub. of the Int. Assoc. of Sed. **15**, 113-123.

Lines, G.C. and Morrissey, D. J. (1983) Hydrology of the Ferron Sandstone aquifer and the effects of proposed surface-coal mining in Castle Valley, Utah. USGS Water-Supply Paper 2195. U.S. Geological Survey, Washington, D.C.

Montgomery, S.L., Tabet, D.E. and Barker, C.E. (2001) Upper Cretaceous Ferron Sandstone: Major coalbed methane play in central Utah. Am. Assoc. of Pet. Geol. Bull. **85** (2), 199-219.

Newman, K.F. and Chan, M.A. (1991) Depositional facies and sequences in the upper Cretaceous Panther Tongue Member of the Star Point Formation, Wasatch Plateau, Utah. UGA Pub. 19. Utah Geological Association, Salt Lake City, pp. 65-76.

Piper, A.M. (1944) A graphic prodecure in the interpretation of water analyses. Am. Geophys. Union Trans. **25**, 914-923.

Rice, C.A. (1999) Waters co-produced with coalbed methane from the Ferron Sandstone in east-central Utah: chemical and isotopic composition, volumes, and impacts of disposal. GSA Abs. with Prog. 31. Geological Society of America Annual Meeting, Denver, Colorado. #6245 (abstr).

Ryer, T.A. (1981) Deltaic coals of the Ferron Sandstone Member of the Mancos Shale: Predictive model for Cretaceous coal-bearing strata of the western interior. Am. Assoc. of Pet. Geol. Bull. **65**, 2323-2340.

Sheppard, S.M.F. (1986) Characterization and isotopic variations in natural waters. In Stable Isotopes in High Temperature Geological Processes (eds. J.W. Valley, H.P. Taylor, Jr. and J.R. O'Neil). Mineralogical Society of America, Washington, D.C. pp. 165-183.

Sumsion, C.T. (1979) Selected coal-related groundwater data, Wasatch Plateau-Book Cliffs area, Utah. Utah Hydrologic Data Report No. 32. USGS Open-File Report 79-915. U.S. Geological Survey, Salt Lake City.

Tabet, D.E. (1998) Migration as a process to create abnormally high gas contents in the Ferron Sandstone coal beds, central Utah. AAPG Abs. with Prog. American Association of Petroleum Geologists Annual Convention, Tulsa. #A646 (abstr.).

Tearpock, D. J. and Bischke, R.E. (2003) Applied Subsurface Geological Mapping with Structural Methods. Prentice Hall, Upper Saddle River.

Tripp, C.N. (1991) Wasatch Plateau oil and gas fields, Carbon, Emery, and Sanpete counties, Utah. UGA Pub. 19. Utah Geological Association, Salt Lake City, pp. 255.

Waddell, K.M., Contratto, P.K., Sumsion, C.T. and Butler, J.R. (1978) Selected hydrologic data from 1931-1977 of the Wasatch Plateau-Book Cliffs Coal-Fields area, Utah. Utah Basic Data Release No. 31. USGS Open-File Report 78-121. U.S. Geological Survey, Salt Lake City.

Waddell, K.M., Contratto, P.K., Sumsion, C.T. and Butler, J.R. (1981) Hydrologic Reconnaissance of the Wasatch Plateau – Book Cliffs Coal – Fields Area, Utah. USGS Water-Supply Paper 2068. U.S. Geological Survey, Washington, D.C.

Witkind, I.J. (1988) Geologic map of the Huntington 30' X 60' quadrangle, Utah. USGS Geol. Map I-1764. U.S. Geological Survey, Washington, D.C.

White, S.P., Allis, J., Moore, J., Chidsey, T., Morgan, C. and Gwynn, M.A. (2003) Injection of CO_2 into an unconfined aquifer located beneath the Colorado Plateau, central Utah, USA. Second Annual Conference on Carbon Sequestration. U.S. Department of Energy, National Energy Technology Laboratory, Alexandria, pp. 15.

Yielding, G., Freeman, B. and Needham, D.T. (1997) Quantitative fault seal prediction. Am. Assoc. of Pet. Geol. Bull. **81** (6), 897-917.

APPENDICES

Appendix A: Interpreted well logs

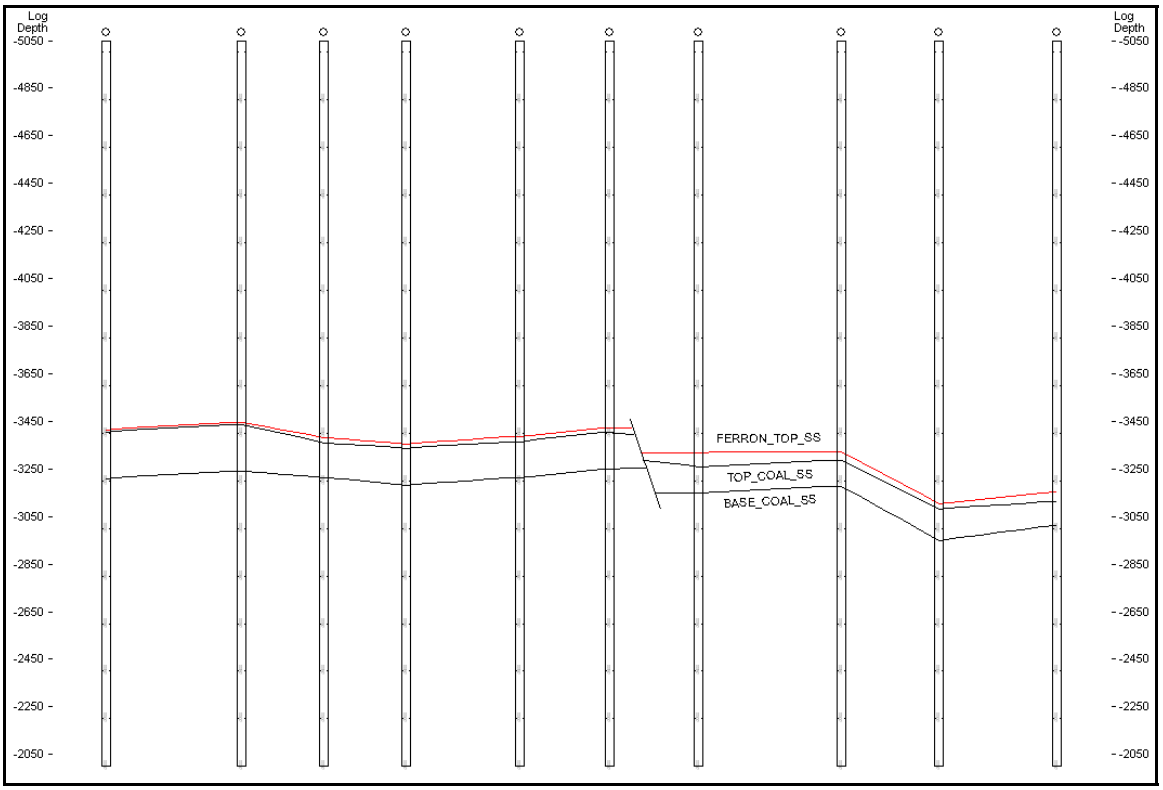

Figure 25: Cross section B-B' with interpreted fault.

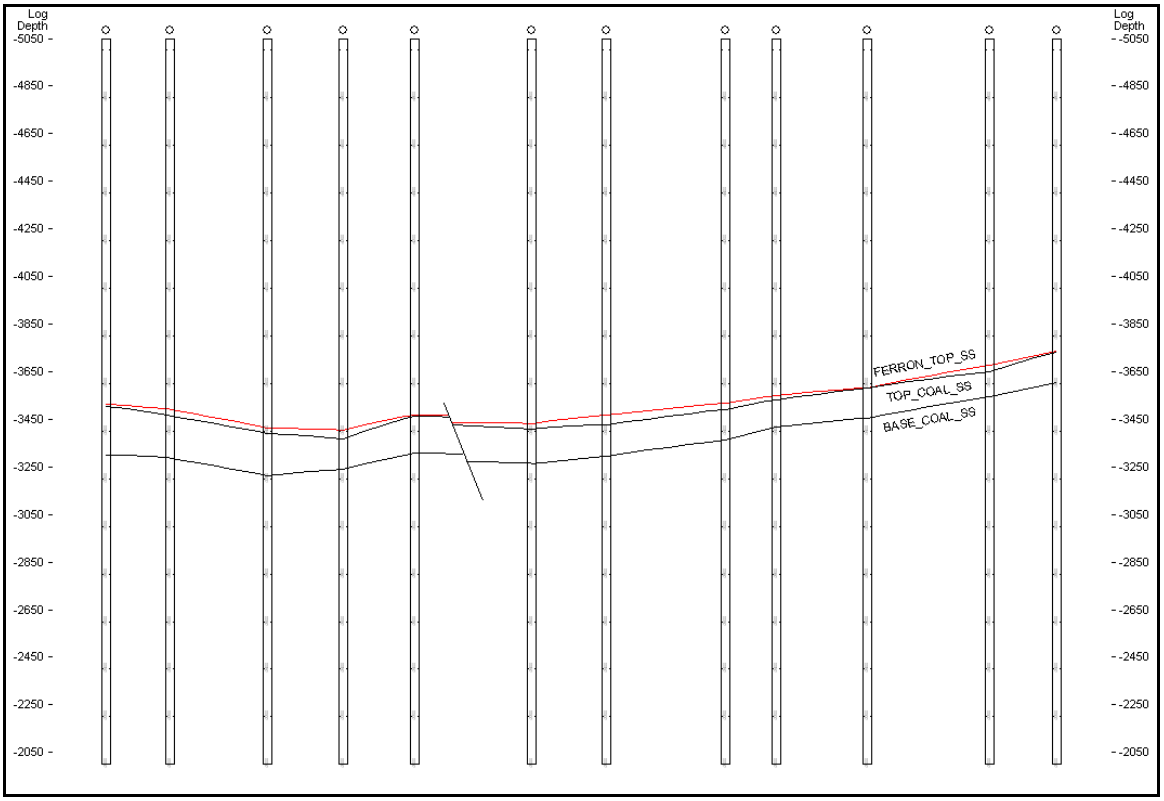

Figure 26: Cross section C-C' with interpreted fault.

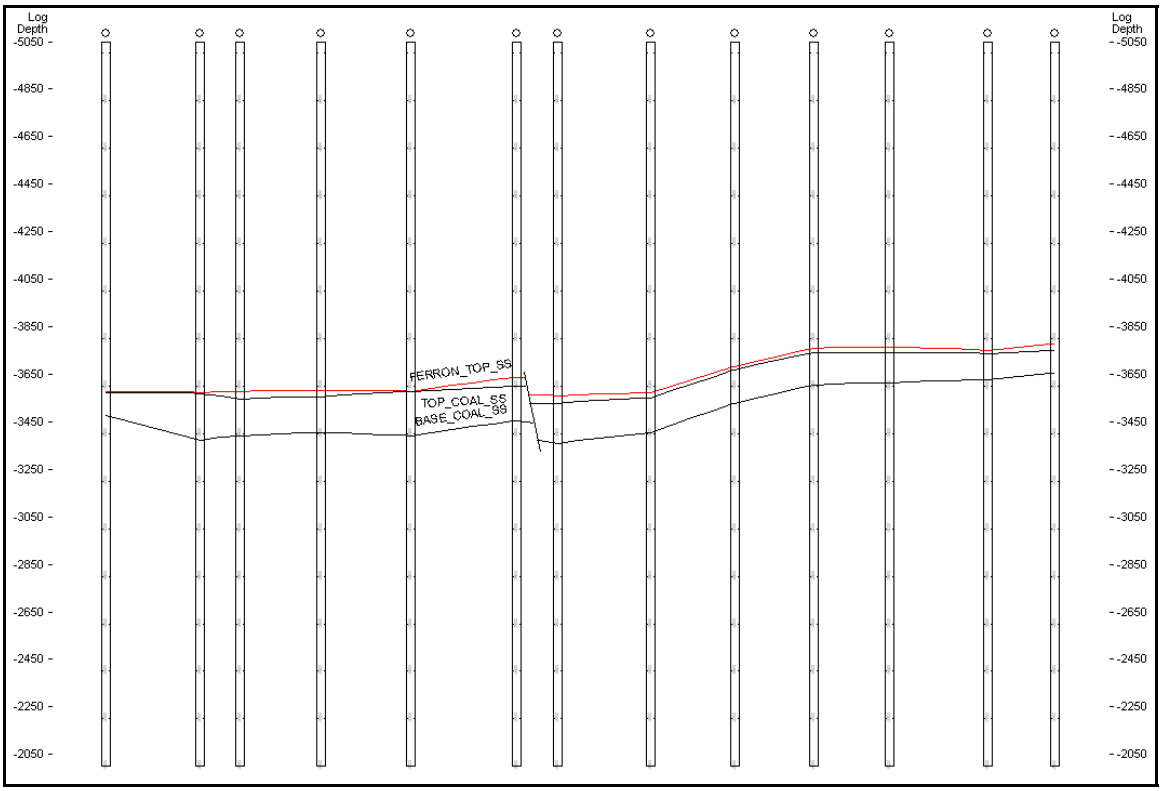

Figure 27: Cross section D-D' with interpreted fault.

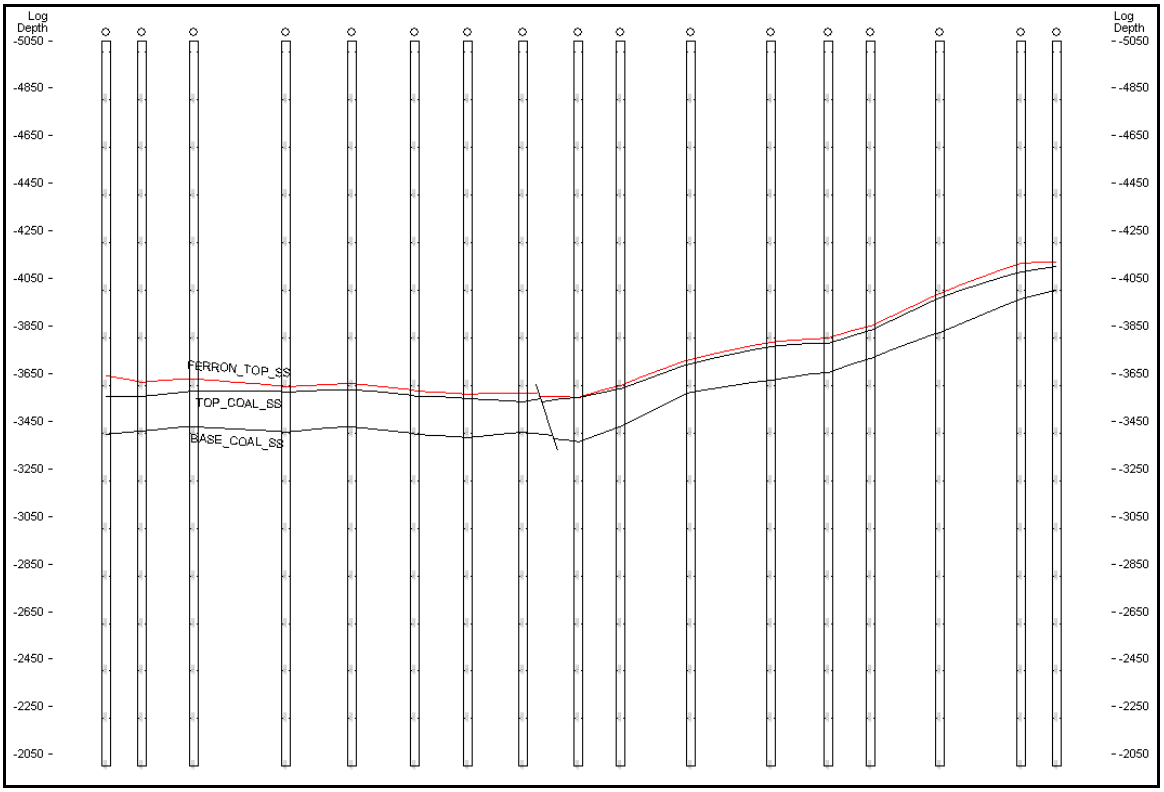

Figure 28: Cross section E-E' with interpreted faults.

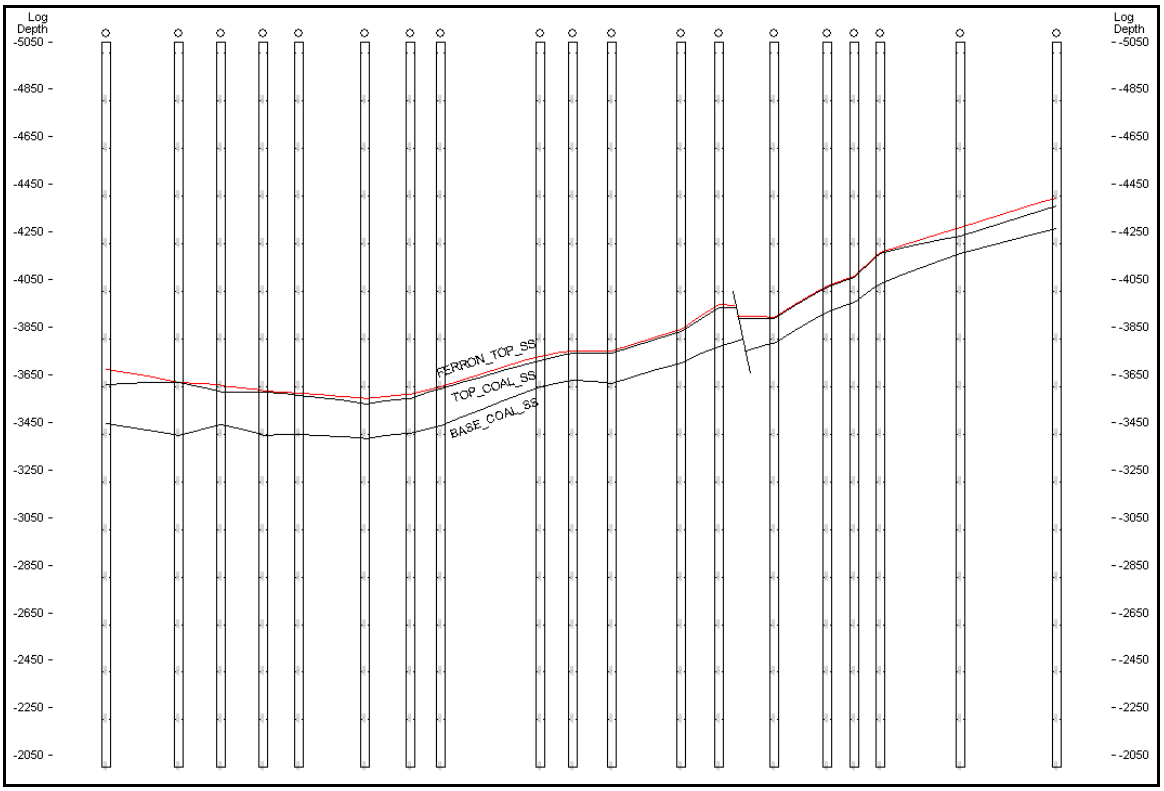

Figure 29: Cross section I-I' with interpreted fault.

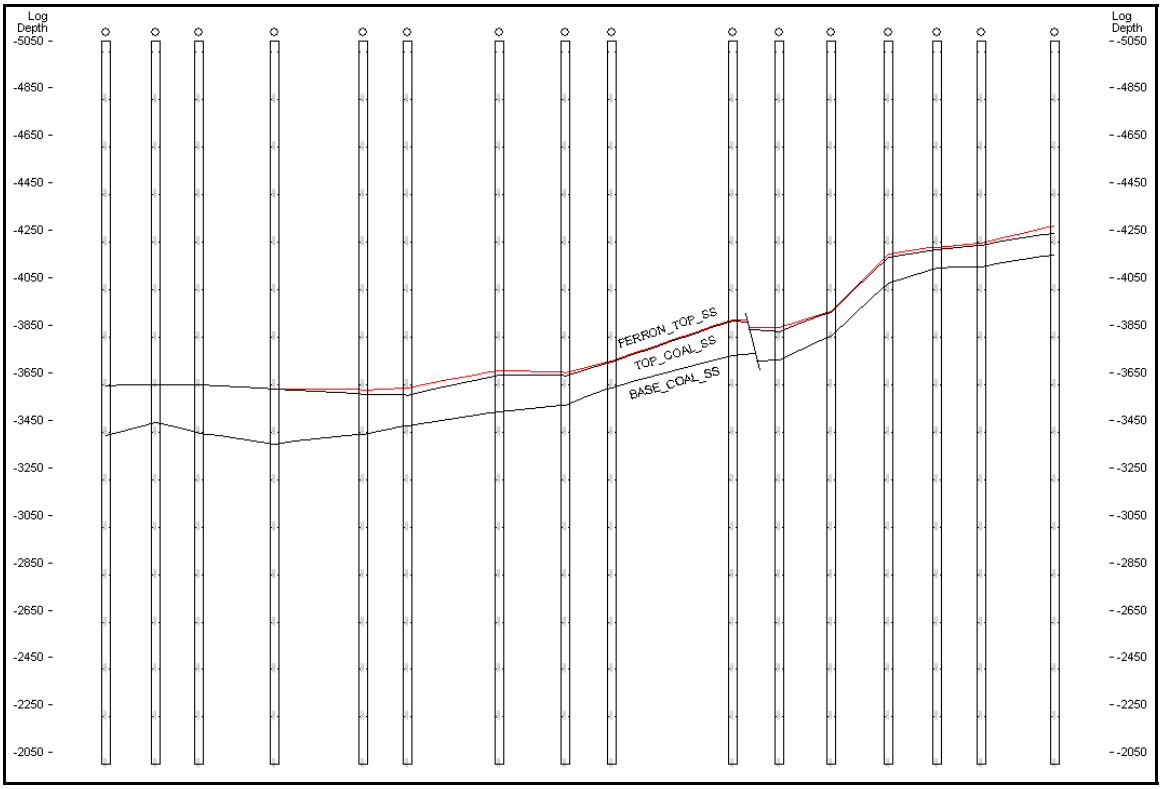

Figure 30: Cross section J-J' with interpreted fault

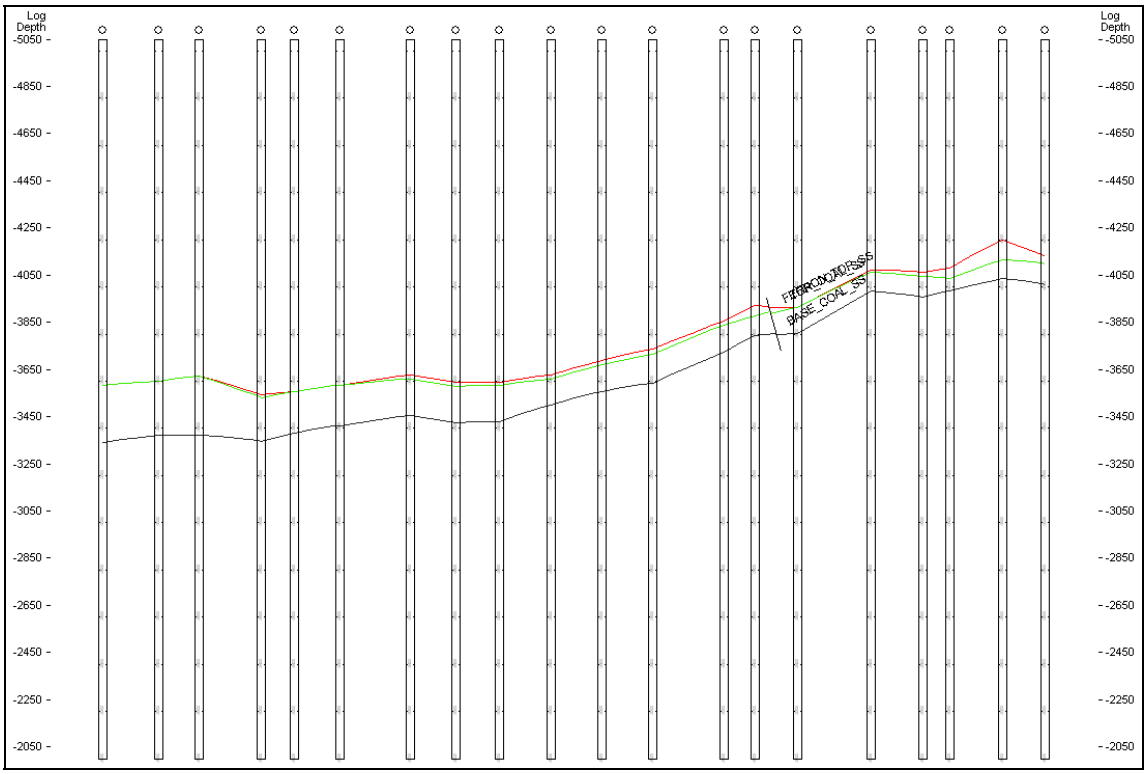

Figure 31: Cross section K-K' with interpreted fault.

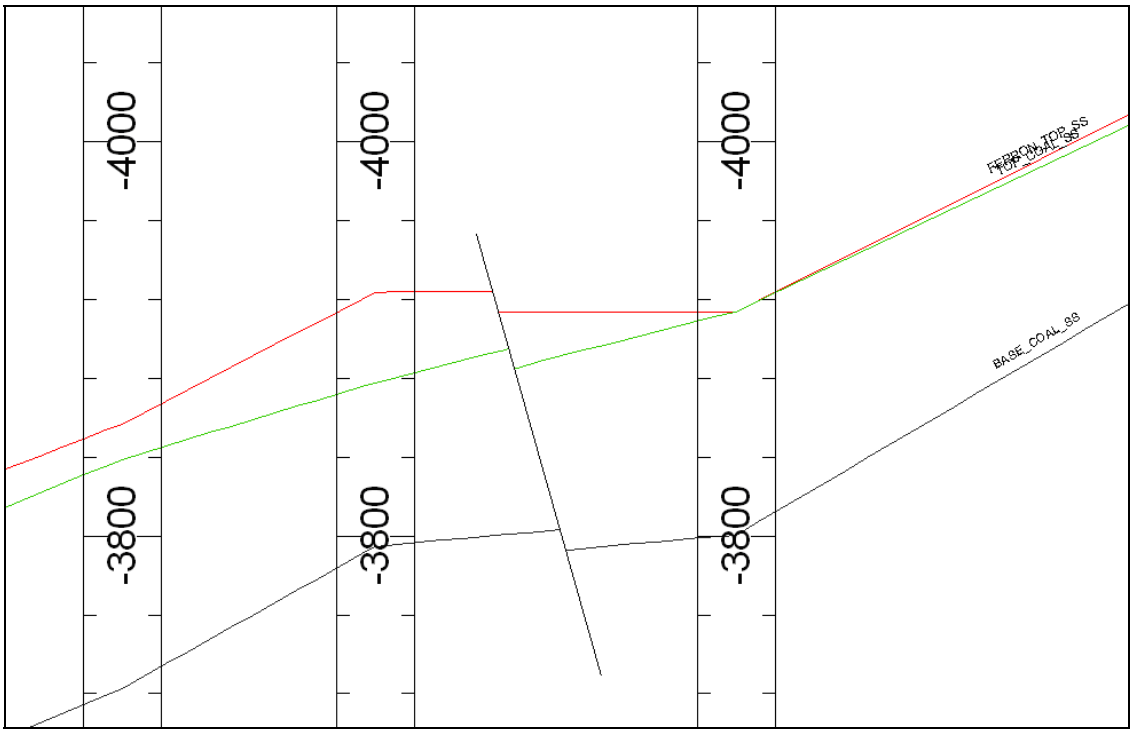

Figure 32: Cross section K-K' close up of interpreted fault showing 10 feet of offset.

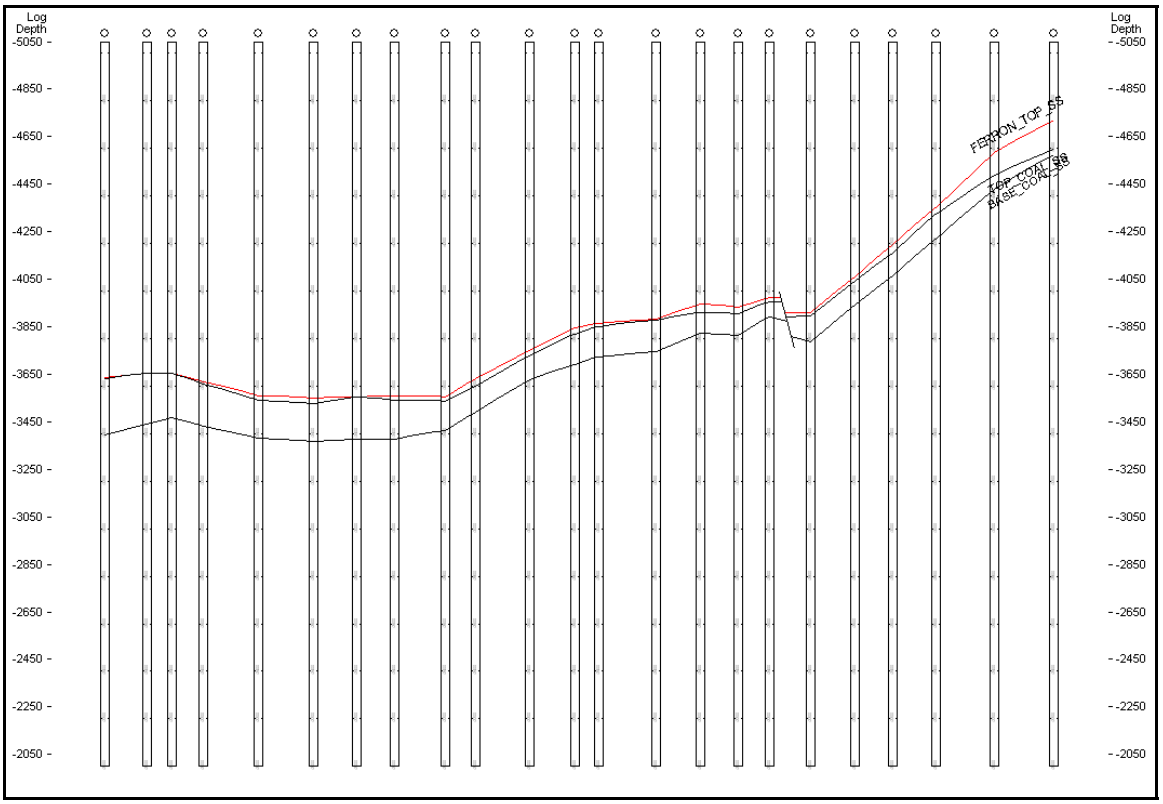

Figure 33: Cross section L-L' with interpreted fault.

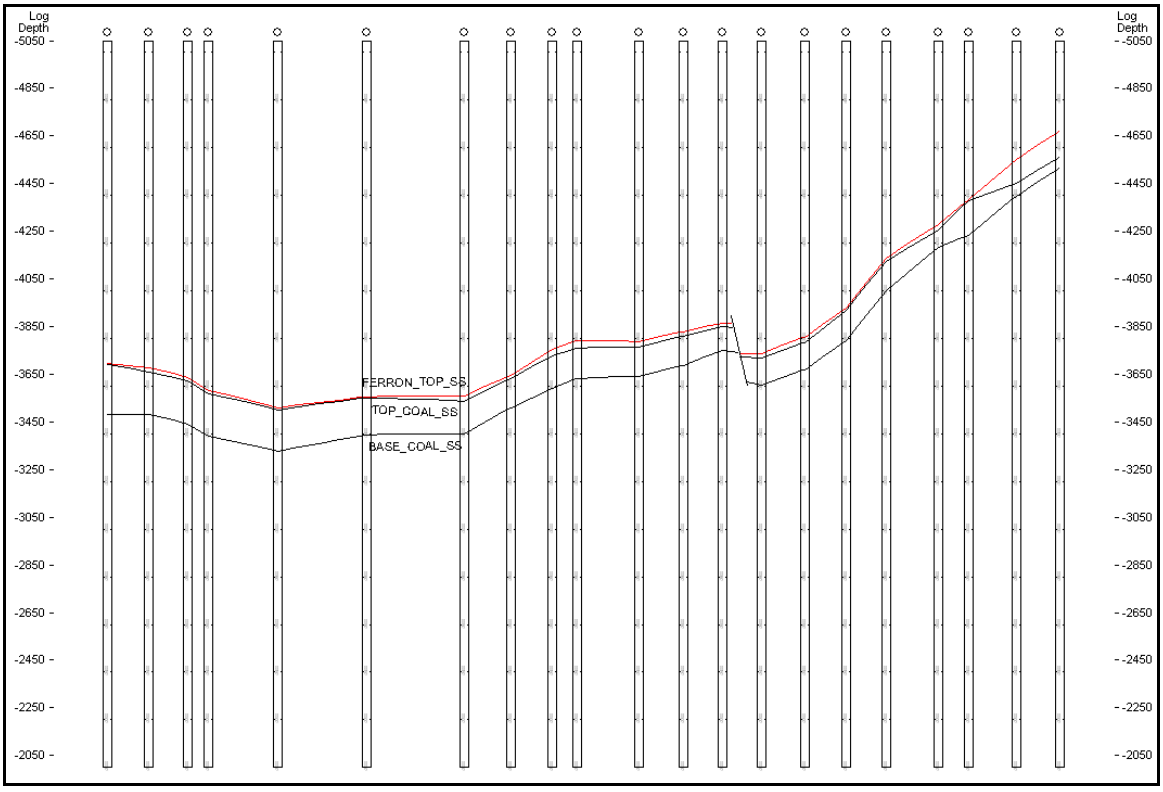

Figure 34: Cross section M-M' with interpreted fault.

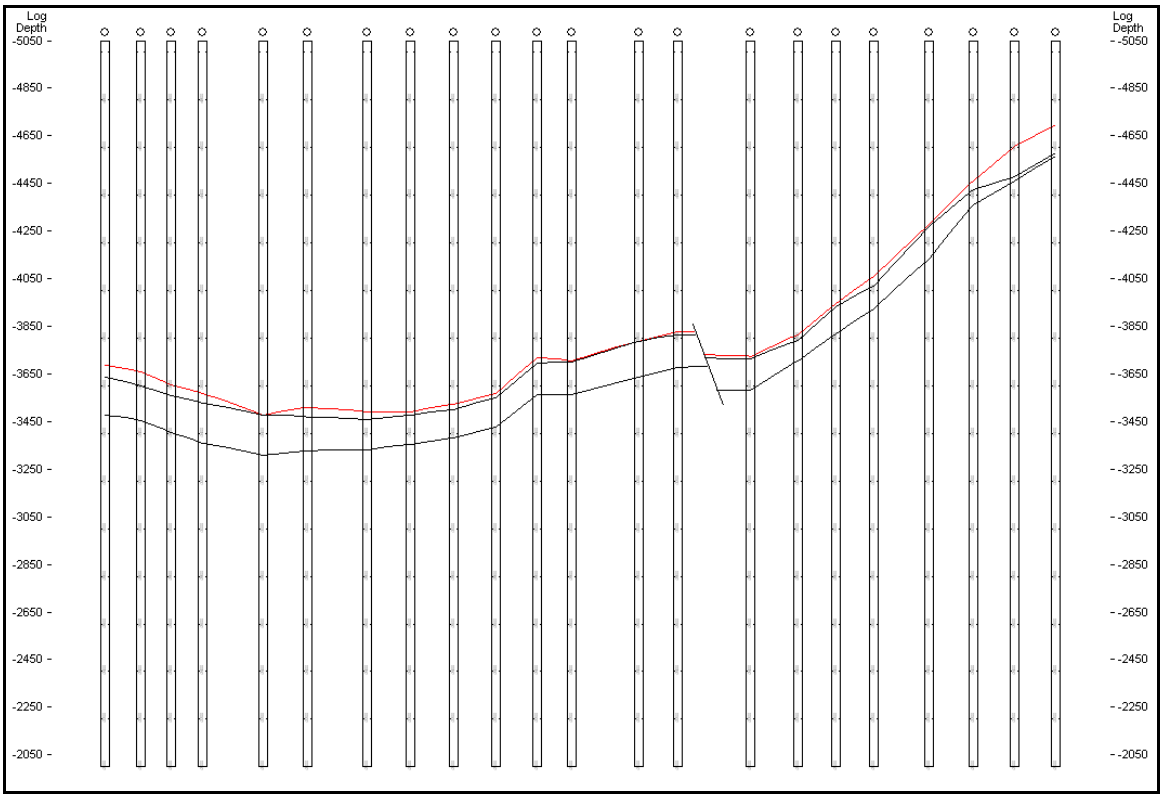

Figure 35: Cross section N-N' with interpreted fault.

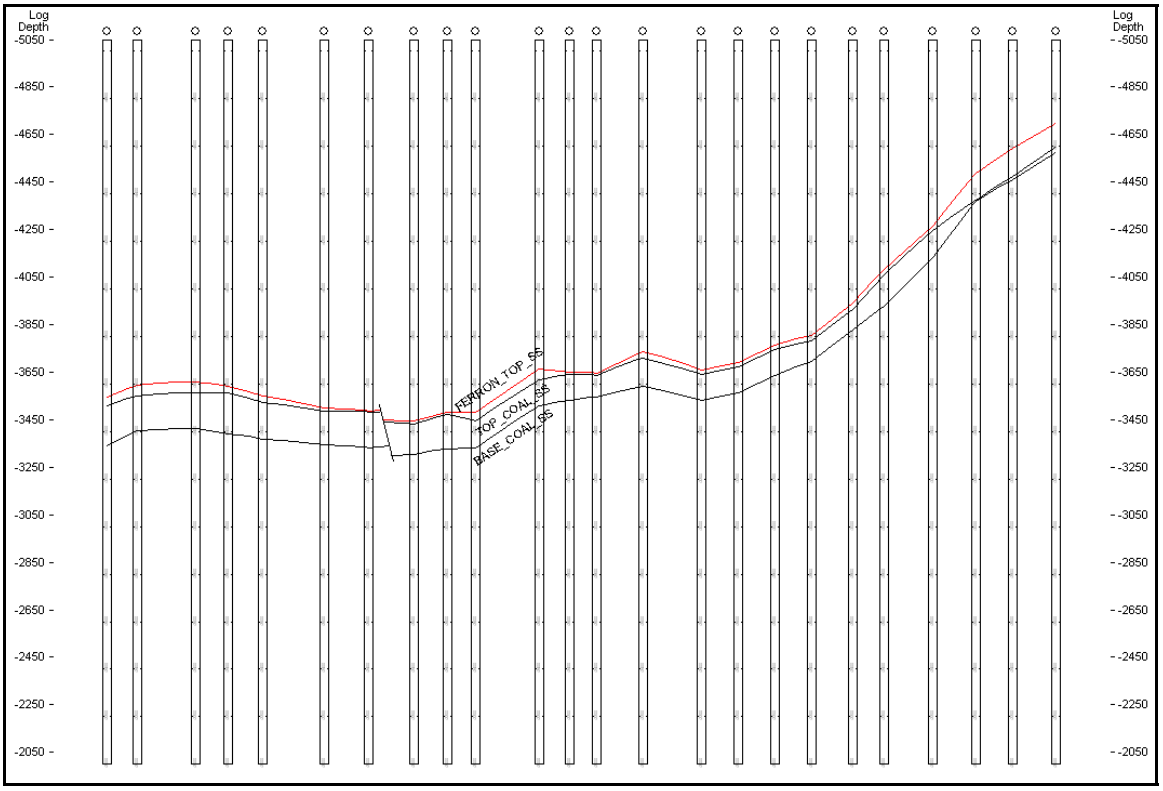

Figure 36: Cross section O-O' with interpreted fault.

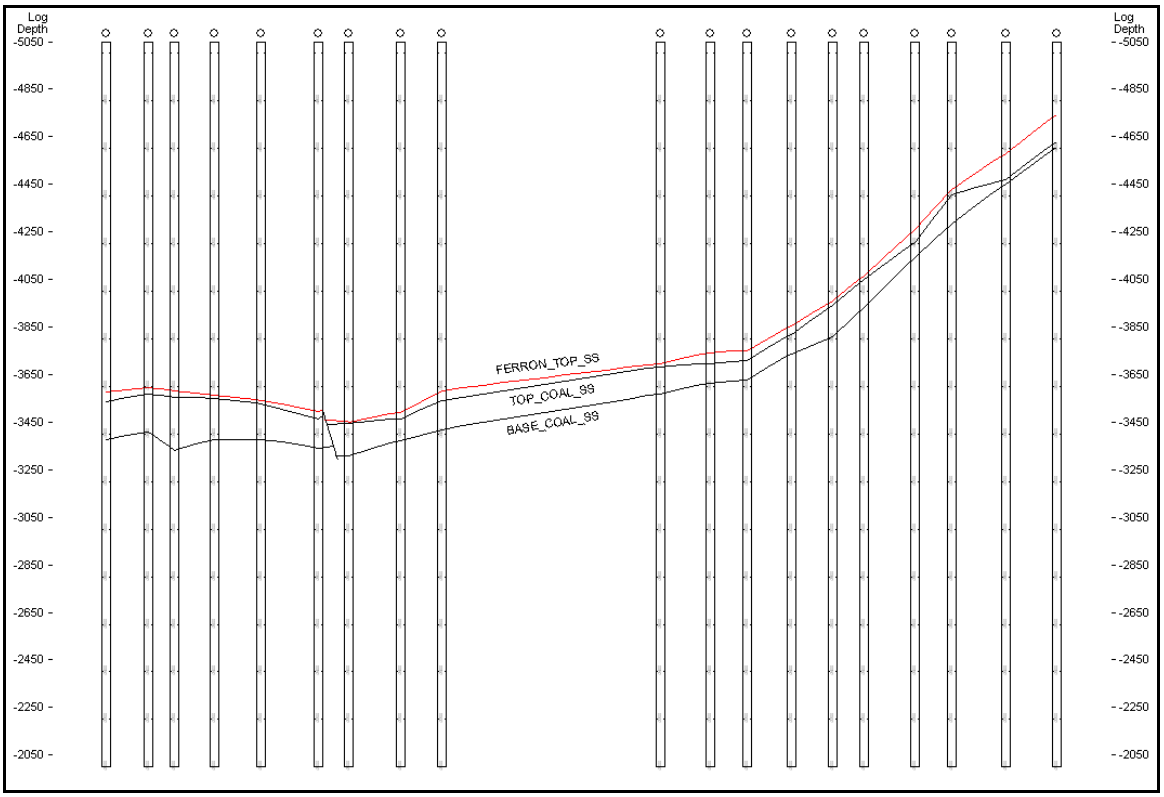

Figure 37: Cross section P-P' with interpreted fault.

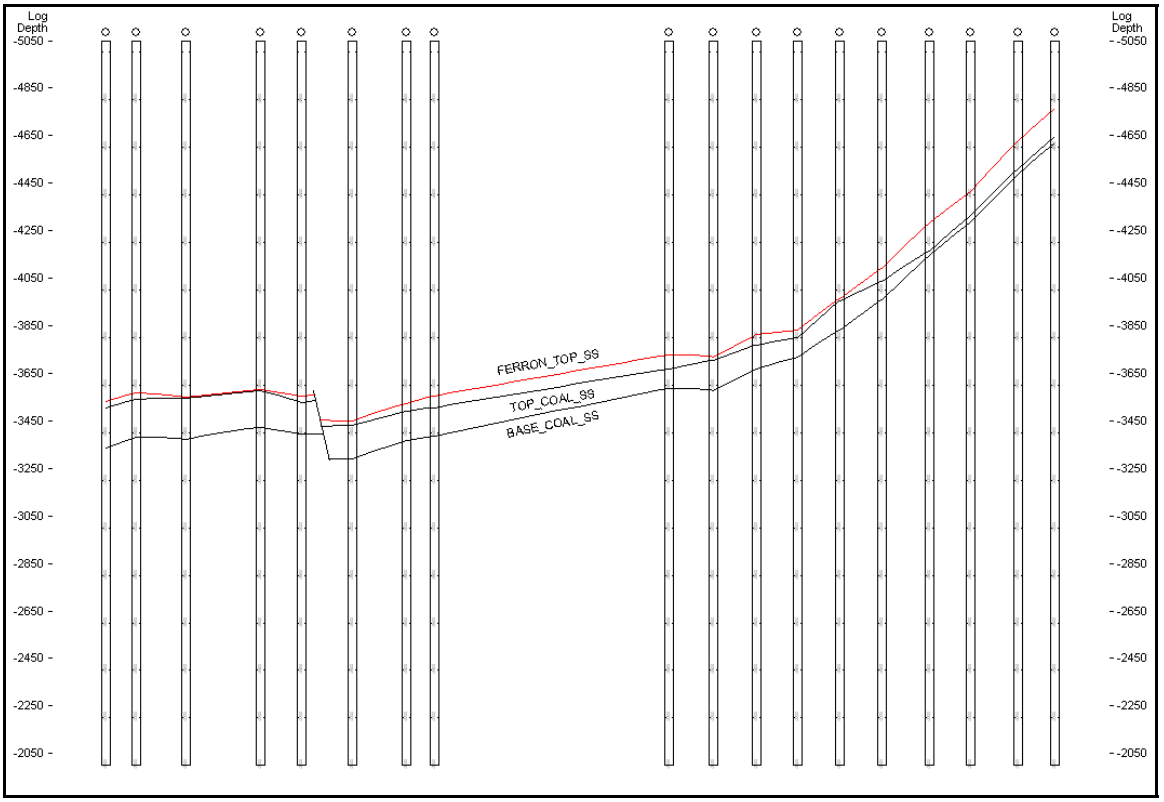

Figure 38: Cross section Q-Q' with interpreted fault.

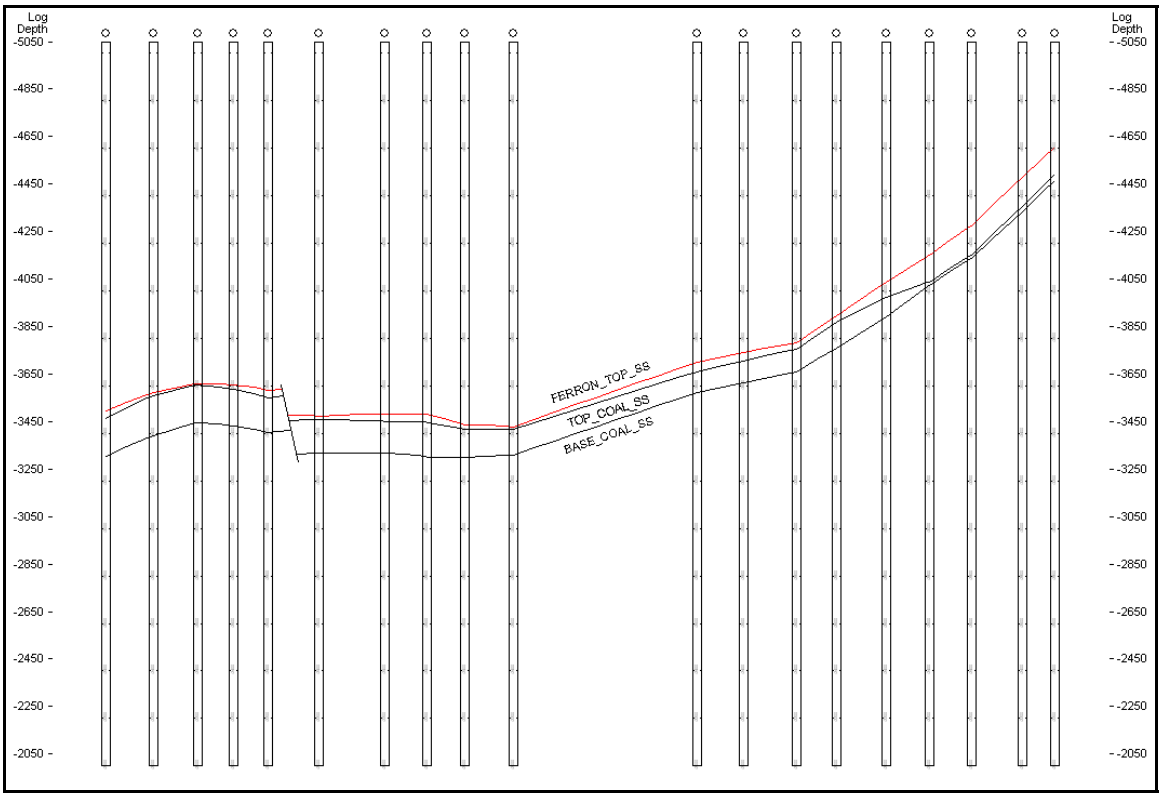

Figure 39: Cross section R-R' with interpreted fault.

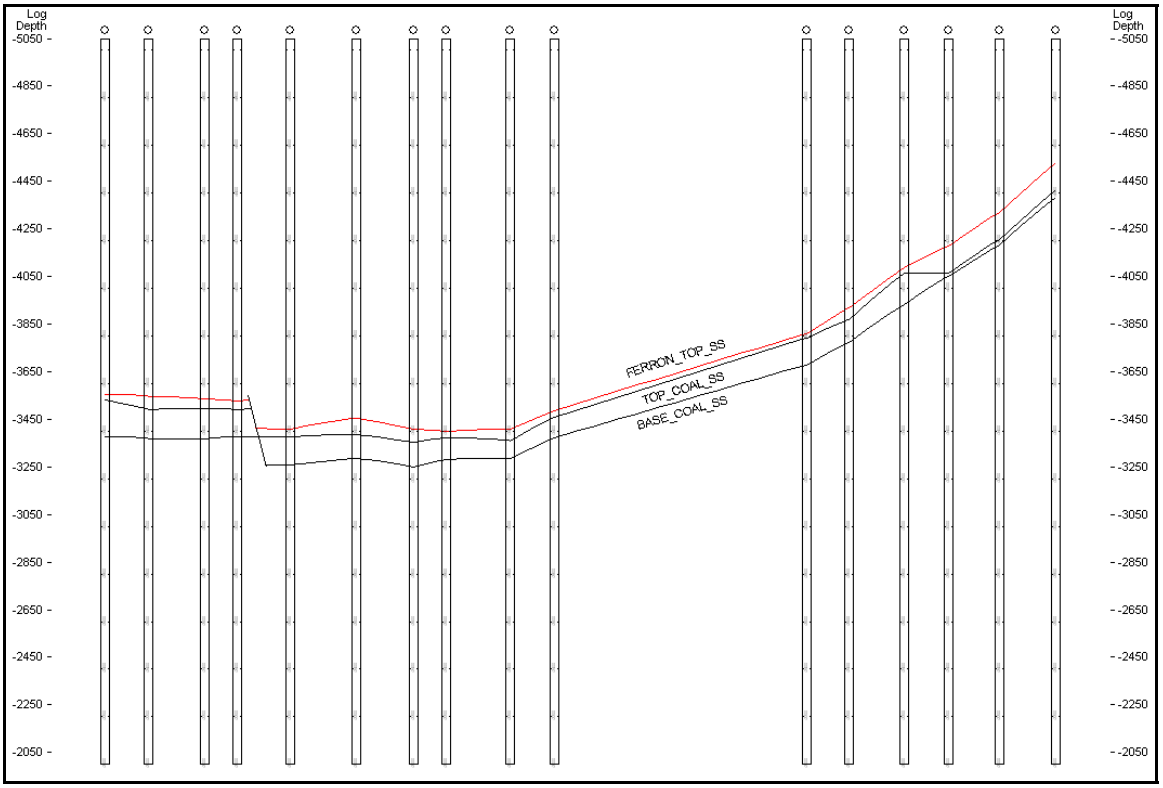

Figure 40: Cross section S-S' with interpreted fault

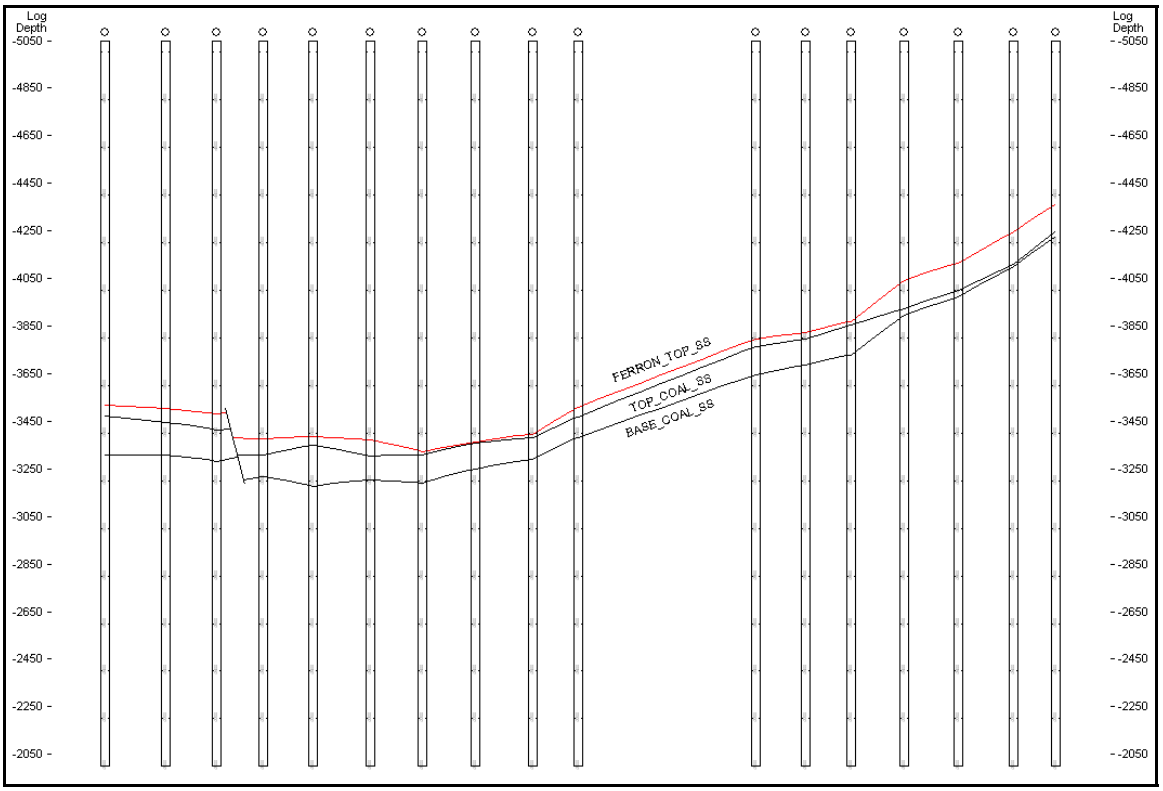

Figure 41: Cross section T-T' with interpreted fault

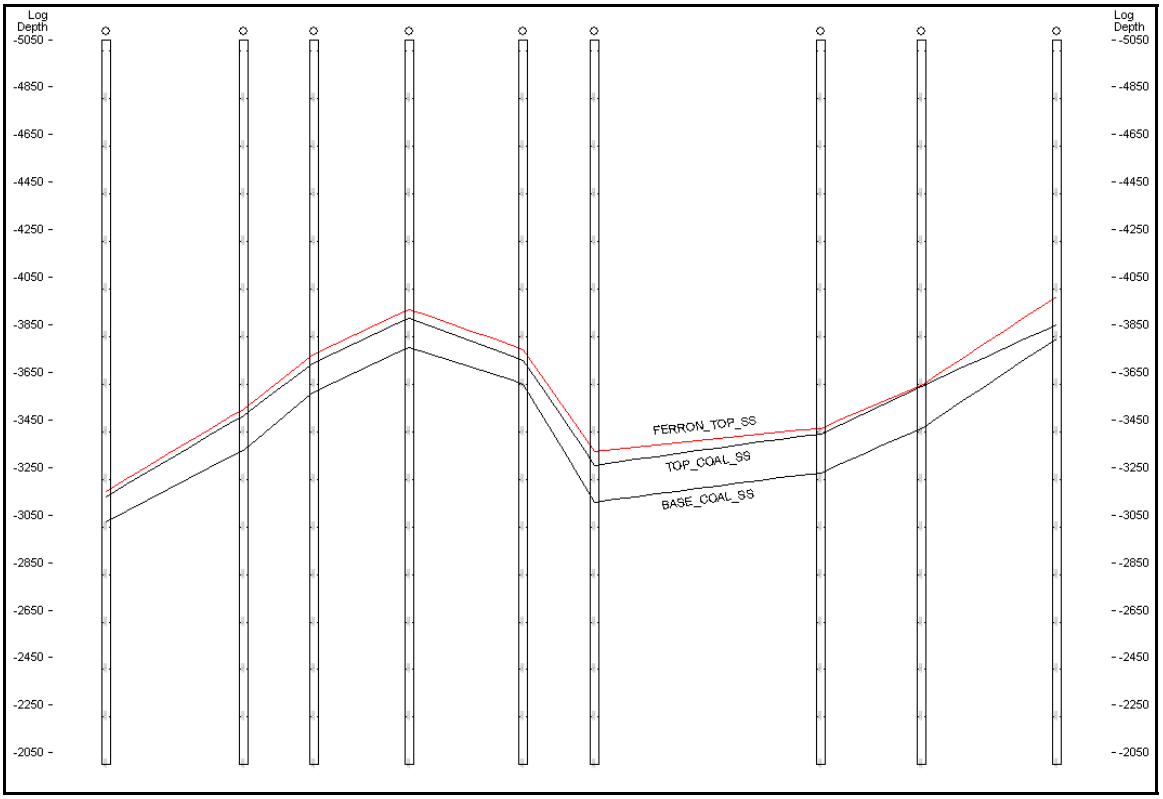

Figure 42: Cross section B1-B2' showing northern part of Huntington anticline.

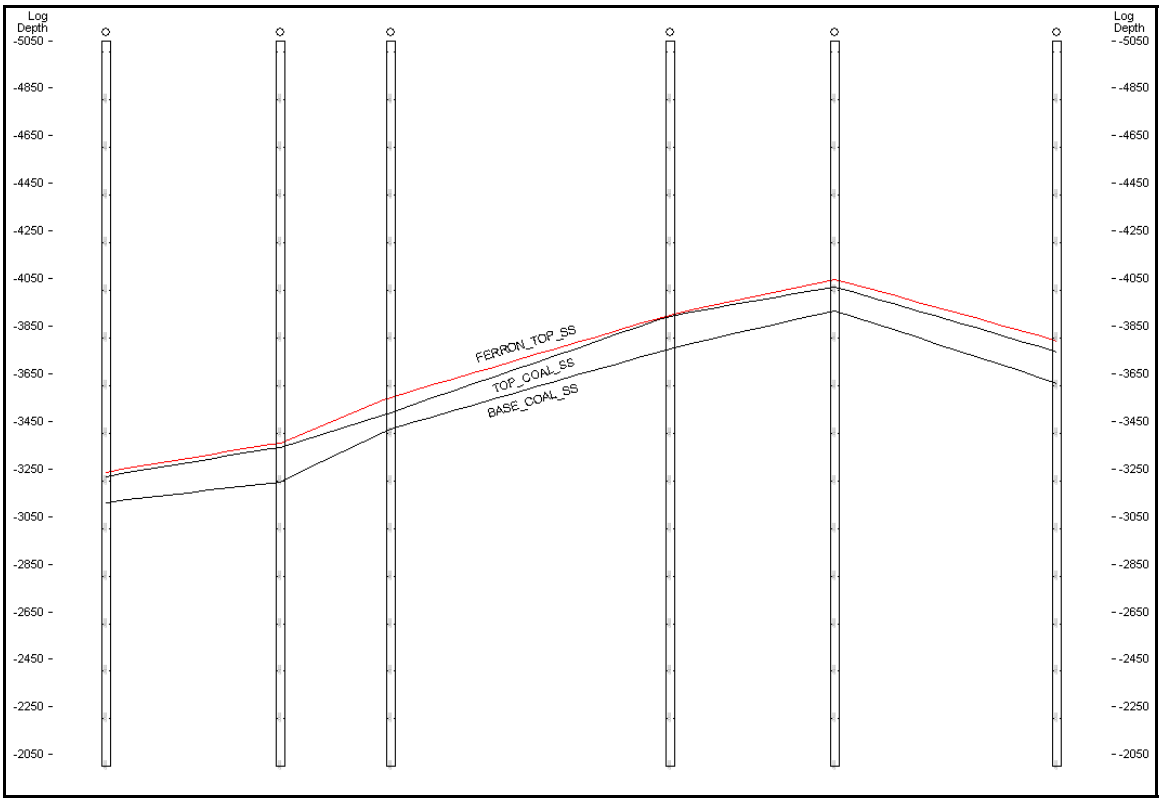

Figure 43: Cross section C1-C2’ showing Huntington anticline.

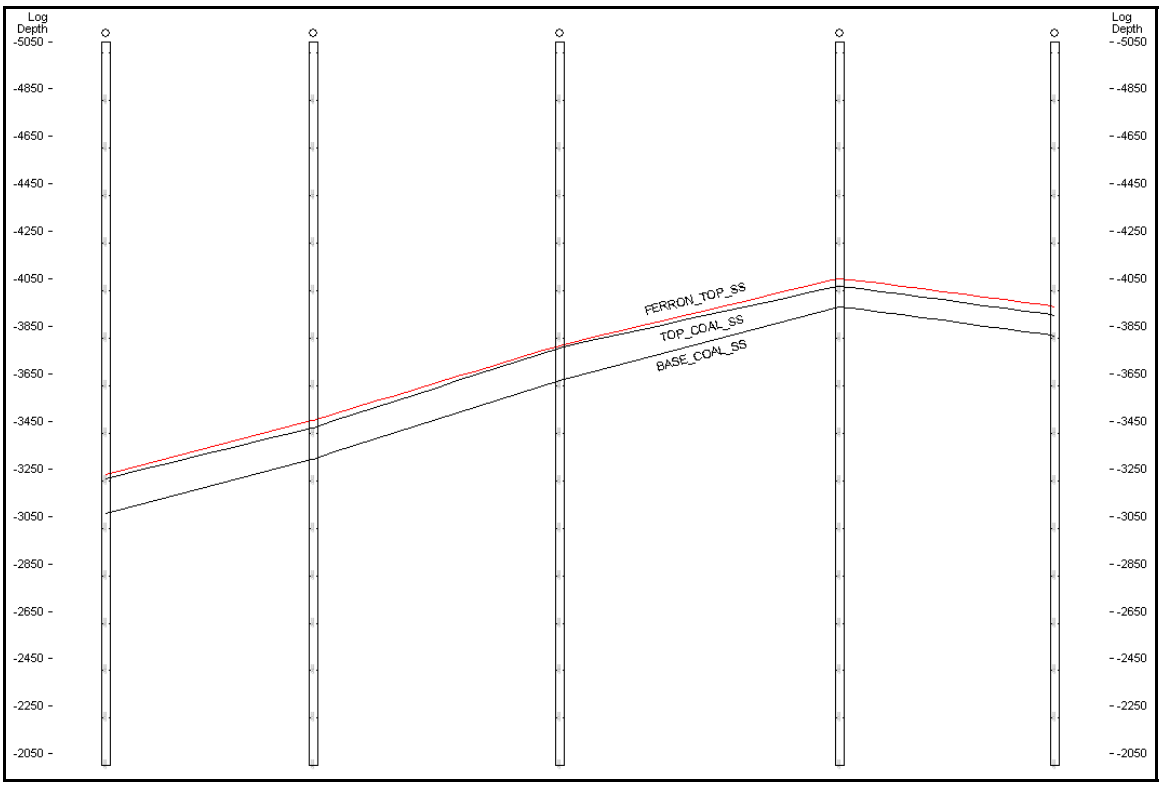

Figure 44: Cross section D1-D2’ showing Huntington anticline.

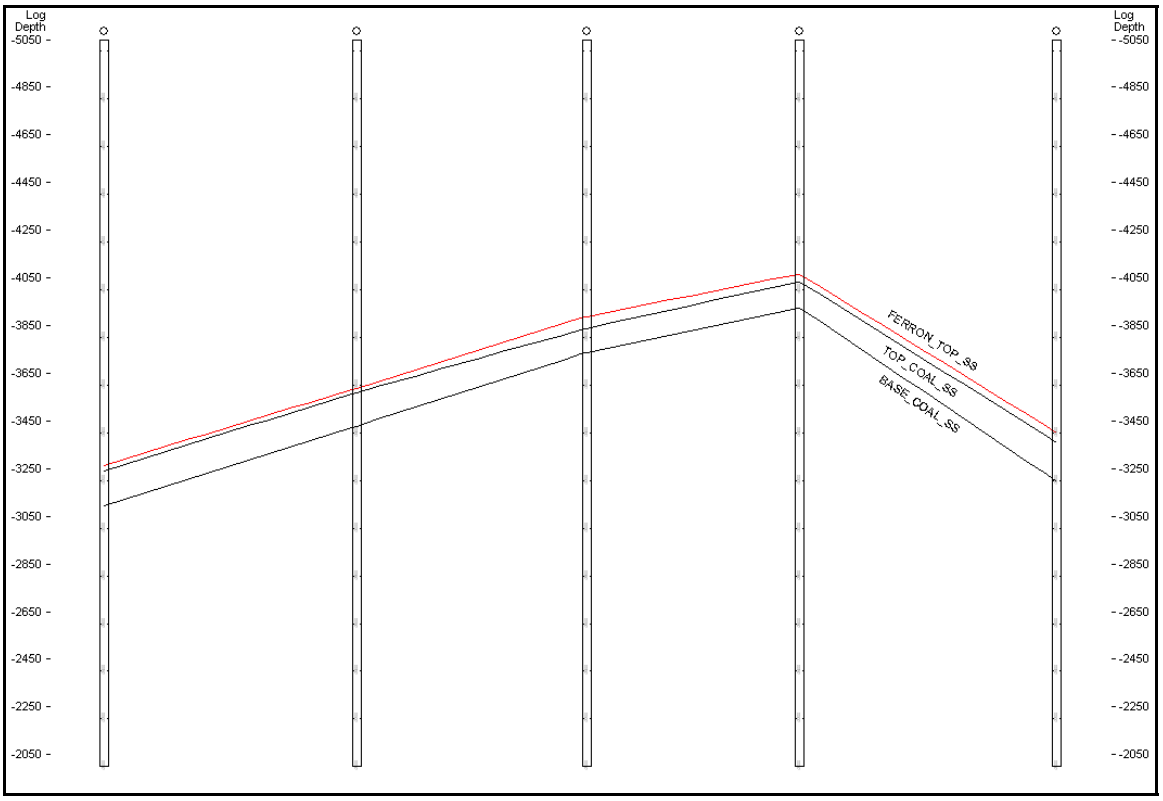

Figure 45: Cross section of E1-E2’ showing southern part of Huntington anticline.

Appendix B: Uninterpreted well logs

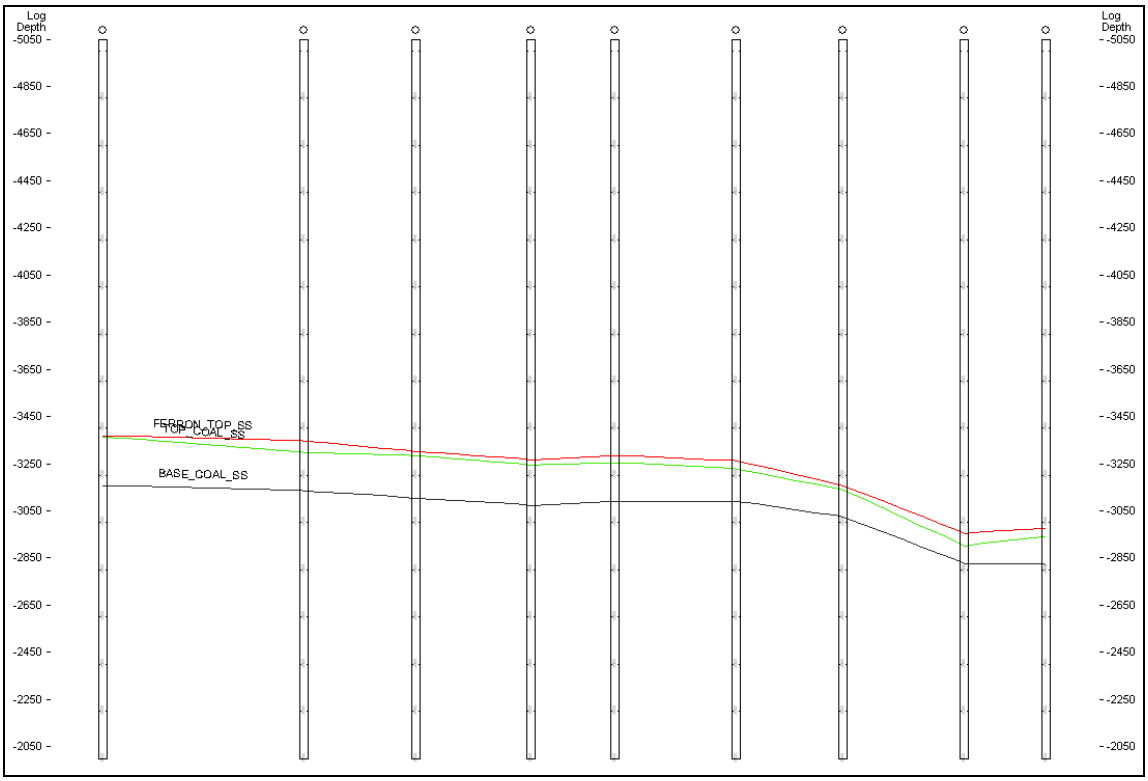

Figure 46: Cross section A-A’ (not interpreted)

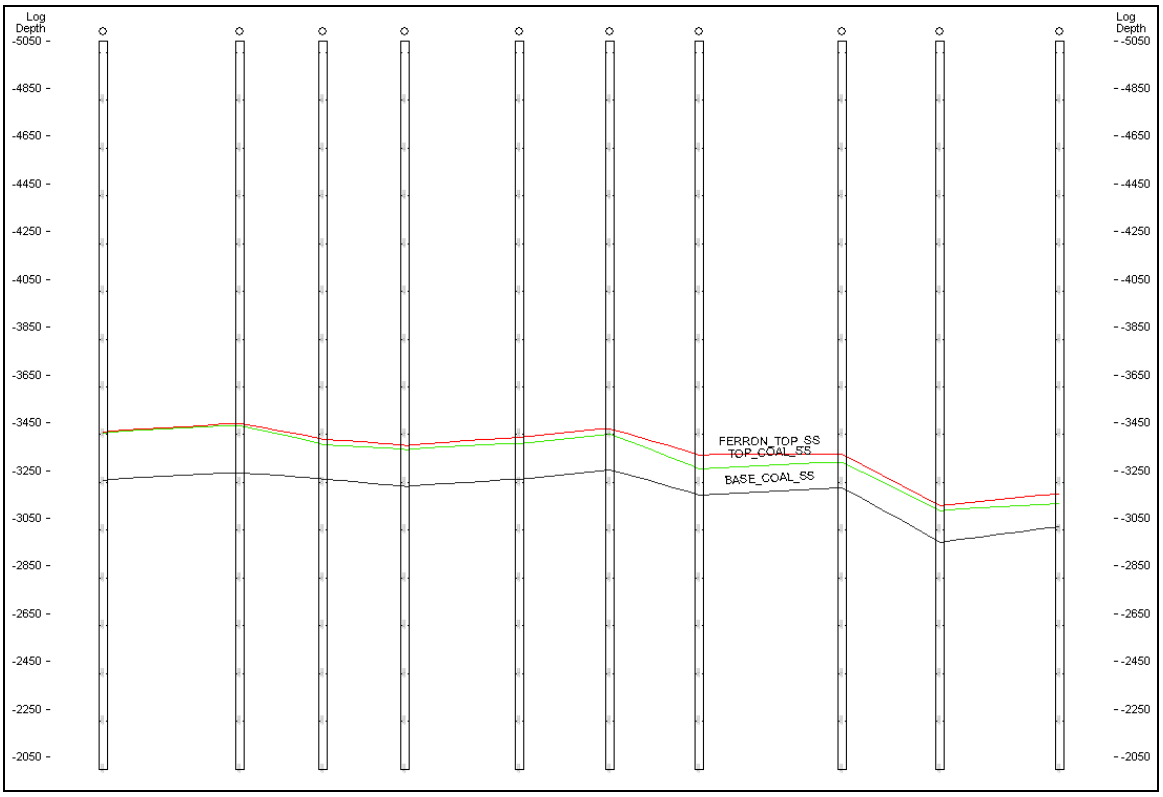

Figure 47: Cross section B-B’ (not interpreted)

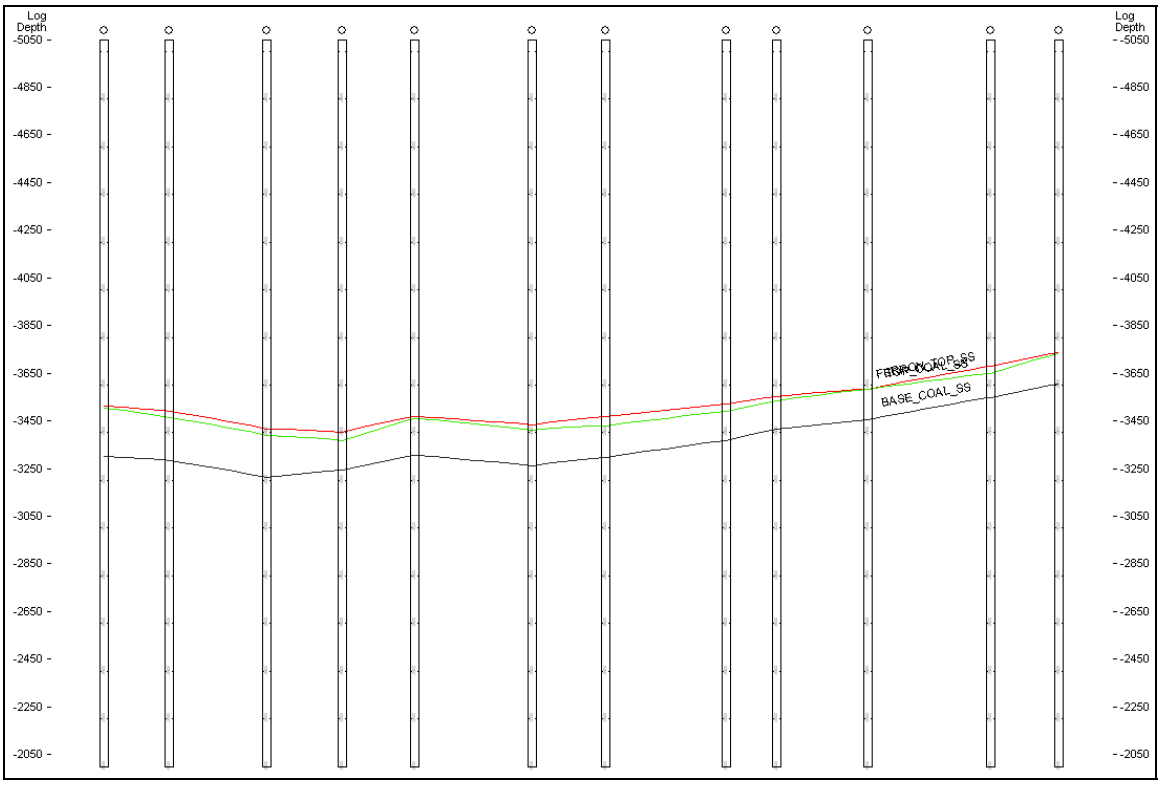

Figure 48: Cross section C-C’ (not interpreted)

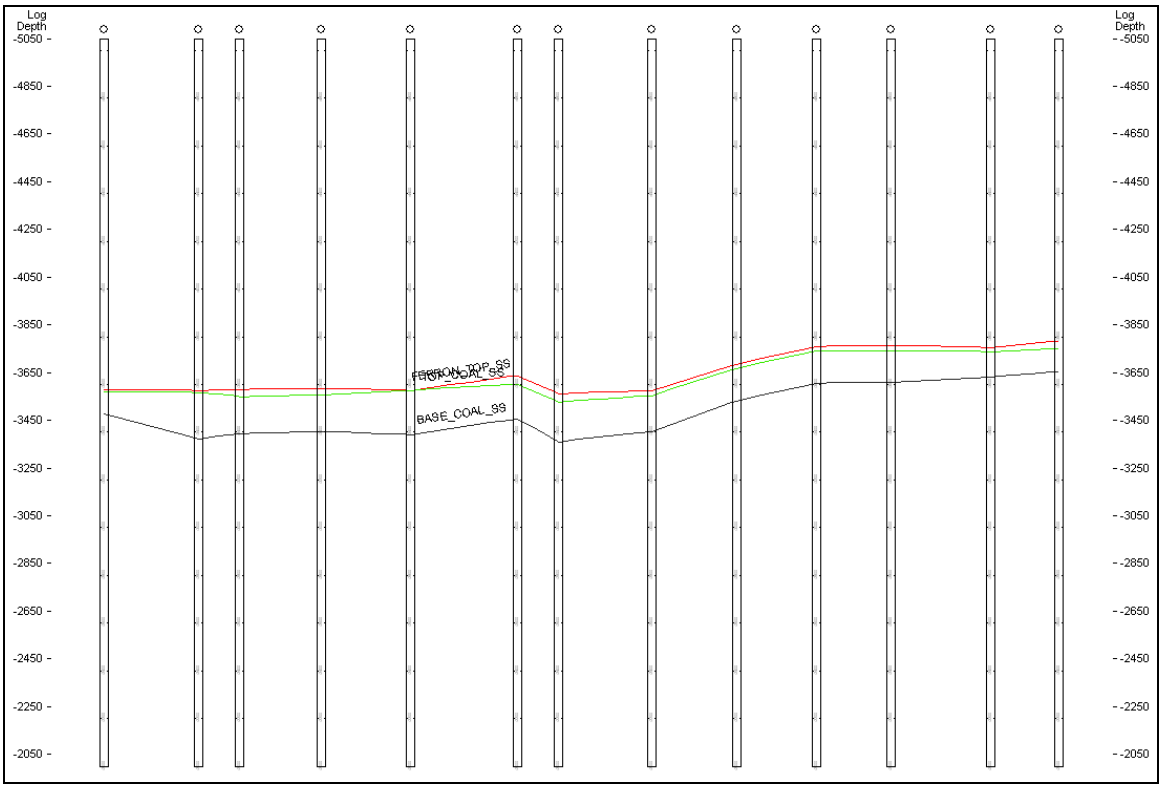

Figure 49: Cross section D-D’ (not interpreted)

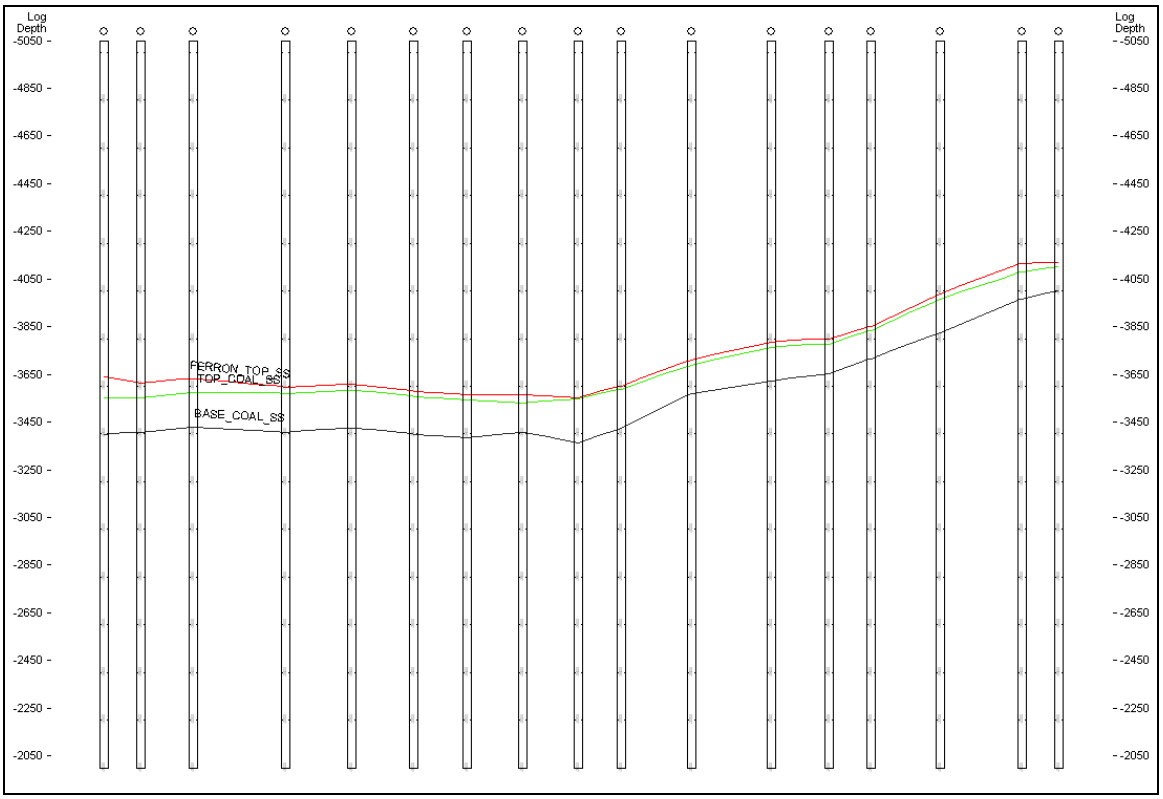

Figure 50: Cross section E-E’ (not interpreted)

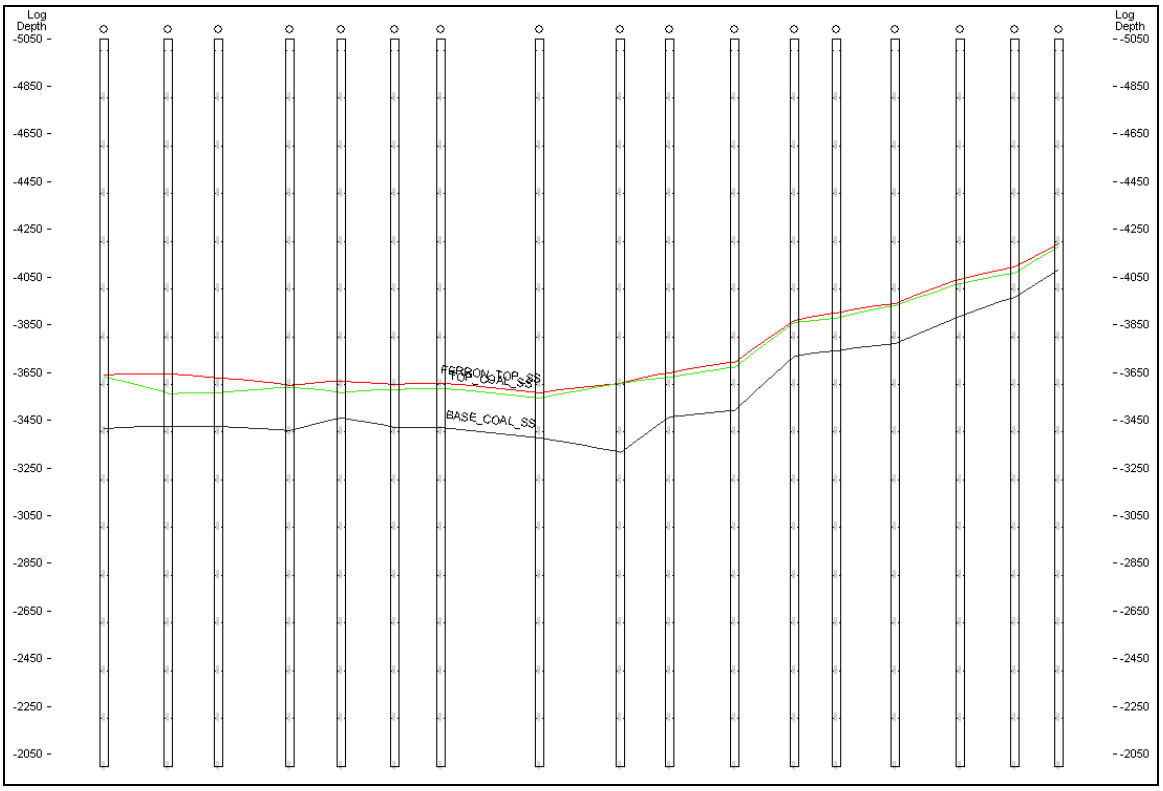

Figure 51: Cross section F-F’ (not interpreted)

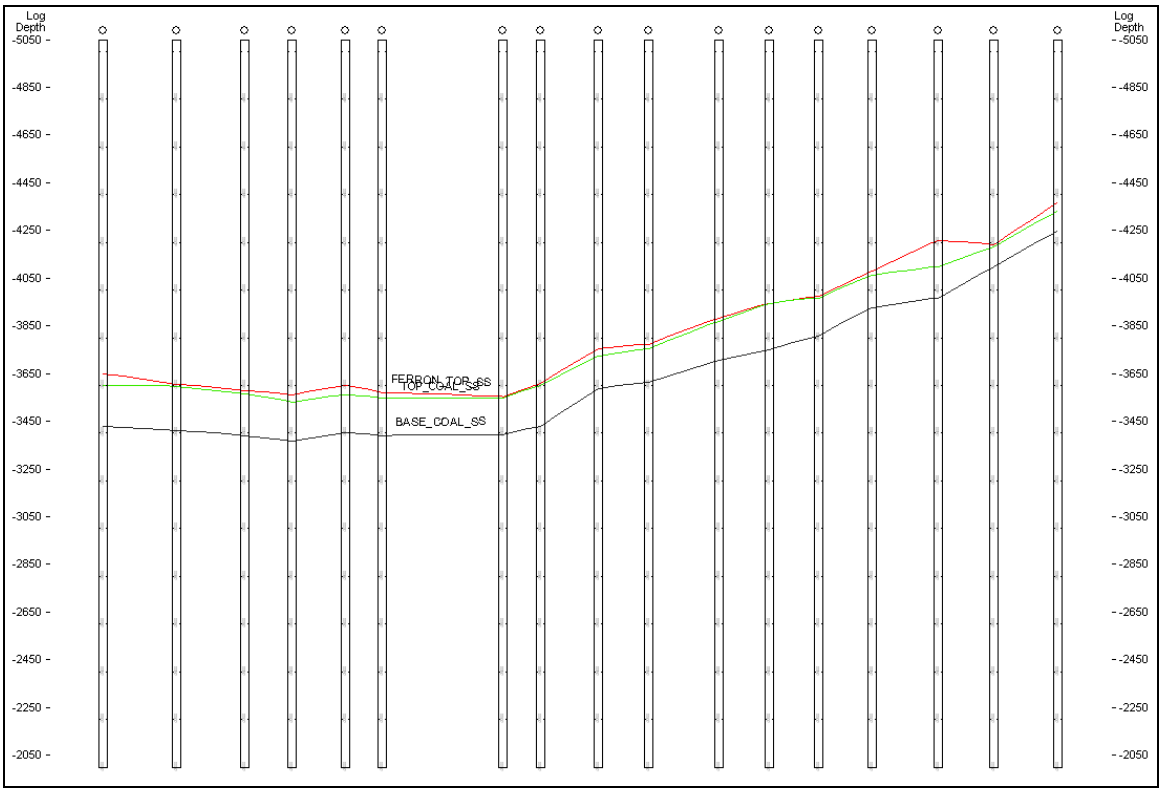

Figure 52: Cross section G-G' (not-interpreted)

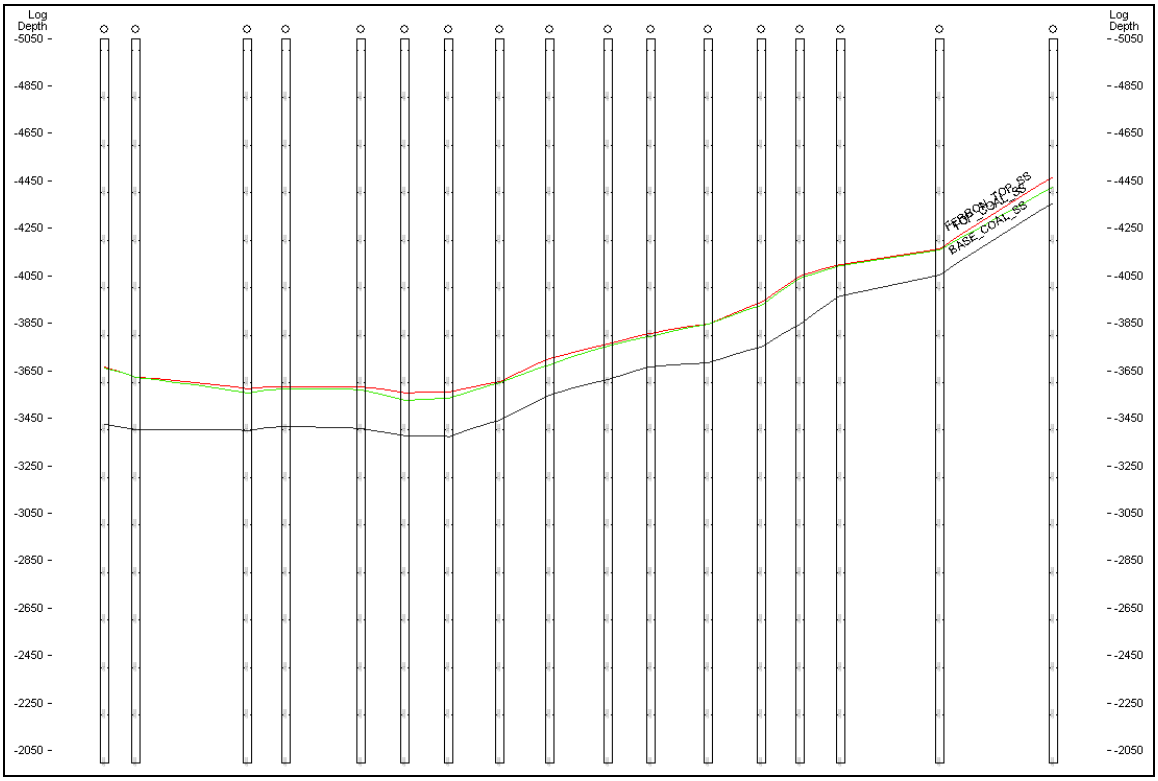

Figure 53: Cross section H-H' (not interpreted)

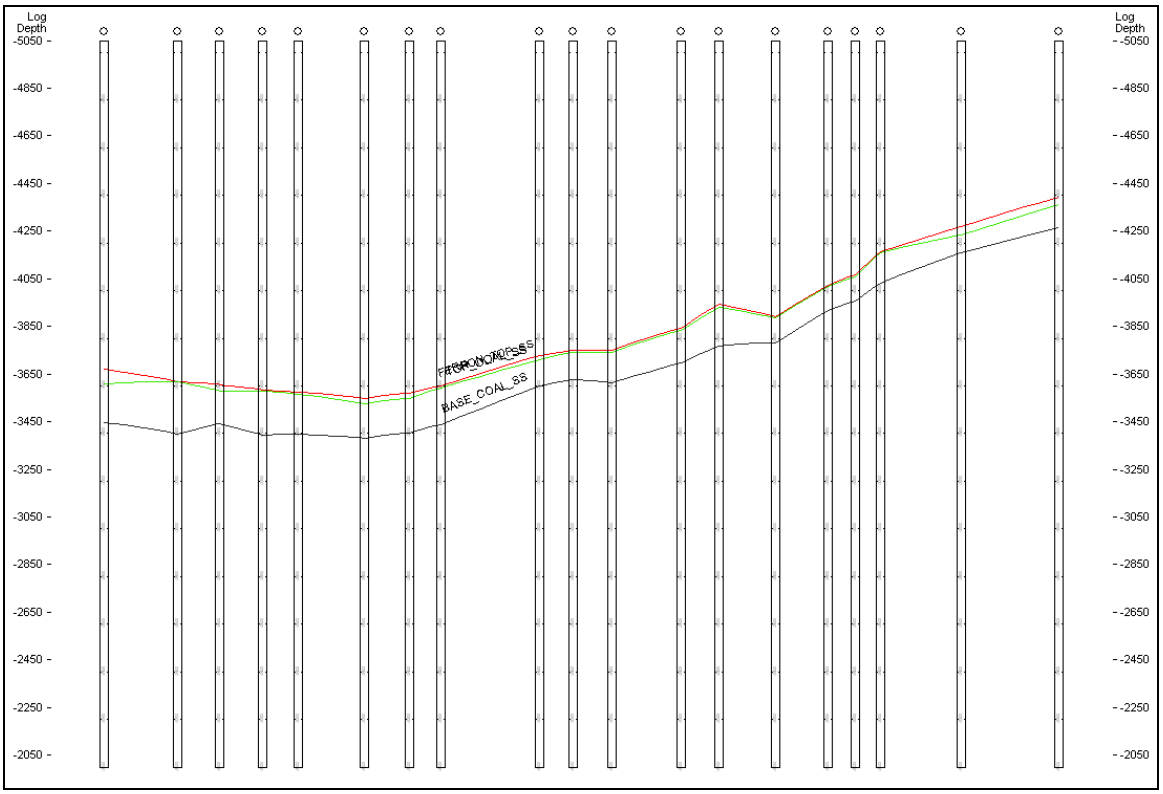

Figure 54: Cross section I-I' (not interpreted)

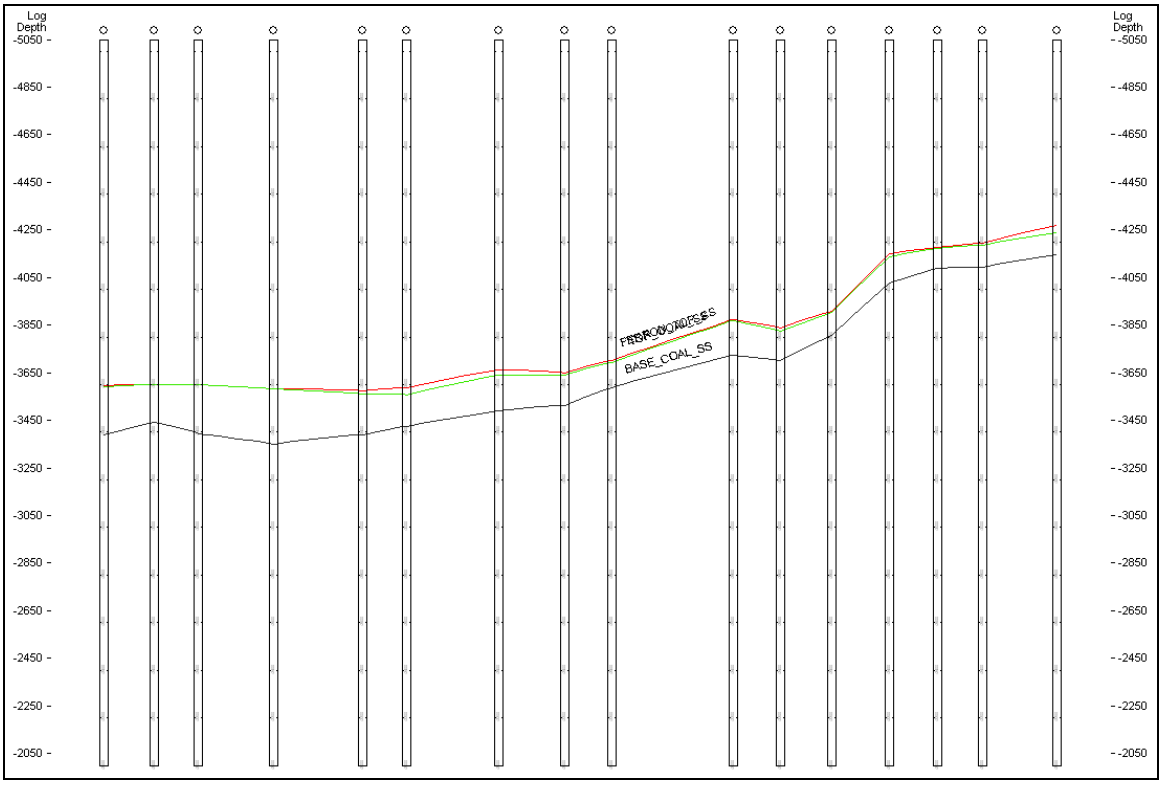

Figure 55: Cross section J-J' (not-interpreted)

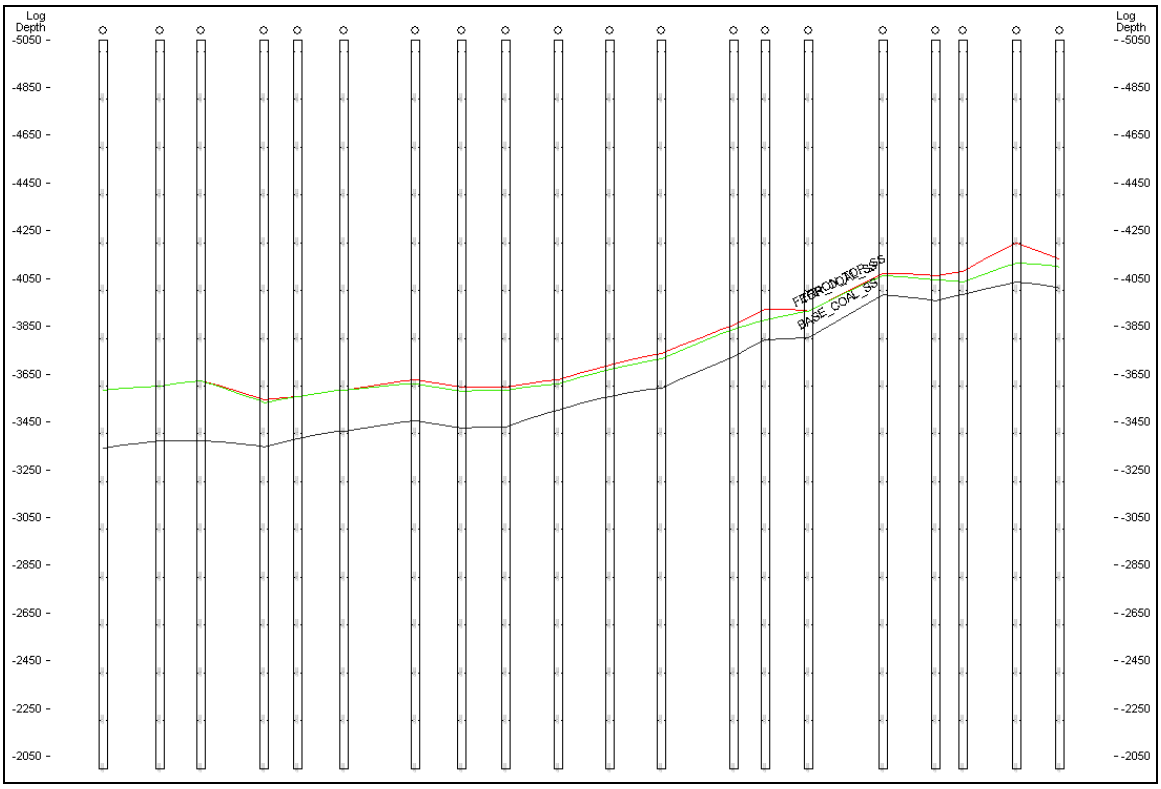

Figure 56: Cross section K-K’ (not interpreted)

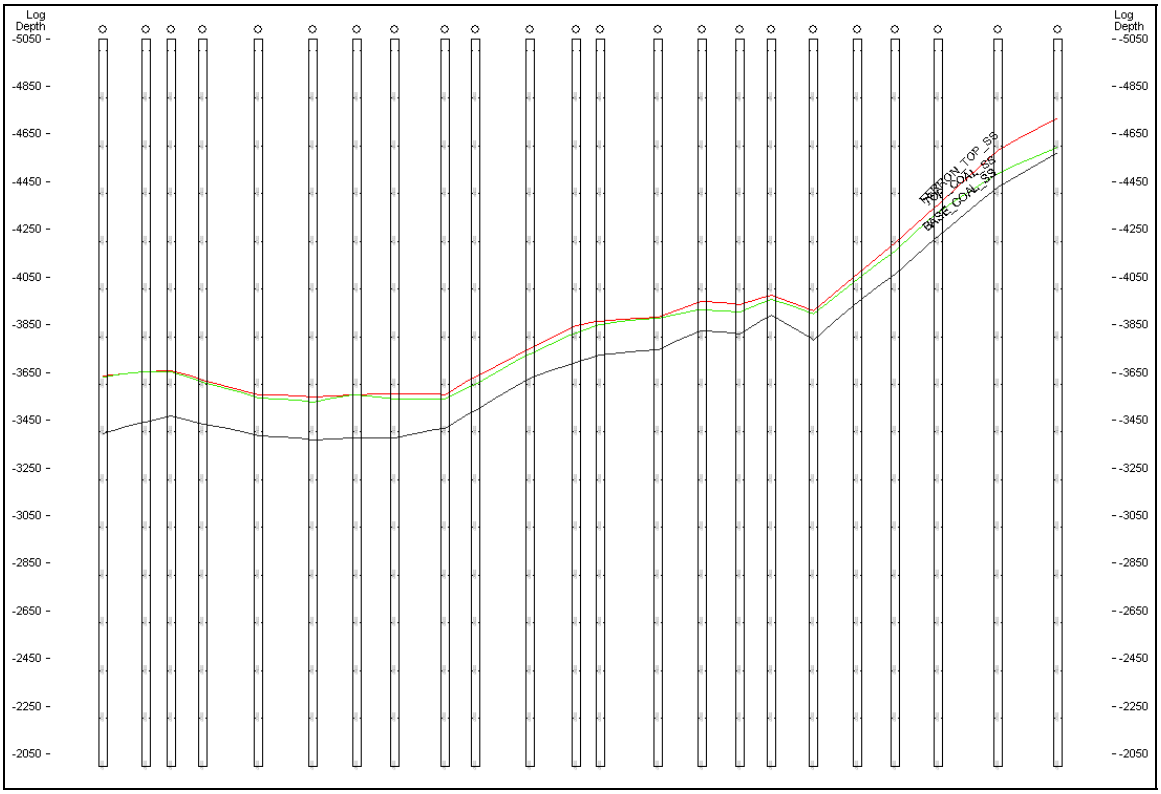

Figure 57: Cross section L-L’ (not interpreted)

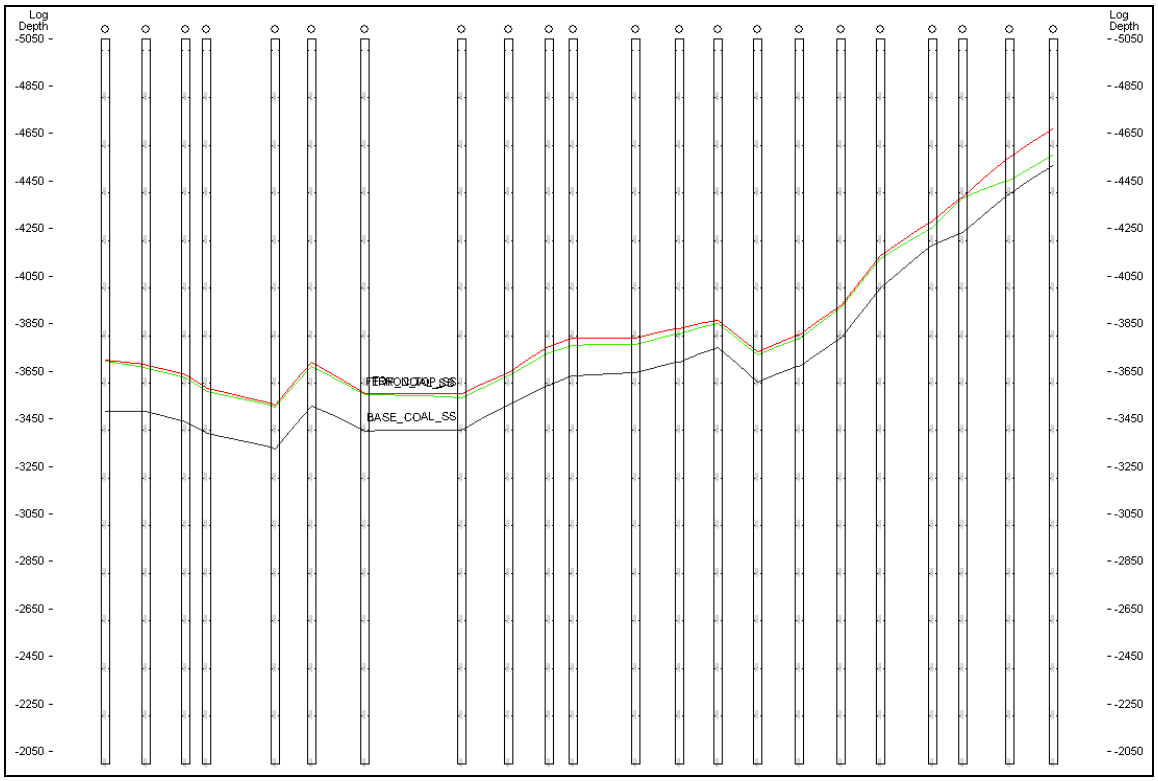

Figure 58: Cross section M-M' (not interpreted)

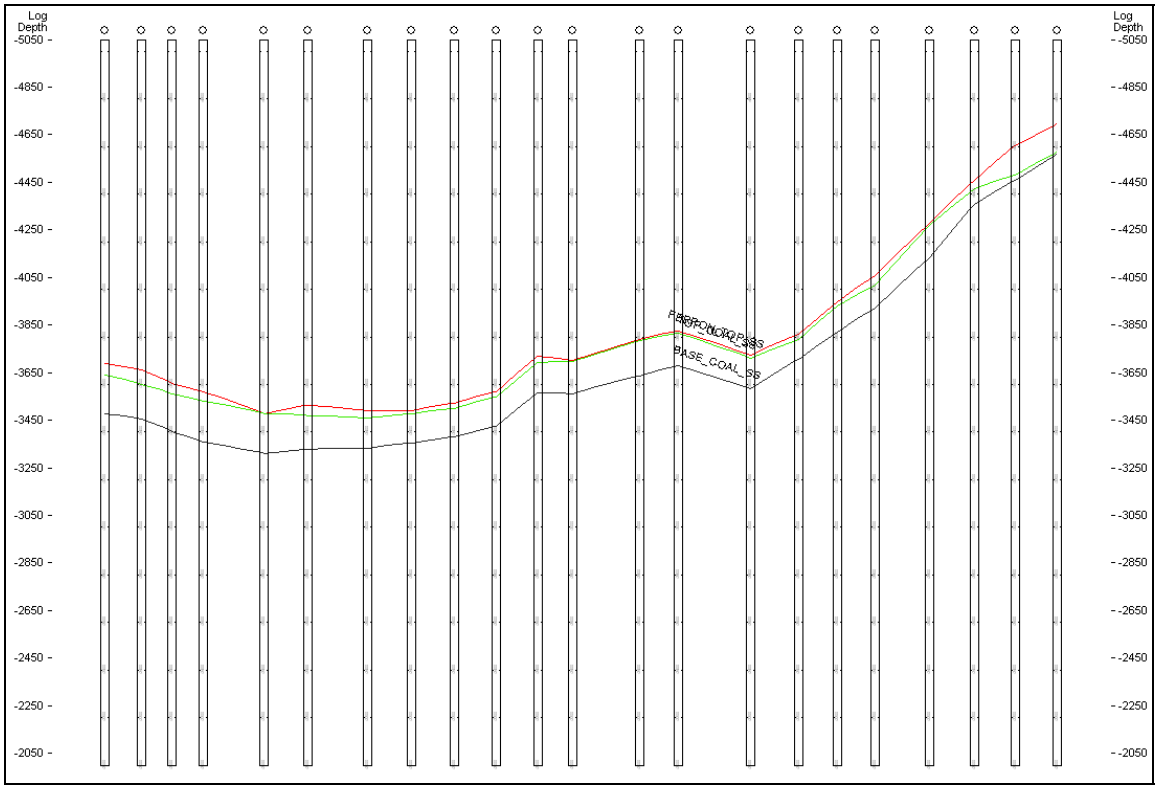

Figure 59: Cross section N-N' (not interpreted)

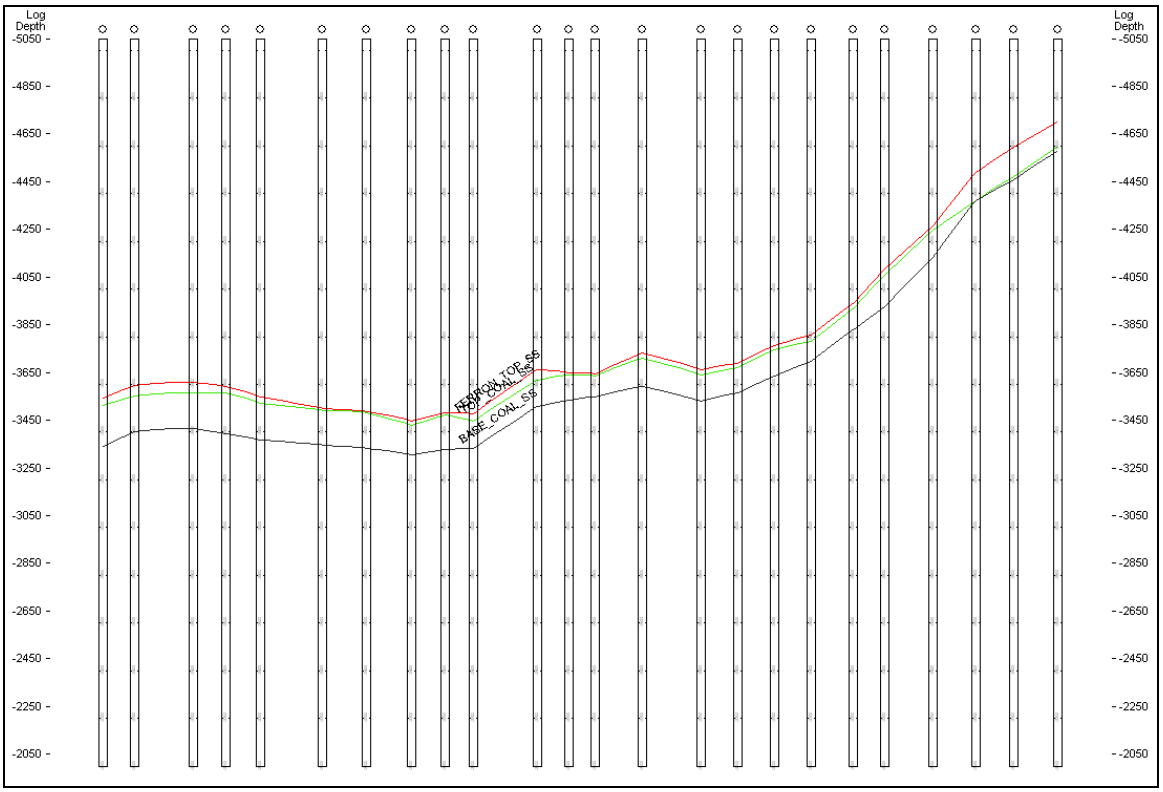

Figure 60: Cross section O-O’ (not interpreted)

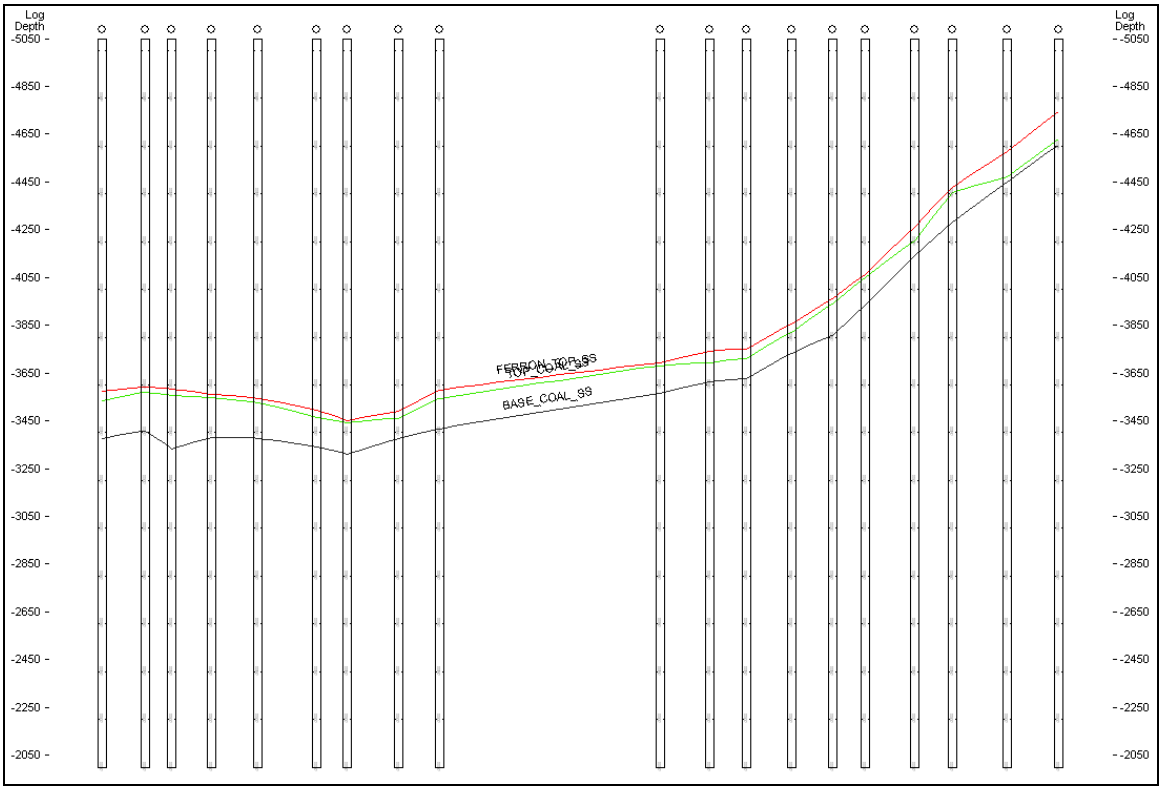

Figure 61: Cross section P-P’ (not interpreted)

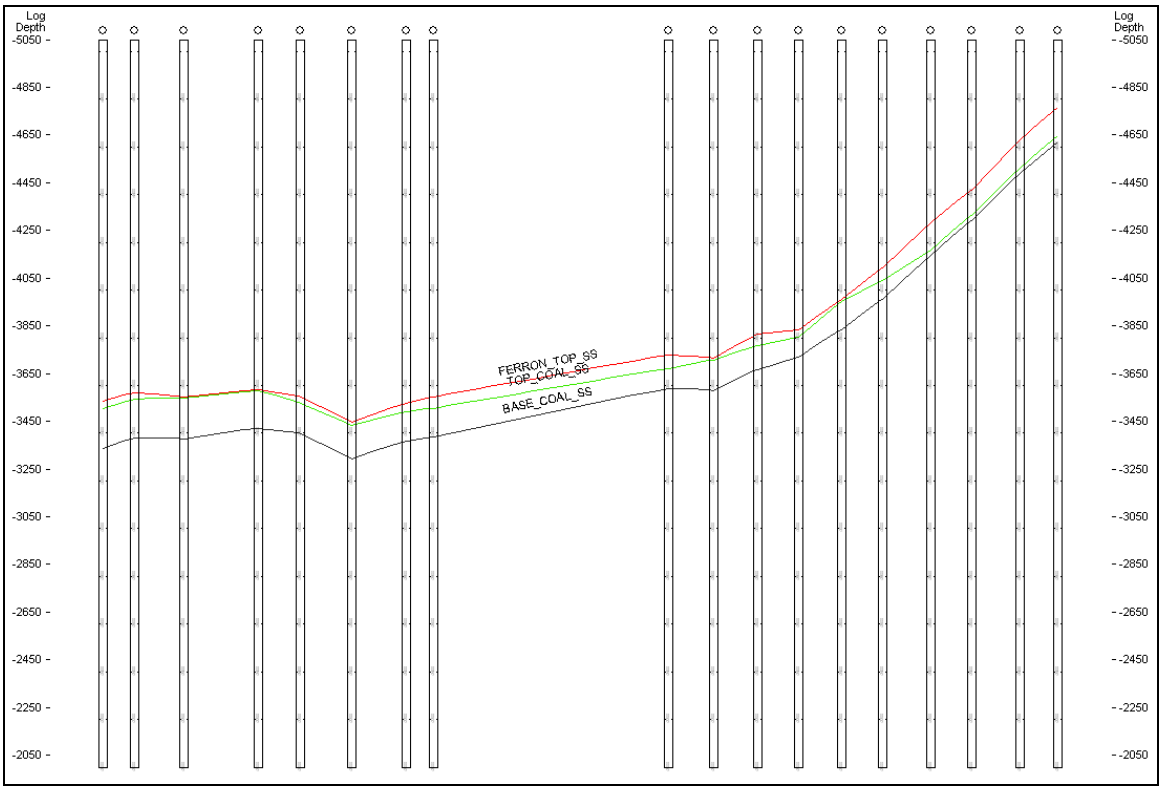

Figure 62: Cross section Q-Q' (not interpreted)

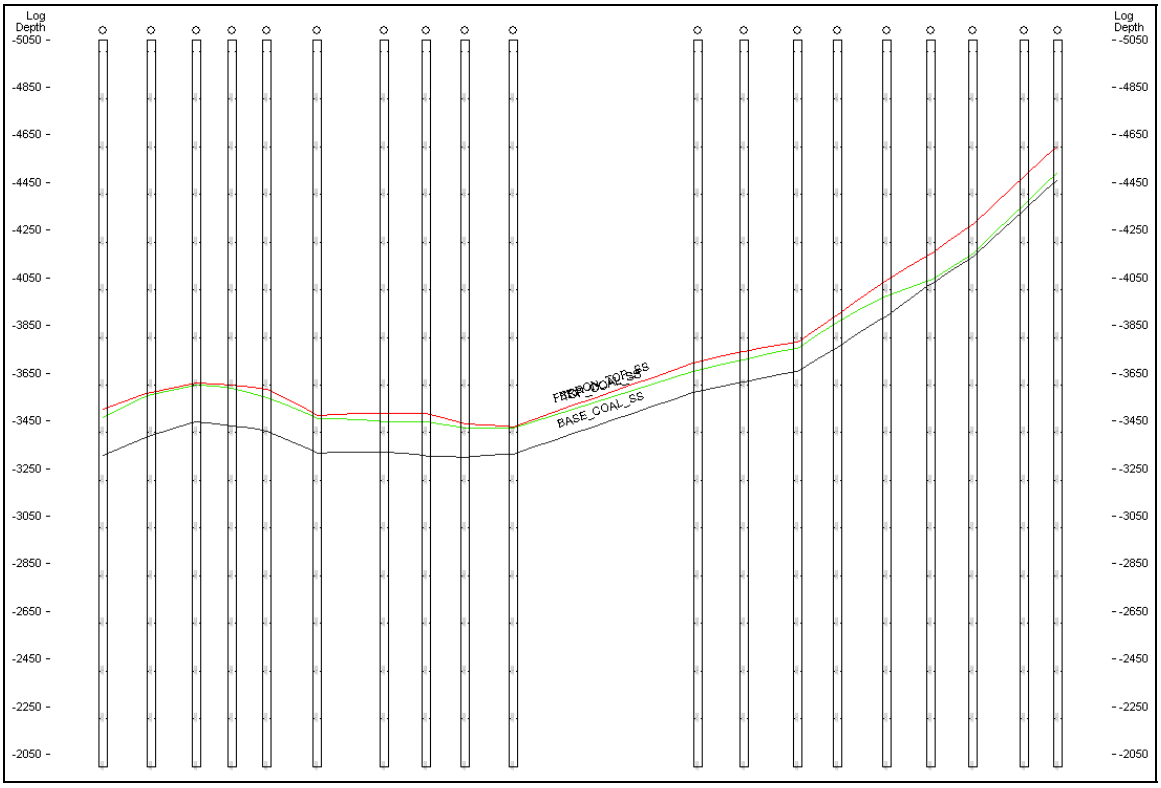

Figure 63: Cross section R-R' (not interpreted)

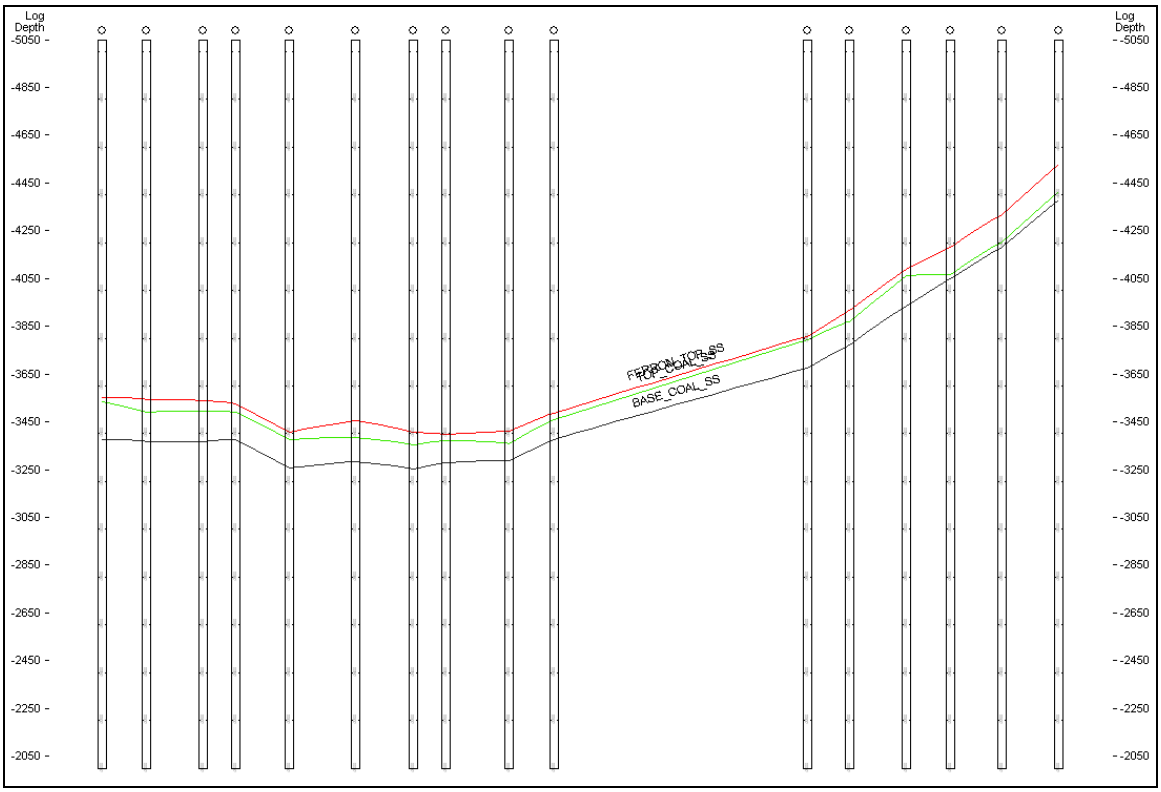

Figure 64: Cross section S-S' (not interpreted)

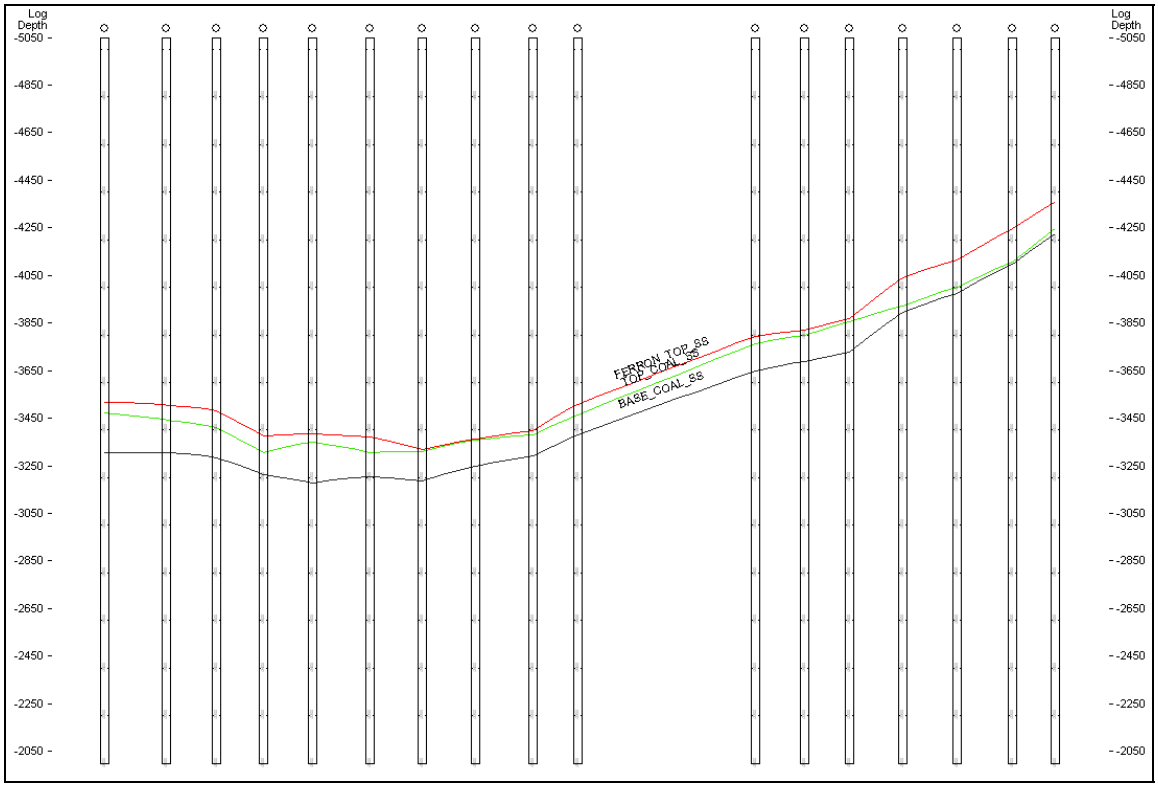

Figure 65: Cross section T-T' (not interpreted)

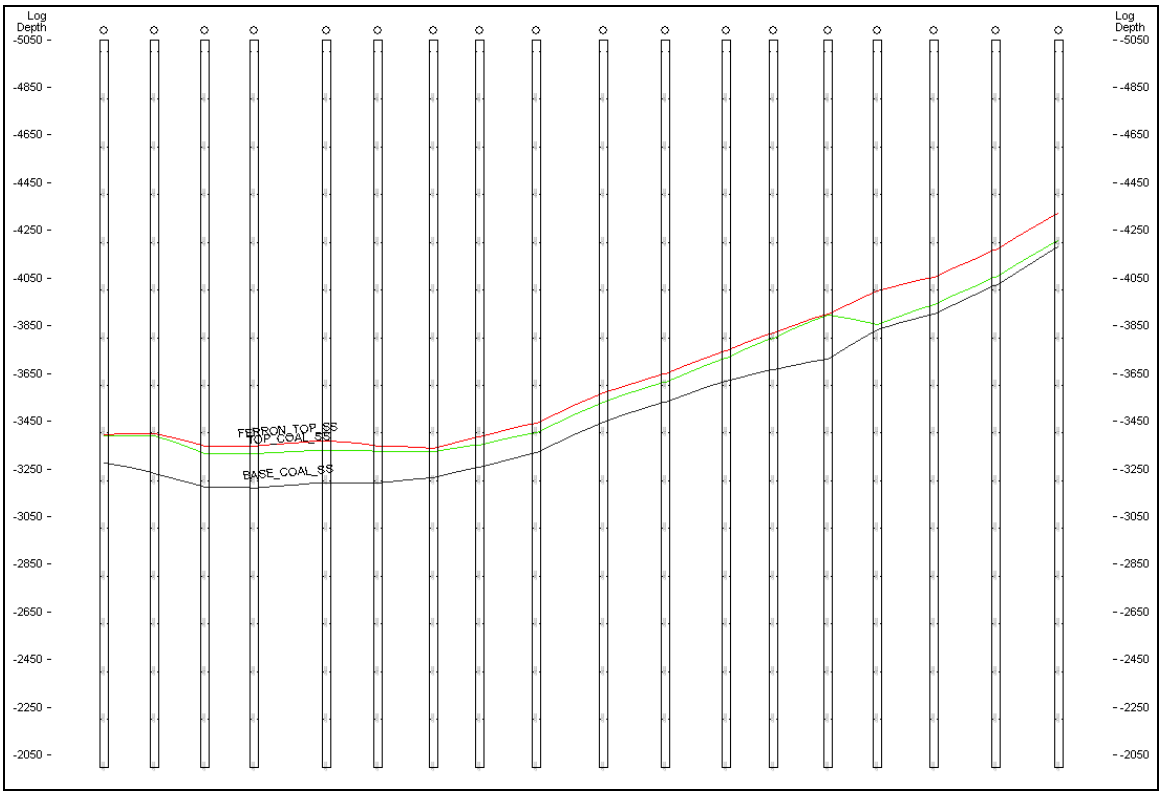

Figure 66: Cross section U-U' (not interpreted)

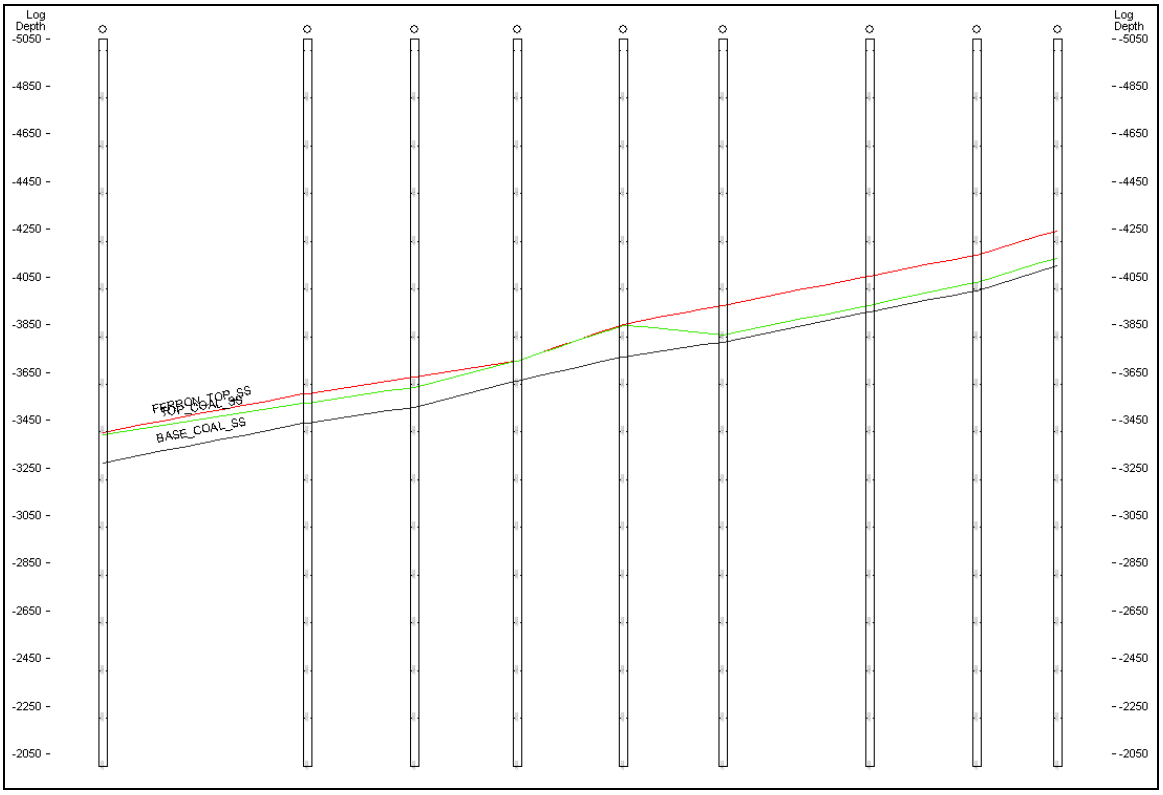

Figure 67: Cross section V-V' (not interpreted)

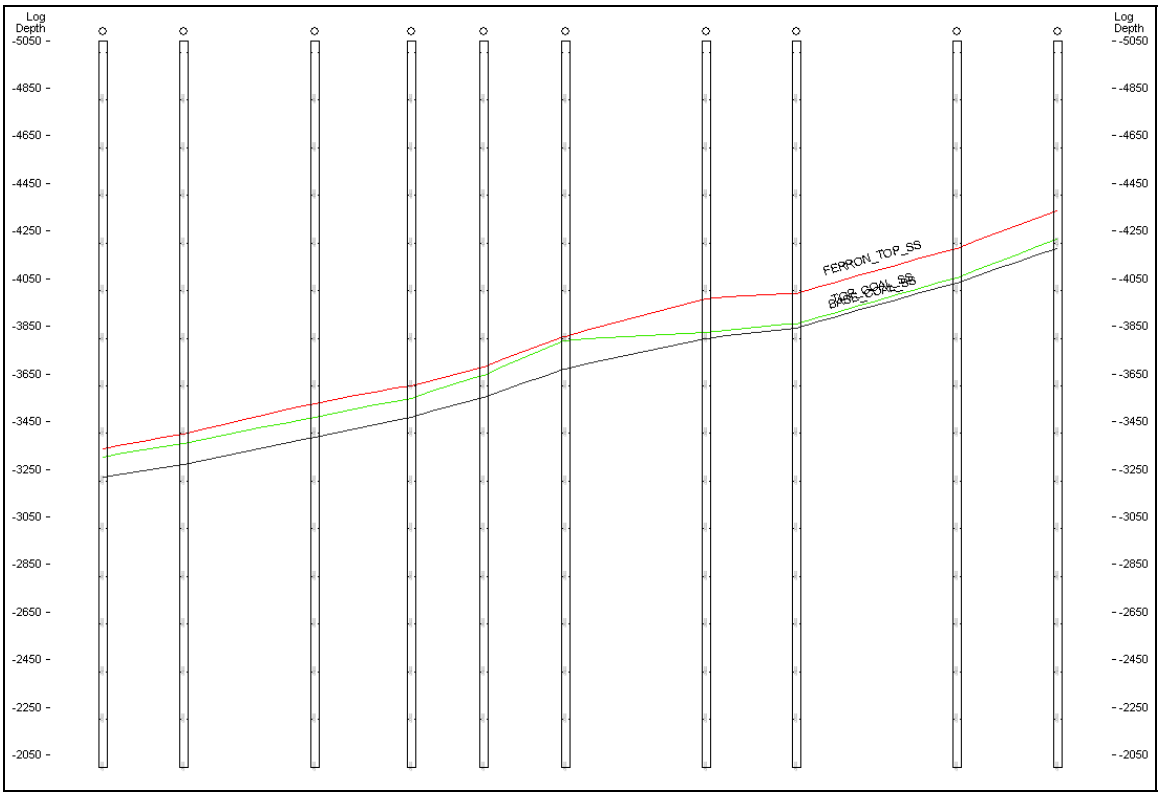

Figure 68: Cross section W-W’ (not interpreted)

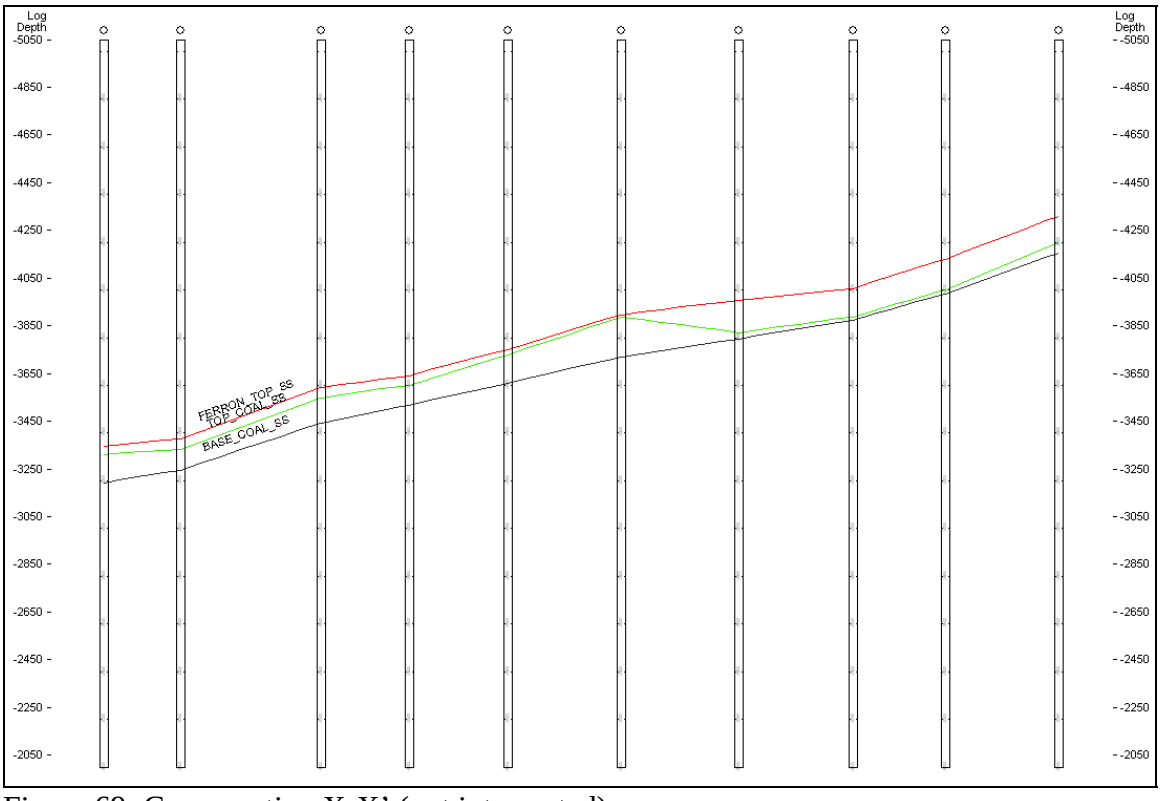

Figure 69: Cross section X-X’ (not interpreted)

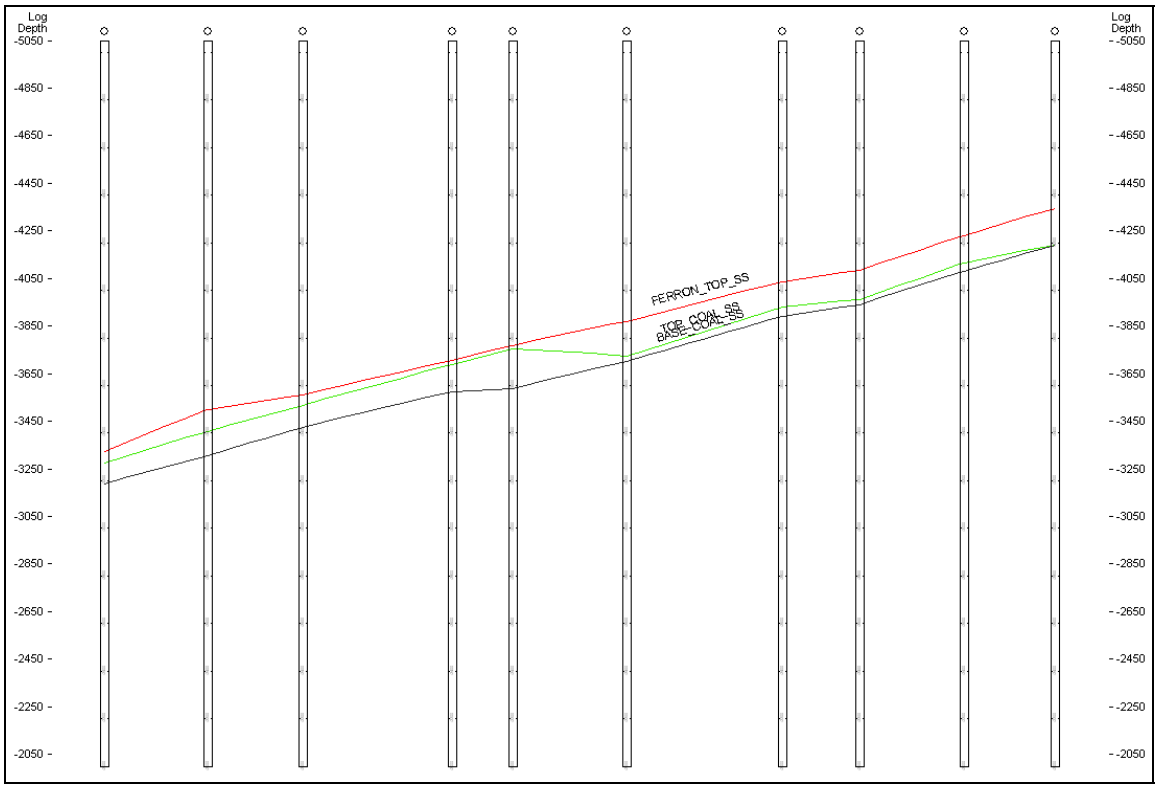

Figure 70: Cross section Y-Y’ (not interpreted)

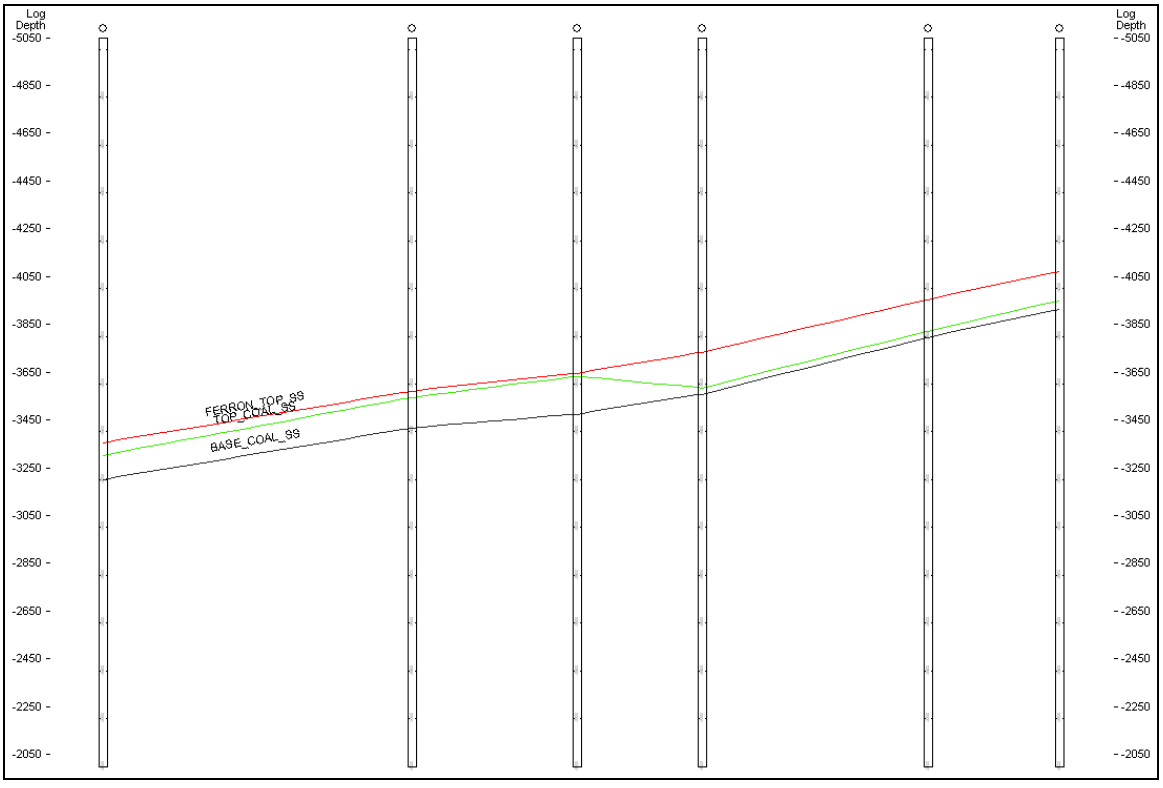

Figure 71: Cross section Z-Z’ (not interpreted)

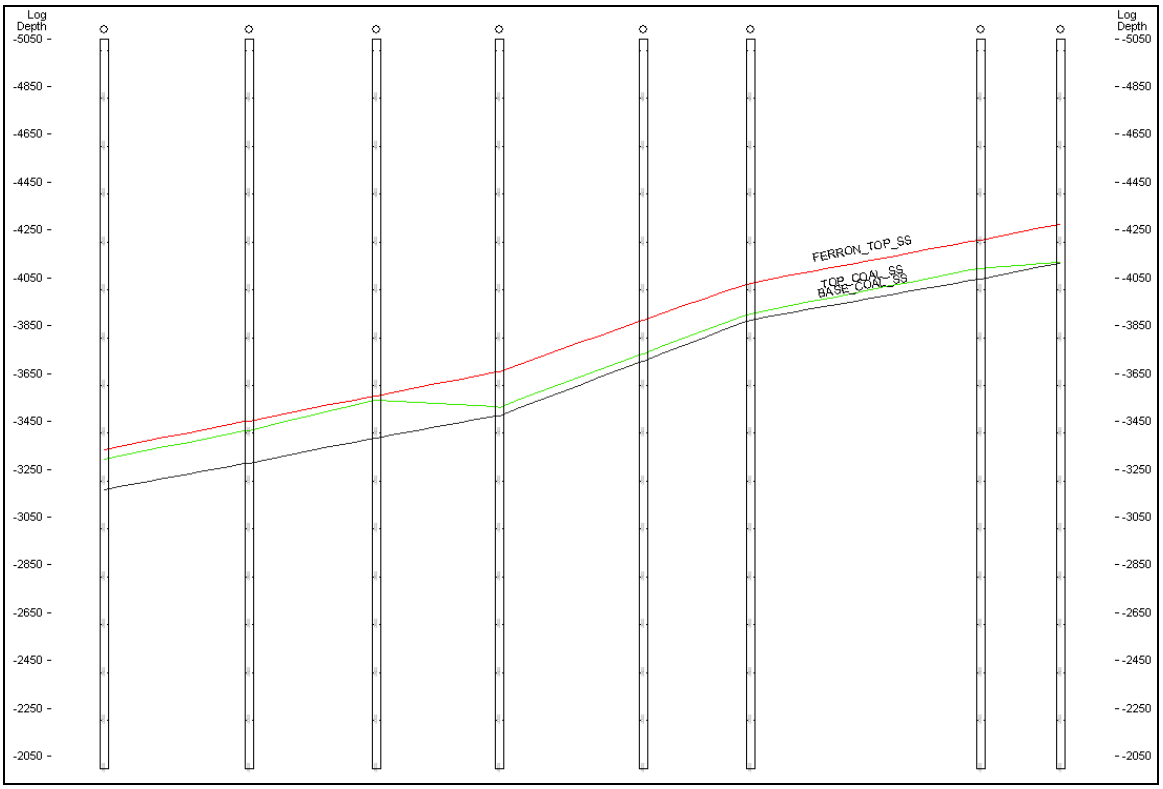

Figure 72: Cross section A1-A2’ (not interpreted)

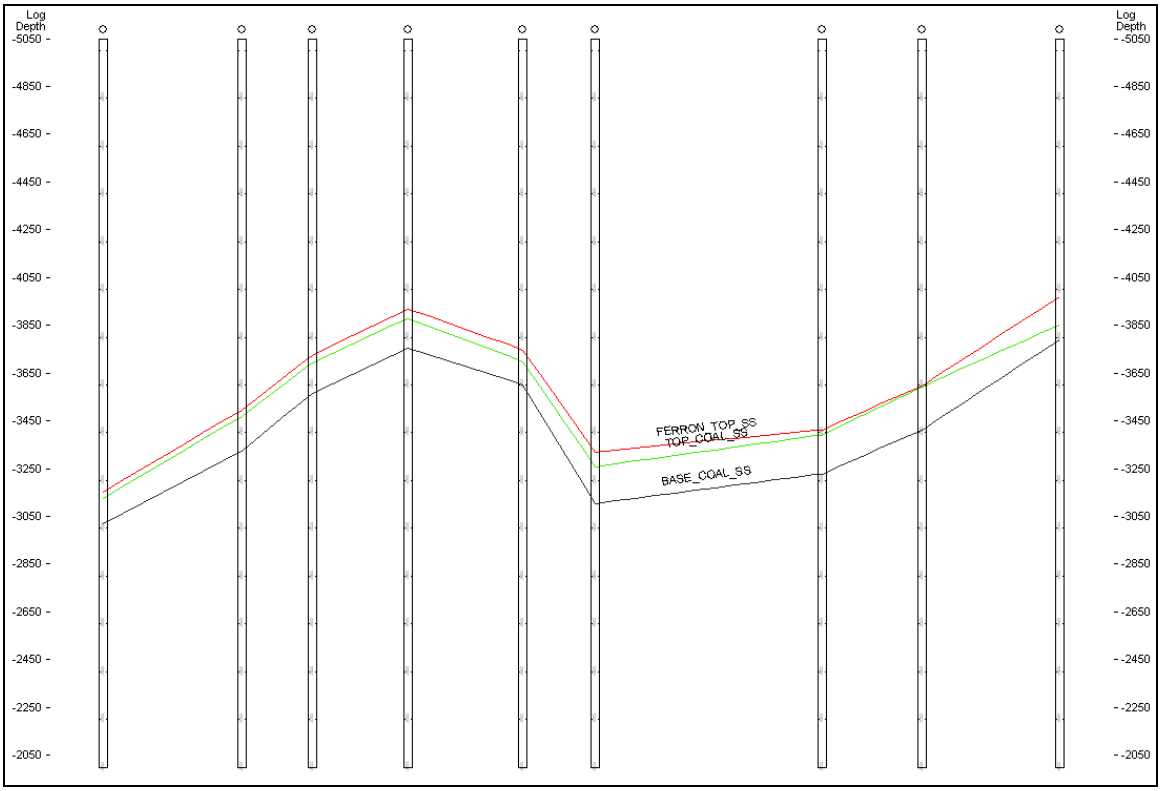

Figure 73: Cross section B1-B2’ (not interpreted)

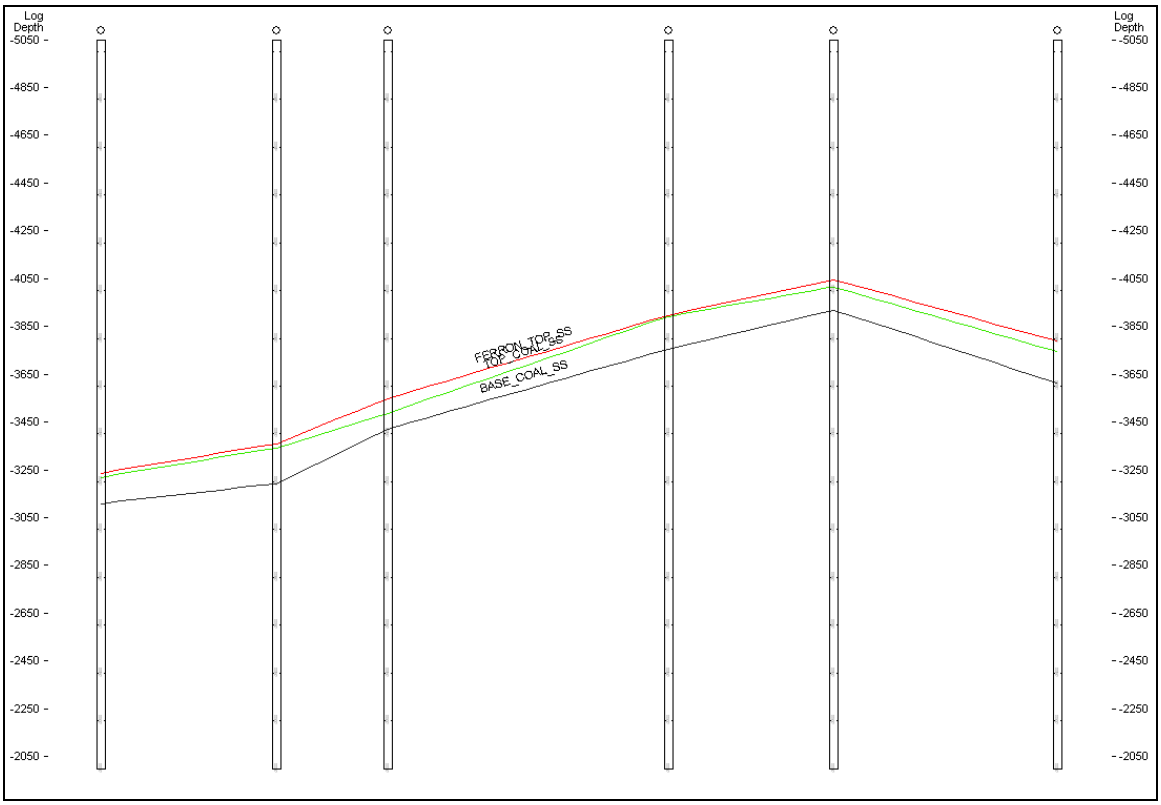

Figure 74: Cross section C1-C2’ (not interpreted)

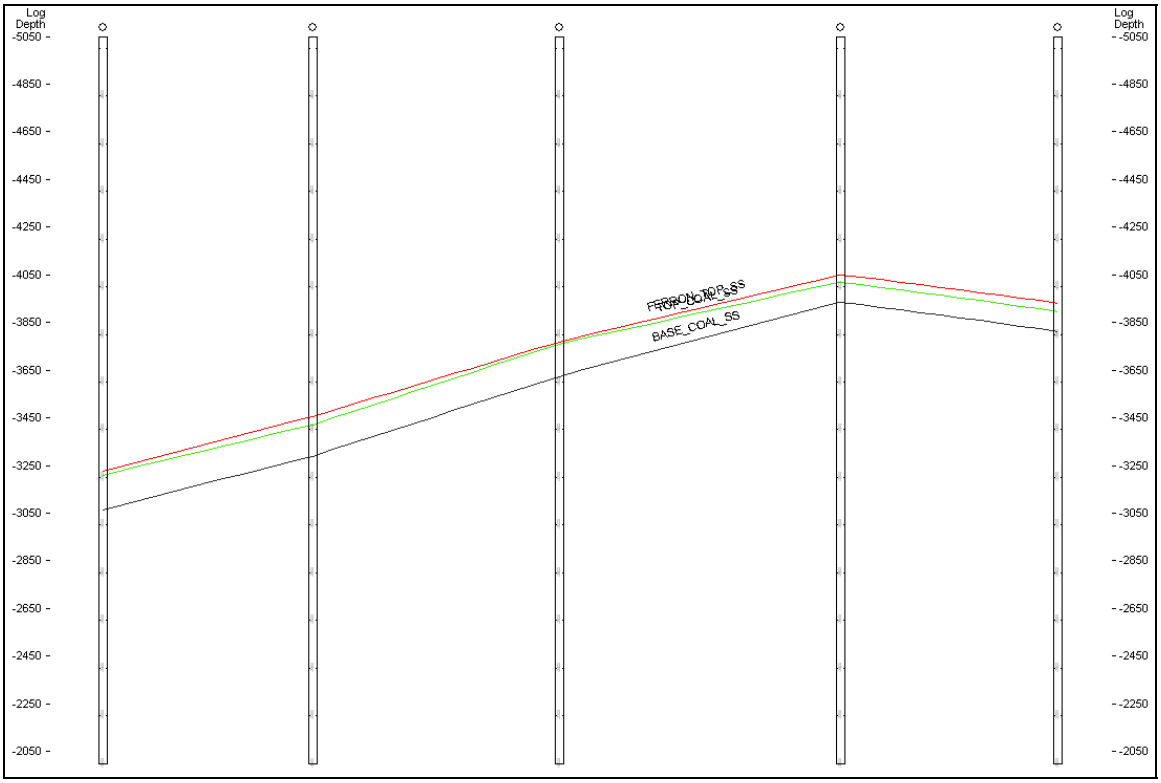

Figure 75: Cross section D1-D2’ (not interpreted)

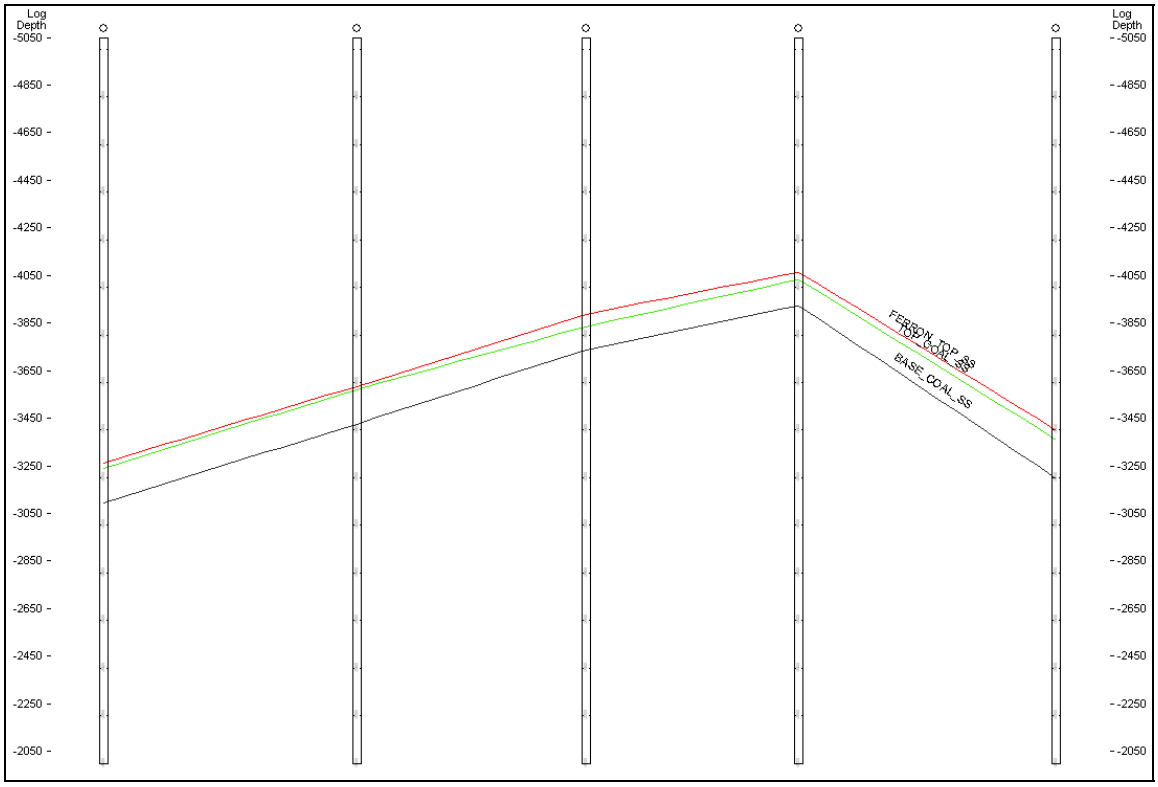

Figure 76: Cross section E1-E2’ (not interpreted)

Appendix C: Contour maps

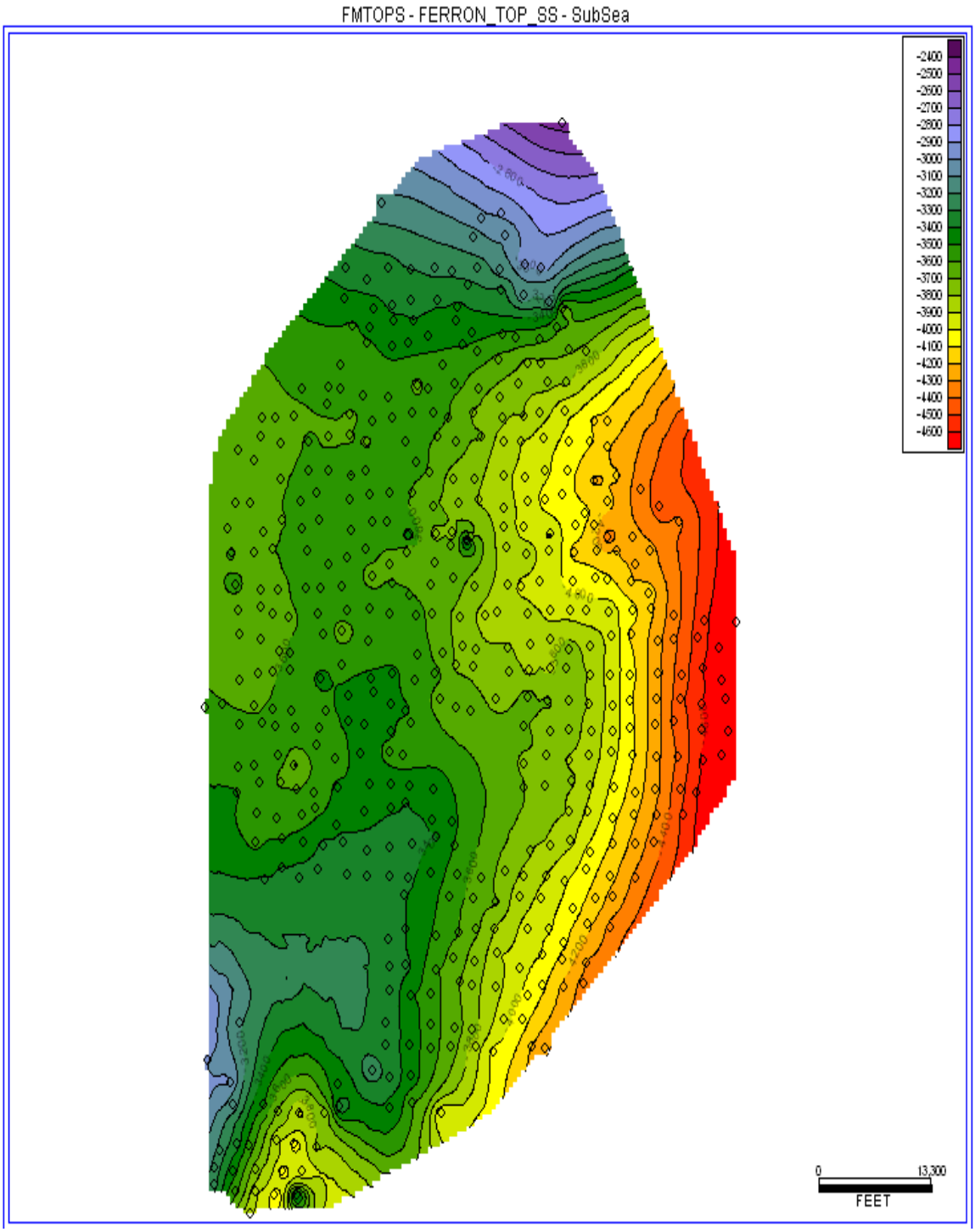

Figure 77: Elevation of top of Ferron Sandstone (ft above mean sea level).

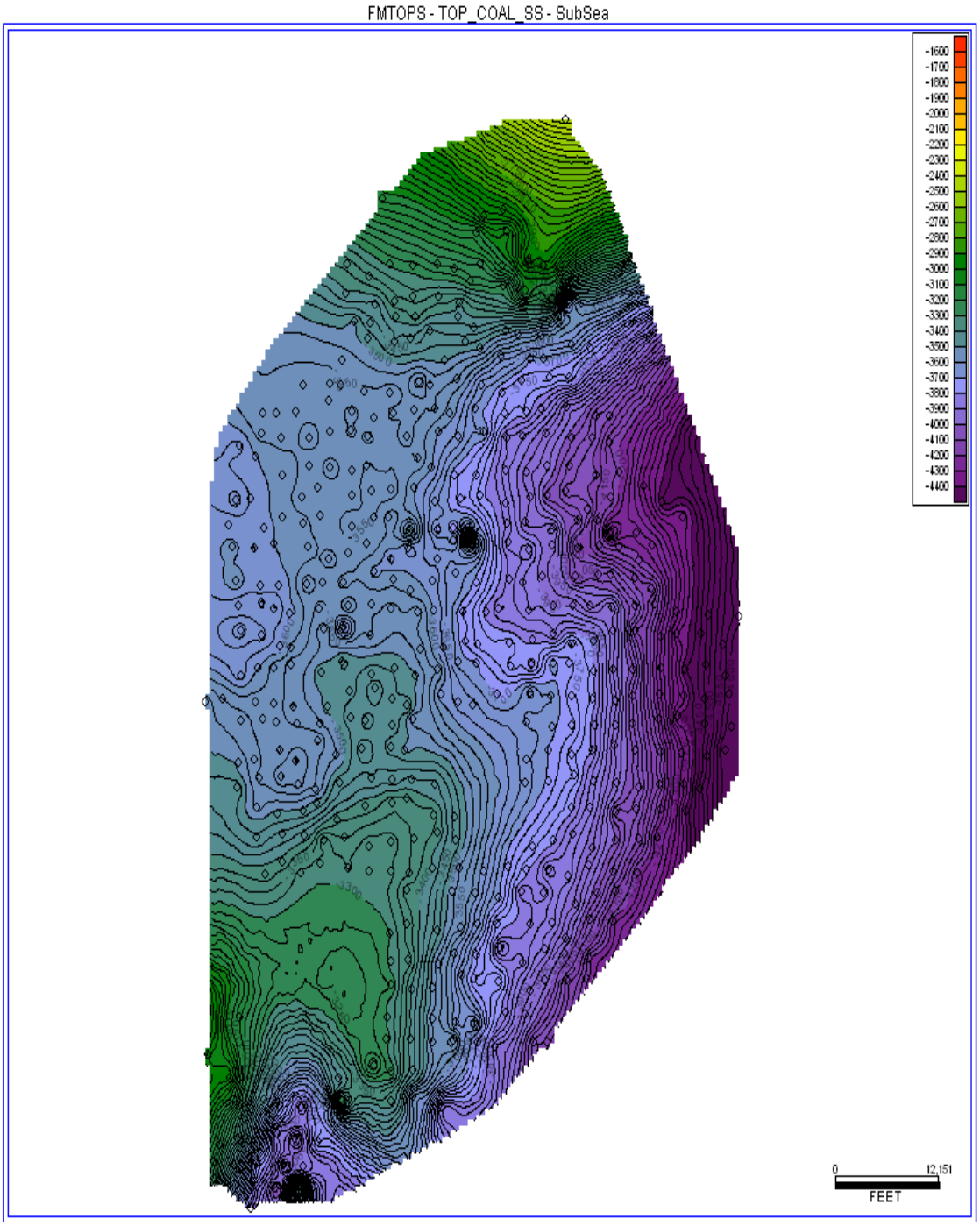

Figure 78: Elevation of top of coal (ft above mean sea level).

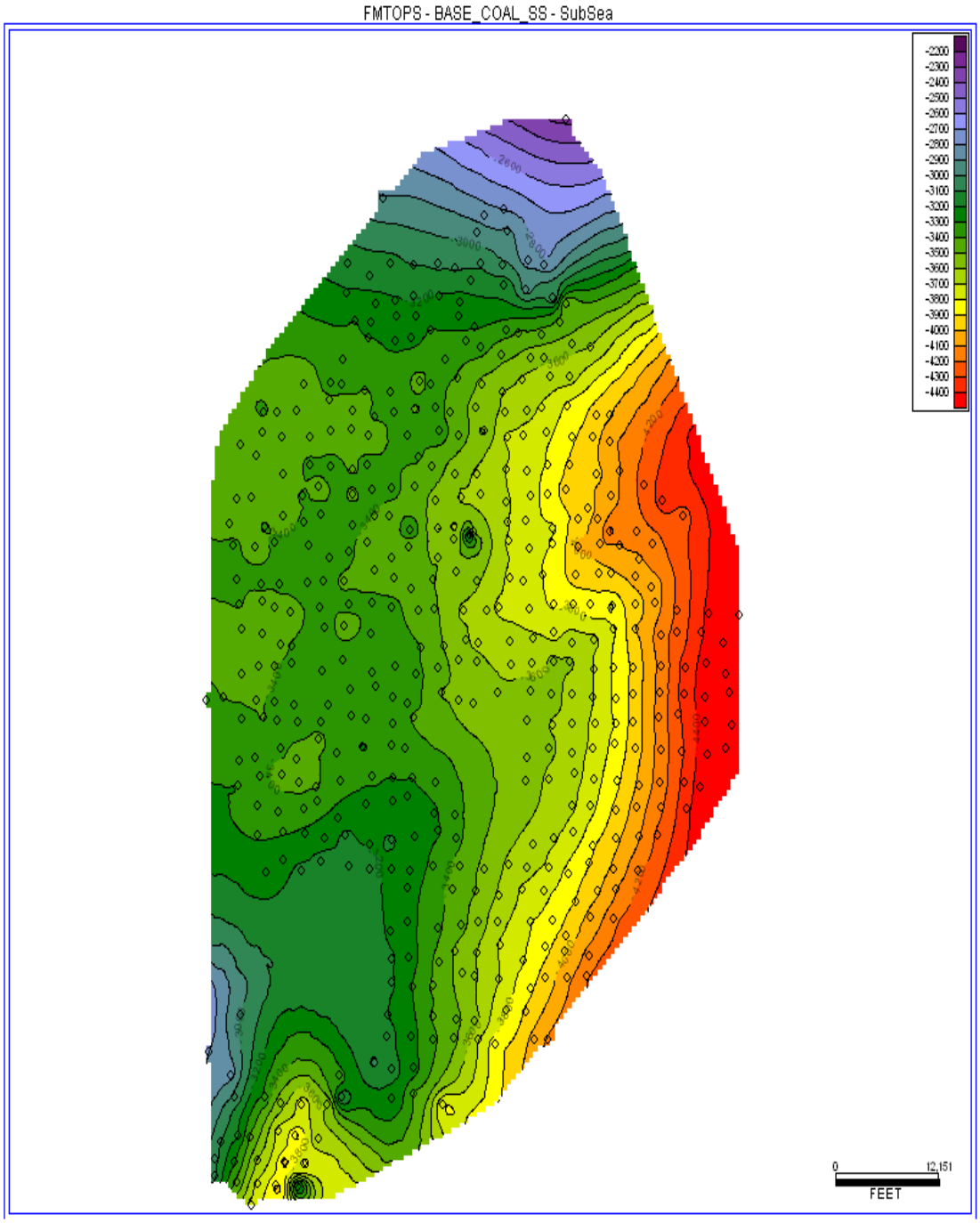

Figure 79: Elevation of base of coal (ft above mean sea level).

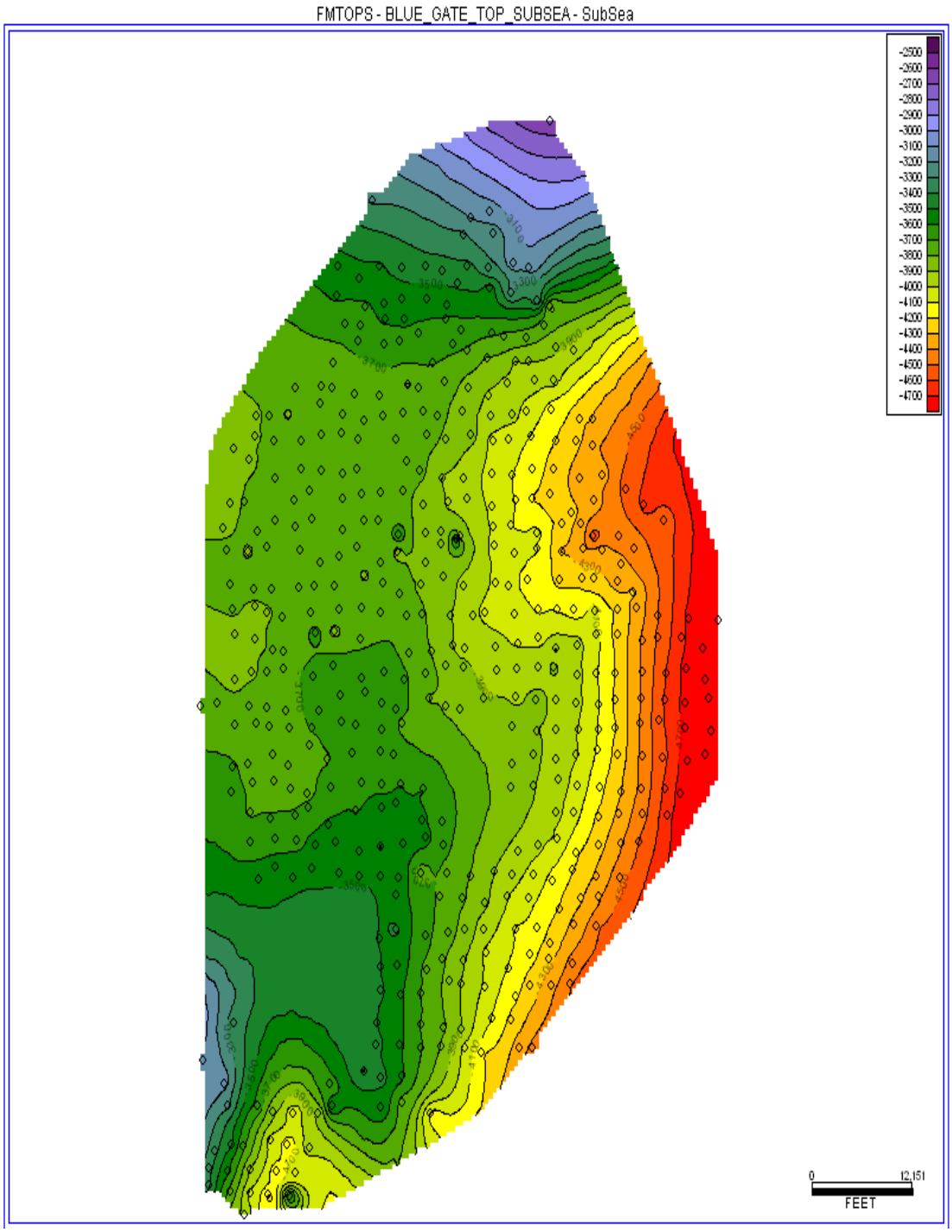

Figure 80: Elevation of top of Blue Gate Shale (ft above mean sea level).